OPTIMIZATION OF MECHANICAL AND MICROSTRUCTURAL PROPERTIES OF WELD JOINTS BETWEEN ALUMINIUM-MAGNESIUM AND ALUMINIUM-MAGNESIUM-SILICON ALLOYS WITH DIFFERENT THICKNESSES

A THESIS SUBMITTED TO
THE GRADUATE SCHOOL OF NATURAL AND APPLIED SCIENCES
OF
MIDDLE EAST TECHNICAL UNIVERSITY

BY
MURAT EKŞİ

IN PARTIAL FULFILLMENT OF THE REQUIREMENTS
FOR
THE DEGREE OF MASTER OF SCIENCE
IN
METALLURGICAL AND MATERIALS ENGINEERING

FEBRUARY 2013

Approval of the thesis:

OPTIMIZATION OF MECHANICAL AND MICROSTRUCTURAL PROPERTIES OF WELD JOINTS BETWEEN ALUMINIUM-MAGNESIUM AND ALUMINIUM-MAGNESIUM-SİLİCON ALLOYS WITH DIFFERENT THICKNESSES

submitted by **MURAT EKŞİ** in partial fulfillment of the requirements for the degree of **Master of Science in Metallurgical and Materials Engineering Department, Middle East Technical University** by

Prof. Dr. Canan Özgen _____
Dean, Graduate School of **Natural and Applied Sciences**

Prof. Dr. C. Hakan Gür _____
Head of Department, **Metallurgical and Materials Eng**.

Prof. Dr. Bilgehan Ögel _____
Supervisor, **Metallurgical and Materials Eng. Dept., METU**

Dr. Caner Batıgün _____
Co-Supervisor, **Weld. Tech. and NDT Res./App. C., METU**

Examining Committee Members

Prof. Dr. Cevdet Kaynak _____
Metallurgical and Materials Eng. Dept., METU

Prof. Dr. Bilgehan Ögel _____
Metallurgical and Materials Eng. Dept., METU

Assist. Prof. Dr. Y. Eren Kalay _____
Metallurgical and Materials Eng. Dept., METU

Assist. Prof. Dr. Kazım Tur _____
Materials Engineering Department, Atılım University

Dr. Caner Batıgün _____
Welding Tech. and NDT Res./App. C., METU

Date: 01 /02/2013

I hereby declare that all information in this document has been obtained and presented in accordance with academic rules and ethical conduct. I also declare that, as required by these rules and conduct, I have fully cited and referenced all material and results that are not original to this work.

Name, Last name: Murat Ekşi

Signature :

ABSTRACT

OPTIMIZATION OF MECHANICAL AND MICROSTRUCTURAL PROPERTIES OF WELD JOINTS BETWEEN ALUMINIUM-MAGNESIUM AND ALUMINIUM-MAGNESIUM-SİLİCON ALLOYS WITH DIFFERENT THICKNESSES

Ekşi, Murat

M.Sc.,Department of Metallurgical and Materials Engineering

Supervisor : Prof. Dr. Bilgehan Ögel

Co-supervisor : Dr. Caner Batıgün

FEBRUARY 2013, 84 Pages

For the last decades usage of aluminium alloys have been increasing tremendously. They have been used in aerospace industry widely and now aluminium alloys are becoming more and more popular in automotive and defense industries. Consequently; successful welding of aluminium alloys gains importance. In this study a research is carried out on weldability of plates having different thicknesses of composition 5754 aluminium and 6063 aluminium in T-fillet geometry using Gas-metal Arc Welding technique. It was aimed to have a successful joint without using pre-weld and post-weld heat treatments. During tests welding current and voltage were the varying parameters as welding speed was held constant. Macro-examinations were performed to see the penetration of the weld metal. It was seen that the type of filler wire greatly effects weld penetration. Hardness tests, tensile tests were done to compare the mechanical properties of the welded joints with different filler wires. Despite having better penetration in 4043 filler wire used weld joints, 5356 filler wire used weld joints had higher tensile strength and ductility.

In the second part of the study, a dynamic loading machine was designed and manufactured to see the behavior of the fillet welds under dynamic loading. The amount of stress and strain given to the specimen on this machine was adjustable but can't be measured. The tests that were made with this machine aimed only to compare the number of cycles of specimens before fracture. For dynamic loading tests two groups of specimens were prepared with filler wire 4043; each group having been welded with different heat inputs. It was aimed to see the effect of welding heat input on service lifes but no significant difference between cycle numbers of specimen groups having been welded with different heat inputs was observed. Microstructure examinations of these specimens revealed that coarsening the grains, grain boundaries, particles in PMZ and HAZ regions between Al 6063 base metal and weld zone made these areas more susceptible and favorable for crack propogation than Al 6063 base metal.

Key Words: Gas-Metal Arc Welding, Aluminium-Magnesium Aluminium-Silicon alloy, Dynamic Loading Machine, Cracking

ÖZ

FARKLI KALINLIKLARDAKİ ALÜMİNYUM-MAGNEZYUM VE ALÜMİNYUM-MAGNEZYUM-SİLİSYUM ALAŞIMLARI ARASINDAKİ KAYNAKLI BİRLEŞTİRMELERİN MEKANİK VE MİKROYAPISAL ÖZELLİKLERİNİN OPTİMİZASYONU

Ekşi, Murat

Yüksek Lisans, Metalurji ve Malzeme Mühendisliği Bölümü

Tez Yöneticisi : Prof. Dr. Bilgehan Ögel

Ortak Tez Yöneticisi : Dr. Caner Batıgün

Şubat 2013, 84 Sayfa

Geçtiğimiz yıllarda alüminyum alaşımların kullanımı önemli miktarda artmıştır. Havacılık sanayiinde sıklıkla kullanılan alüminyum alaşımları otomotiv ve savunma sanayiinde de gittikçe daha da popüler olmaya başlamıştır. Sonuç olarak alüminyum alaşımlarının başarılı bir şekilde kaynağı da büyük önem kazanmıştır. Bu çalışmada farklı kalınlıklardaki alüminyum 5754 ve alüminyum 6063 kompozisyondaki plakaların köşe kaynağı şeklinde gaz-metal ark kaynağı yöntemi kullanılarak kaynaklanabilirliğine yönelik bir araştırma yapılmıştır. Kaynak öncesi ve kaynak sonrası ısıl işlem kullanmadan başarılı bir birleştirme yapılması amaçlanmıştır. Testler sırasında kaynak hızı sabit tutulup, kaynak akımı ve kaynak voltajı sürekli değişen parametreler olarak seçilmiştir. Kaynak metalinin nüfuziyetini görmek için makro incelemeler yapılmıştır. Dolgu telinin çeşidinin kaynak nüfuziyetine etkisinin çok büyük olduğu görülmüştür. 4043 teli kullanılarak yapılan kaynaklarda daha iyi nüfuziyet elde edilmiş olmasına rağmen, 5356 teliyle yapılan kaynaklarda daha yüksek mukavemet ve süneklik değerleri gözlemlenmiştir.

Çalışmanın ikinci kısmında köşe kaynaklarının dinamik yük altındaki davranışlarını görmek için bir dinamik yükleme makinesi tasarlanmış ve imal edilmiştir. Yüklenen gerilim ve oluşan gerinim değiştirilebilir olup, ancak bu makinada miktarları ölçülememektedir. Bu makinede yapılan testler sadece kaynakların kırılmadan önceki çevrim sayılarını karşılaştırmayı amaçlamıştır. Dinamik yükleme testleri için 4043 dolgu teliyle iki grup kaynaklı numune hazırlanmış olup gruplar arası ısı girdisi farkı vardır. Isı girdisinin numunelerin kullanım ömürlerine nasıl etki ettiğini gözlemlemek amaçlanmış fakat değişik ısı girdileri ile kaynaklanmış numunelerin çevrim sayıları arasında belirgin bir fark görülememiştir. Bu numuneler üzerinde yapılan mikro yapı araştırmaları sonucunda Al 6063 ana metal ve kaynak bölgesi arasındaki kısmı erimiş bölge ve ısıdan etkilenmiş bölge, Al6063 ana metaline göre tane irileşmesi, tane sınırı kalınlaşması, parçacık irileşmesi gibi sebeplerden dolayı çatlak ilerlemesine daha meyilli hale gelmiştir.

Anahtar Kelimeler: Gas-Metal Ark Kaynağı, Alüminyum-magnezyumalaşımı, alüminyum-silisyum alaşımı, Dinamik yükleme makinesi

ACKNOWLEDGEMENTS

First of all, I would like to extent my sincere gratitude to my supervisor Prof. Dr. Bilgehan Ögel and co-supervisor Dr. Caner Batıgün for his guidance, cooperation, and support throughout my master education and this thesis.

Thanks to my examining committee: Prof. Dr. Cevdet Kaynak, Assist. Prof. Dr. Y. Eren Kalay, Assist. Prof. Dr. Kazım Tur for their most valuable comments, suggestions and support on several aspects of this master thesis.

Thanks to all the members of METU Welding Technology and Non-Destructive Testing Research and Application Center for for helping me with their best intentions throughout my study.

My special thanks to my colleagues Murat Tolga Ertürk, Oğuz Özlem for their technical supports and friendship.

I want to extend my appreciation to all my friends especially Onur Akın, Ekin Ağsarlıoğlu, Özgür Soydemir, Mehmet Akgül for their moral support and friendship.

Additionally, I would like to express my deepest feelings to my family for their full support at every step of my life.

TABLE OF CONTENTS

LIST OF FIGURES

FIGURES

LIST OF TABLES

TABLES

To My Beloved Karoş

CHAPTER 1

INTRODUCTION

With the improving production and heat treatment techniques, there has been serious progress on producing high strength aluminium alloys. Consequently they have been used more and more in aerospace, automotive and defense industries.

Welding can be defined as joining two different parts by creating atomic bonding having a neutral electron configuration between each other. This is often done by melting the two parts and filler wire between them to form a pool of molten material followed by resolidification. Different energy sources are used such as gas flame, electric arc, laser, electron beam, friction, and ultrasound.

Welding is the main joining method used in the industry. Gas-metal arc welding and gas-tungsten arc welding are the most used welding types for aluminium. However, there are still important problems in welding process of aluminium to overcome when compared to steels. Complex behavior of the intermetallics and sensitivity of aluminium alloys to heat can create problems.

In this study the aim was to perform a successful welding with an economical welding method under the most difficult conditions. Gas metal arc welding method using argon as inert gas is thought to be convenient as it is very widespread in the industry and suitable for automation with industrial robots. The plates to be welded are selected to have a large thickness difference and having a chemical composition difference as it is a common case in the joining processes and this situation created great difficulty during optimizing the weld parameters. Hot cracking is one of the most struggling problems in aluminium welding but no pre-heat treatment was applied to overcome this problem to lower the cost of the process. Two different filler wires are used in this study to overcome hot cracking with determining the weld parameters precisely.

Throughout the study; firstly welding parameters was optimized to have a successful joint with no discontinuities between aluminium- magnesium and auluminum-magnesium-silicon alloys using different filler wires. Afterwards mechanical and microstructural properties of the produced welded specimens were examined. Fatigue behavior of the aluminium fillet weld has also been a subject of curiosity. A machine was designed and manufactured in order to compare service lifes of the joints under dynamic loading. The dynamic loading machine is able to load and unload the specimens 360 times in a minute. Manufactured machine is more practical than the conventional fatigue test machines and easy to use for a fillet weld. Certainly some improvements can be made on the constructed machine such as attaching a cycle counter and attaching a unit that can measure the given stress. Finally the fracture surface examinations were carried out using scanning electron microscopy.

CHAPTER 2

THEORY

2.1 Aluminium and its Alloys

Aluminium heat treatment and production techniques are being developed tremendously for the last decades. Since aluminium has higher specific strength (strength / density) than steels and is cheaper than titanium, it is being more widely used in defense and transportation industry day by day.

Aluminium has advantages such as good machinability and good shapeability however it has problems while welding especially those which have different chemical compositions.

Hydrogen porosity is one of the main problems of aluminium welding. Oxygen and nitrogen gases are not as soluble as hydrogen in molten aluminium [3] and as a result of this they don't create porosities in the weld pool.

One of the most helpful reviews on hydrogen porosity is published two decades ago by Devletian and Wood [4], they say that the ratio of the solubility of hydrogen in the superheated molten to the solubility in the metal at solidification temperature is far more greater when compared to another structural metals. The authors also believe that alloying elements influence solubility data. They give some examples that alloying elements effects porosity concentration. As a result one can understand that porosity in aluminium welds is very much related to bead chemical composition.

The main sources of hydrogen entering the weld pool [4]

a) Hydrogen contained in the filler metal or parent metal
b) hydrogen bearing contamination or hydrated oxide films on filler metal and parent metal surfaces
c) Hydrogen and water vapor in shielding gas

So it is very important to clean the aluminium plates and filler wires before welding. Cleaning process is also very important to eliminate the oxide layers that immediately form on aluminium surfaces. Before welding the surfaces must be exposed the mechanical cleaning such as machining, filing, wire brushing, scraping or chemical cleaning. Otherwise oxide particles may enter the weld pool causing reduction in ductility, lack of fusion and weld cracking possibility. Another favor of using shielding gas such as argon in our study is to prevent re-forming of the oxide layer. [5]

One of the most important properties of aluminium concerning weldability is thermal conductivity. Aluminium's thermal conductivity (k - W/(m.K)) is half of the thermal conductivity of copper and four times greater than thermal conductivity of low-carbon steel. The big difference in the amount of this property between aluminium and steel is interesting and means that aluminium must be heated four times faster than low-carbon steel. However this high thermal conductivity may be useful in some cases such as the fast cooling of the liquid weld-pool in out-of-position welding [5]

Considering weldability, another important property of aluminium that differs from steel a lot (twice as much) is the coefficient of linear thermal expansion which is a measure of the change in length of a material with a change in its temperature. The relative large amount of this property means that one must be careful for keeping the joint space to remain uniform. In this study parts are preliminary joined by tack welding to overcome this problem. [5]

Melting temperature, volumetric specific heats and heats of fusion is lower than steel for aluminium and this situation results in lower heat input is required for aluminium welding. Melting ranges is also low when compared to steel. Pure Aluminium melts at 660^0 Cand its alloys melt between 350^0C-660^0C [5]

Aluminium can be alloyed with many other metals to improve physical and mechanical properties. Table 1 shows the major alloying elements in wrought aluminium alloys. [28]

Table 1 Major alloying elements in wrought aluminium alloys

Series	**Primary Alloying Element**
1xxx	Aluminium - 99.00% or Greater
2xxx	Copper
3xxx	Manganese
4xxx	Silicon
5xxx	Magnesium
6xxx	Magnesium and Silicon
7xxx	Zinc

Aluminium wrought alloys can be divided into two groups such as non-heat treatable alloys and heat treatable alloys.

According to EN 573 standards aluminium alloys are represented as 4 digit numbers representing their alloying elements. In this system in 5nxx series the main alloying element is magnesium and in 6nxx series the main alloying element is silicon. “n” indicates alloy modification.

Initial strength of the non-heat treatable alloys comes from the hardening effect of the alloying elements such as silicon, iron, manganese and magnesium. These elements increase strength by existing as dispersed phases or by solid solution strengthening. The non-heat treatable alloys are mainly in 1000, 2000, 3000, 4000 and 5000 series. Magnesium is the most effective solution strengthening element in non-heat treatable alloys. Aluminium-Magnesium alloys of the 5000 series have relatively high strength in annealed condition. All of the non-heat treatable alloys of aluminium are work hardenable. To remove the effects of cold working in order to increase ductility non-heat treatable alloys can be heated to a uniform temperature. Upon fusion welding which the joining method used in this study, non-heat treatable alloys may lose strength coming from strain hardening in a narrow zone adjacent to weld zone.

The initial strength of heat treatable aluminium alloys depend only on the alloy composition. Heat treatable aluminium alloys increase their properties by solution heat treating, then quenching and finally natural or artificial aging. Cold working may add additional strength and annealing may add additional ductility if it is necessary.

2.2 Gas-Metal Arc Welding

2.2.1 The Process

Gas-metal arc welding is a welding method that joins metals by melting. An arc is created and used for heating and melting metal pieces. Argon or helium gases are used to create a protective

atmosphere and that is why this process is called metal-inert gas (MIG) welding. Here in our study, welding aluminium is done by metal-inert gas method and the protective atmosphere is ensured by argon gas. This method is the most widely used arc welding method for aluminium alloys. A schematic representation of gas-metal arc welding is given in Figure 1. Unlike gas-tungten arc welding direct current electrode positive is used is GMAW. So we can obtain a stable arc, smooth metal transfer with low spatter loss and good weld penetration. [10]

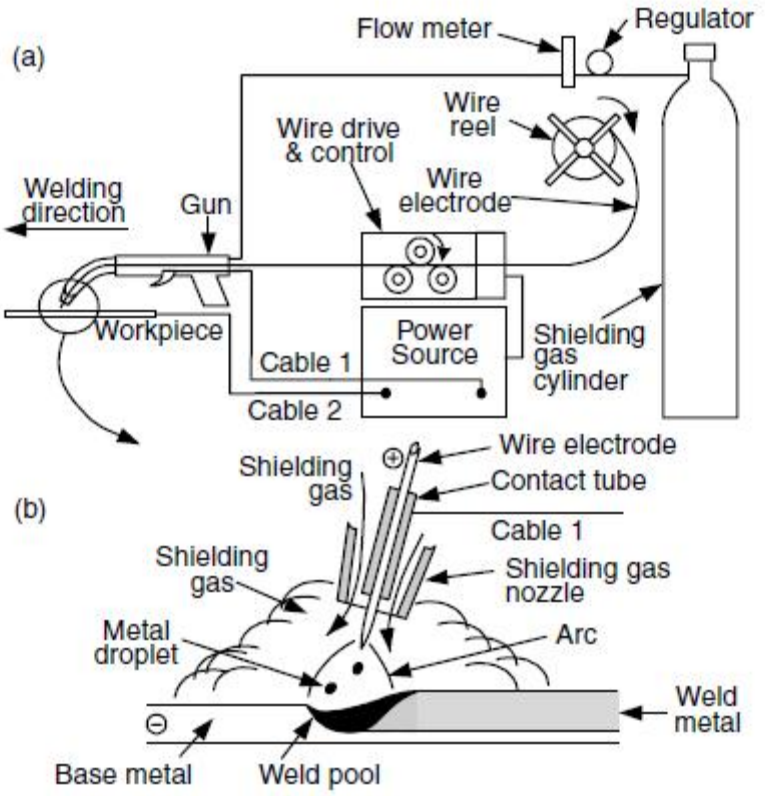

Figure 1 Gas-metal arc welding a) overall process; b) welding area enlarged [10]

2.2.2 Shielding Gases

For non-ferrous metals such as aluminium argon, helium and their mixtures are used. argon has lower thermal conductivity than helium so the arc energy is more uniformly dispersed in a helium arc than an argon arc. As a result of this Argon arc has higher energy arc plasma core and has lower thermal energy in outer mantle. So through Argon arc plasma; a stable, axial transfer of metal droplets is obtained. The weld transverse cross-section which is achieved by using argon as protective gas is characterized by a papillary (nipple) type of penetration [7] shown in Figure 2 (left). On the same figure at right a protective gas of mixture 75% He and 25% Ar is used and broad, parabolic type of penetration is observed [10].

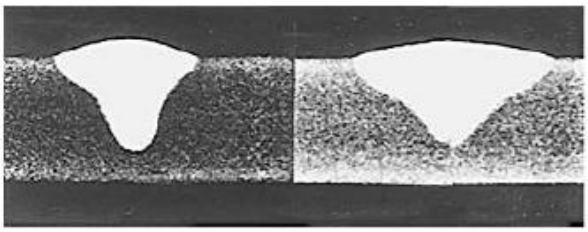

Figure 2 Gas-metal arc welds in 6.4-mm-thick 5083 aluminium made with argon(left) and 75% He-25% Ar(right) [8].

2.2.3 Modes of Metal Transfer

There are three transfer modes of molten metal at the electrode tip to the weld pool. [10]

a) Globular Transfer*:* Metal drops that are equal or larger in diameter than electrode tip drops to weld pool under the effect of gravity. In Figure 3 globular transfer can be seen during GMAW of steel 180 A and Ar-2% O_2 as protective atmosphere [9]. Because that globular transfer is not smooth no matter what the shielding gas is spattering occurs at low welding speeds. However with He, it can occur at all welding speeds.

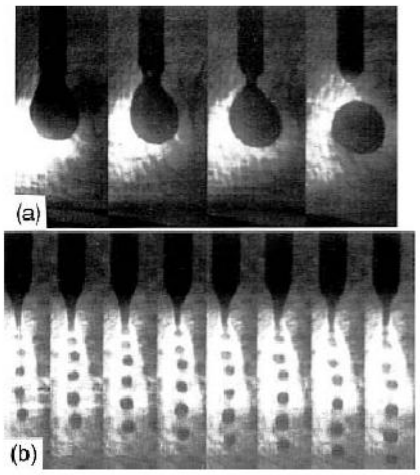

Figure 3 Metal transfer during GMAW of steel with Ar–2% CO2 shielding: (a) globular transfer at 180A and 29V shown at every 3 ¥ 10^{-3} s; (b) spray transfer at 320A and 29V shown at every 2.5 ¥ 10^{-4} s. [9]

b) Spray Transfer: At high currents small discrete metal droplets transfer occurs through the arc by electromagnetic force at much higher speed and frequency than globular mode. At Figure 3 (b) an illustration of spray transfer is given. The critical current level above which spray transfer occurs is dependent on material and size of the electrode and the shielding gas composition.

c) Short-circuiting Transfer: In this type of transfer metal passes when electrode touches the pool surface in other words when short circuiting happens. It is used when welding thin sections or in out-of-position welding because a smaller and fast freezing weld pool is produced.

2.2.4 Advantages and Disadvantages

GMAW is a very clean welding method especially with an inert gas. The deposition rate is much higher in GMAW than in GTAW. This is a great advantage when welding thick pieces. In our study the reason that GMAW is chosen to work with is that it is convenient for automatic welding. Unlike GTAW there is no need of human skill to maintain a short and stable arc length. GMAW torches can be bulky and can create difficulty when welding small areas but in our study it is not important for us. [10]

2.3 Weld Regions

Welding is a process that high amount of heat is given to base metal in order to melt the initial base metals and create metal bonding between them when solidifying together.

The first zone to be mentioned is the weld metal where filler material and base metal is completely melted and solidified. Weld metal is not only the area that is affected from heat input. There is also another zone called heat affected zone (HAZ). The difference of this area is that melting does not occur here but still microstructural changes happen. Weld metal is separated with a fusion line in which the temperature is liquidus. Inside HAZ starting from fusion line up to a point where temperature is solidus there is also another zone called partially melting zone (PMZ).

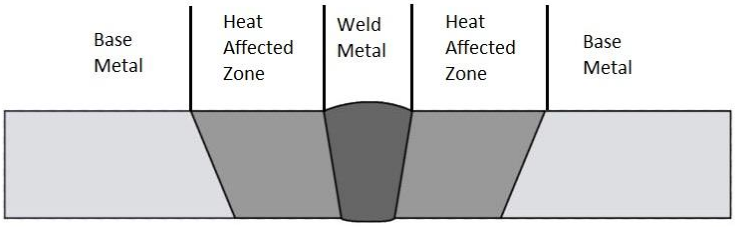

Figure 4 Zones in a weld

2.3.1 Weld Metal

This is the area that is subjected directly to the heat of the arc and that's why base metal and filler metal is completely melted creating a weld pool. Size and composition of the weld pool is related with the heat input and weld parameters.

Understanding basic solidification concepts is very important in order to explain weld metal microstructure. Temperature gradient (G) and growth rate (R) is two important factors defining microstructure and they are affected by weld parameters. Figure 5 briefly shows how G and R effects the morphology and size of solidification structure.

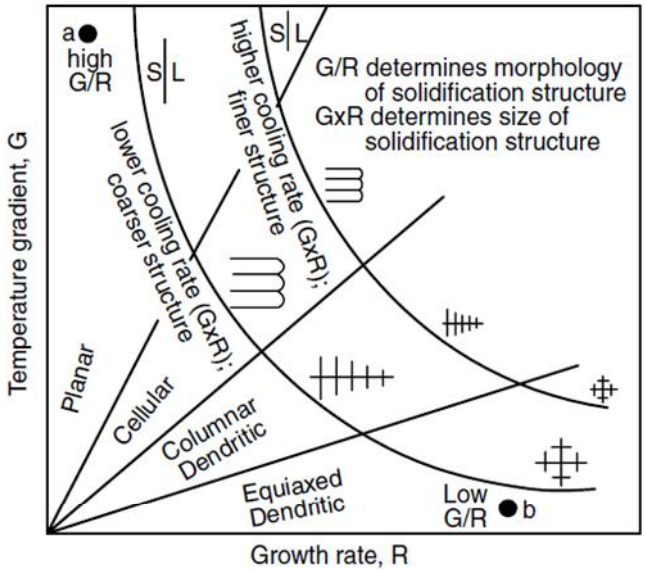

Figure 5 Effect of temperature gradient and growth rate on weld metal solidification [10]

G/R determines morphology of solidification and GxR determines size of the solidification structure. G is highly affected by heat input. As the given heat increases temperature gradient will be lowered and this can change the solidification morphology cellular to dendritic [10]. Given line energy (Q/V) in other words heat input and welding speed is also important as it determines the cooling rate. It is known that decreasing line energy (Q/V) in other words decreasing heat input or increasing welding speed results in finer microstructure.

2.3.2 Heat Affected Zone

Heat affected zone is adjacent to weld metal and separated by fusion line from it. This zone's microstructure and properties are changed after the welding operation. The heat given to metal and cooling afterwards is the reason of this change in the area. The amount of property change depends on mainly the base metal, filler metal and the heat input. Weld parameters again get important as they define the heat given to the material.

Thermal conductivity is another important property that has influence on the width of heat affected zone. If the thermal conductivity of the metal increases then the heat affected zone will be narrow because the heat is easily transferred to surrounding and the zone temperature couldn't get high. So the cooling rate is high making the heat affected zone narrower. This is actually the case in aluminium welding. Inversely low thermal conduction leads to slow cooling rate and a larger HAZ.

Welding process type also plays an important role in determining the size of the HAZ. For example processes like oxyacetylene welding create large HAZ because of the high input. On the other hand processes like electron beam welding or laser beam welding use intense and lower heat and create a narrow HAZ. Gas-Metal arc welding used in this study is a type that lies in the middle of the range [11].

2.3.2 Partially Melted Zone

Partially melted zone is a zone that is actually inside the heat affected zone. It starts from the fusion line where the temperature is liquidus and lies into HAZ until the temperature is solidus. Melting is incomplete in this zone and it is wider in aluminium alloys as the solidification range is wider.

Liquation cracking occurs mainly in partially melted zones and this is one of the most important problems in aluminium welding.

2.4 Weld Defects

Actually every weld is a defect in the material because it disturbs the microstructure by giving heat. However most of the times it has no alternative in order have a successful joint. It is nearly impossible to produce a perfect weld but it is possible to keep the defects in accepted limits that are specified by standards.

Some of the reasons causing weld defects are environmental effects, applied current magnitude, solidification rate, dimensions and position of the electrode and the presence of flux, high residual stresses, orientation and size of the welded materials.

In this section a brief discussion is going to be made about general weld defects especially the ones that caused great problems in this study.

2.4.1 Incomplete or Insufficient Penetration

When the weld metal does not penetrate to the required depth in the base metal, this defect is called incomplete or insufficient penetration.

The reasons for this defect are low current, low preheat, tight root opening, fast travel speed, short arc length. For prevention these factors must be corrected.

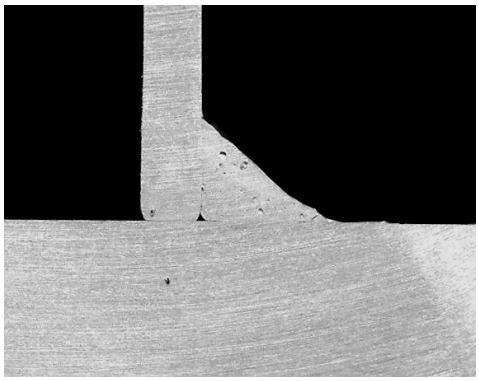

Figure 6 Insufficient penetration (Magnification 3X, Etchant: Flick's solution)

2.4.2 Incomplete Fusion

Sometimes weld metal does not form a cohesive bond with the base metal which is of course not wanted.

Reasons for this weld defect can be described as low current, steep electrode angles, fast travel speed, short arc gap, lack of preheat, too small electrode, unclean base metal, arc off seam.

Figure 7 shows a good example of incomplete fusion. This section which is perpendicular to the welding direction was taken from one of the experiments of this study.

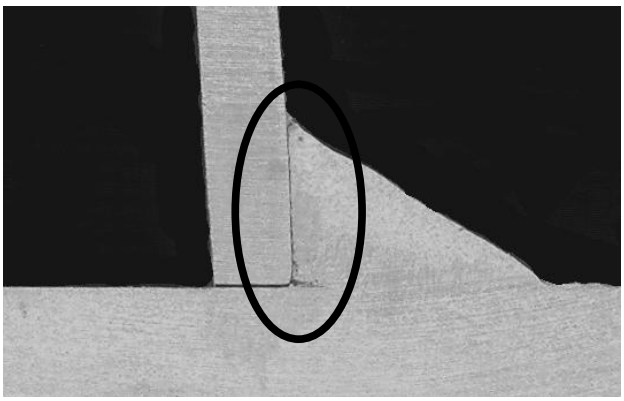

Figure 7 Incomplete Fusion (Magnification 3x, Etchant: Flick's solution)

This welding defect can be prevented by eliminating the possible causes. It can also be repaired by removing and rewelding the defected area but this can be very difficult sometimes.

2.4.3 Undercut

A groove cut at the toe of the weld (Figure 8) which is left unfilled is called undercut.

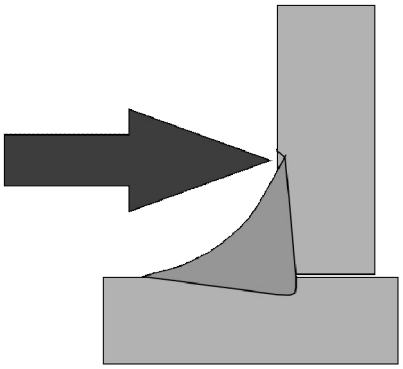

Figure 8 Undercut

Main reason for this weld defect is the wrong torch angle and the other reasons are high current, long arc length and rust. This problem is very difficult to overcome but can be lowered to some acceptable limits. Selecting the optimum torch angle and cleaning the metals may be useful.

2.4.4 Misalignment

This type of geometric defect is generally caused by a setup/fit up problem, or trying to join plates of different thickness. (Figure 9)

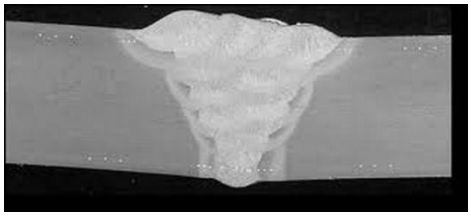

Figure 9 Misaligned vertical plate (Magnification 5X, Etchant: Flick's solution)

2.4.5 Overlap

When the face of the weld extends beyond the toe of the weld this is considered a weld defect called overlap (Figure 10). Improper welding techniques, wrong torch angles, wrong travel speed can be the cause of this problem.

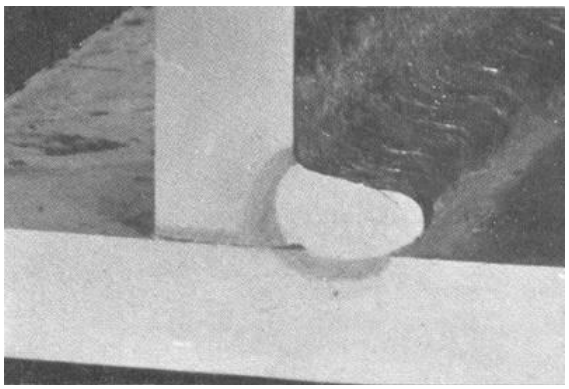

Figure 10 Overlap (Magnification 3X)

2.4.6 Porosity

This weld defect can shortly be described as gas being entrapped inside weld metal. Contamination of weld metals, moisture on the filler metal or base metals, long arc length and improper weld parameters (excessive current) are the possible reasons for porosity.

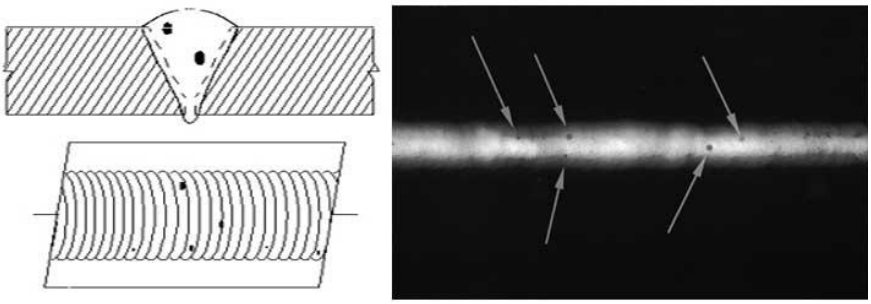

Figure 11 Porosity

Contamination can of course easily be eliminated by cleaning the base metals and if the filler wires are stored properly moisture on them would not cause defect. Lastly optimizing weld parameters will overcome the excessive current problem.

Porosity is a much bigger problem when it comes to aluminium welding. In aluminium liquid hydrogen solubility is too high and solubility increases with increasing temperature. In section 2.1 a more detailed explanation is done.

2.5 Cracking

In the previous section some weld defects that are considered to be important are discussed but cracks are more important since a small crack can grow and lead to failure. All welding standards show zero tolerance to cracks whereas other defects are accepted up to some limit. All welds include local defects that raise stress enough to induce cracks. So the engineer must study the stress environment and toughness. The ways for increasing toughness may be controlling alloy chemistry and post-weld heat treatment and there are also remedies for reducing stress such as changing the joint design for lowering tensile load, preferably having compressive loads at possible crack locations.

In this section a brief discussion is going to made about three types of weld defects which are hot crack, cold crack and fatigue crack.

2.5.1 Hot Crack

As the name implies this type of cracking is observed at high temperatures during solidification assisted by cooling stresses induced in the weld. Hot cracks generally occur when the alloying element has low solubility in the first appearing solid. As the solidifying grains grow, they push the alloying elements/impurities towards the center. The alloying elements/impurities tend to react with the main element which is aluminium in this study and form a low strength compound. Hot cracks are usually found at the center of the weld, extending through the weld direction producing a longitudinal crack. There are two other regions that hot cracks can be seen. They can occur at the end of the weld in a star shape, called crater cracks. These types of cracks also become a problem in this study. In aluminium alloys hot cracks can form in the heat affected zones adjacent to fusion lines. Special name for this zone is partially melted zone as already mentioned [12].

A collection of hot cracking theories has been done by Eskin et. al. [13]. They are not going to be discussed in this thesis widely, actually only a summary is given in this section. One of the theories says that hot crack formation is determined by the ductility of the semi-solid body [14, 15].

W.S Pellini stated that [16] the strain on the liquid film between dendrites is a reason for solidification cracking which is a subtitle under hot cracking.

Pumphery and Jennings' theory which is called shrinkage-brittleness theory [17] suggests that mushy zone can resist strain up to some limit and strains greater than that limit cause cracking

Borland's generalized theory [18] examines solidification into three stages (Figure 12). At the first stage liquid and solid move independent of each other. At the second stage a dendritic skeleton is being formed but still no strain on the liquid. At the third stage dendritic network no more allows for the liquid flow thus healing of pores and cracks. So when the strain generated is greater than the semi solid can handle crack forms.

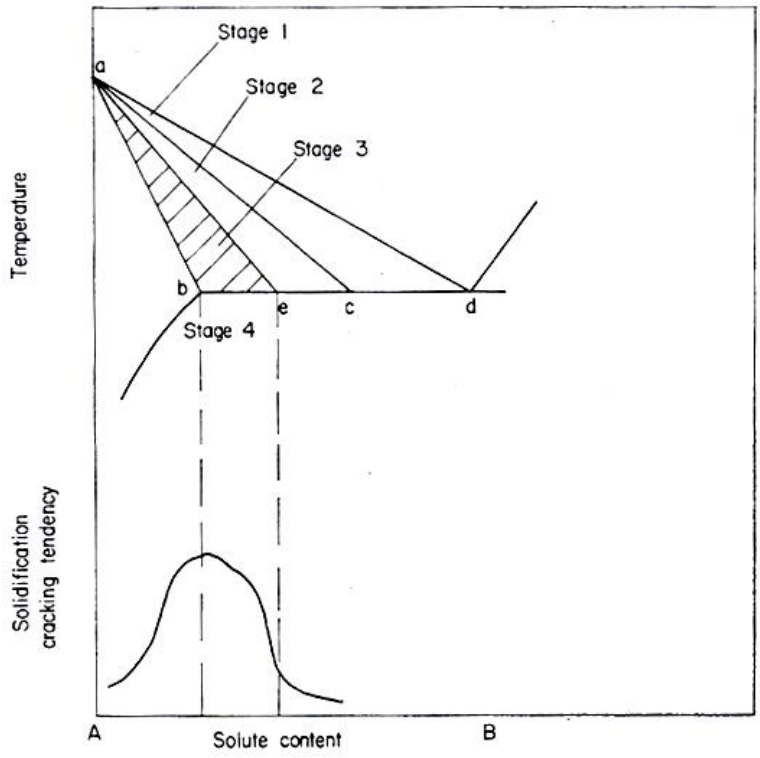

Figure 12 Stages of solidification according to Borland's generalized theory [18]

2.5.2 Cold Crack

Cold cracks form in the joint after the weld is cooled. Two main reasons are shown for this type of crack. First reason is the excessive residual stress in the weld and the second reason is the hydrogen remained in the weld diffusing into dislocations. The diffused hydrogen form pockets which expands the defects creating cracks. In this situation presence of hydrogen is not enough; actually a microstructure having a tendency to crack growth is also necessary. Suck cracks can form in the weld but they are generally found in heat affected zones [12].

Cold cracks can form even 48 hours after the welding. Hydrogen-assisted cold cracking can be reduced by preheating the weld metals as the cooling rate decreases and hydrogen is allowed to diffuse outside the material. [12].

2.5.2 Fatigue Crack

Since this study includes design and building of a dynamic loading machine, it is essential to discuss fatigue cracks. Figure 13 shows a typical crack in a fillet weld joint.

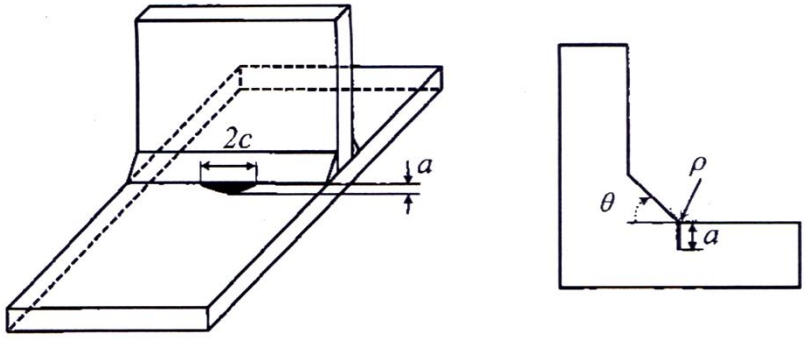

Figure 13 Typical geometry and crack in a fillet welded joint [22]

Residual stresses assist external fatigue stress for the growth and initiation of fatigue cracks which can be seen in the regions near the weld zone. These cracks are observed in the heat affected zones but there must be residual surface tensile stresses present [12].

On a macroscopic scale, and under essentially elastic conditions in isotropic materials metallic materials most fatigue crack tend to propagate in Mode I (Figure 14). Thus researchers predicting fatigue crack paths focus on this mode [19].

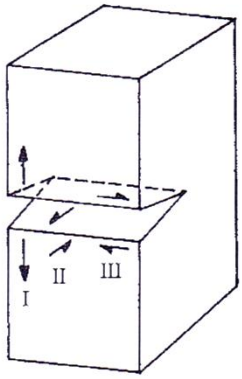

Figure 14 Notation for modes of crack surface displacement [25]

There are two types of crack propagation in these types of cracks [20]. The first type of crack propagation is dominated by maximum principal stress. In this type, cracks of Mode I approximately perpendicular to the direction of the maximum principal stress are called maximum stress dominated. So it can be thought that fatigue cracks tend to propagate perpendicular to the maximum principal stress direction. [19]

The second type of fatigue crack propagation is dominated by shear stress. It usually forms on maximum shear stress planes and it is often seen when the crack tip plastic zone is large [21]. A shear dominated fatigue crack propagates in either mode II or mode III [19].

2.6 Fatigue

2.6.1 Introduction

Fatigue is the progressive damage on the material that is subjected to cyclic loading. The amount of the load and stress is below the ultimate tensile strength of the material and it may also be below the yield strength of the material.

Fatigue occurs when the material is continuously loaded and unloaded. When the amount of the load is above some limit microscopic cracks will begin to form on the surface. Finally those cracks reach to a certain length and sudden fracture occurs.

Due to the morphology of the specimen fatigue can be classified into two topics:

a) The uncracked situation: In this condition fatigue lifes are dominated by crack initiation rather than crack propagation. Plain metallic specimens such as gears, crank shafts are examples of this type
b) The cracked situation: In this type cracks are present at the beginning thus the fatigue lifes are dominated by crack propagation. Welding and casting introduces cracks into specimens. For determining the fatigue life it is necessary to find the number of cycles from initial cracks size to the final crack size at which static failure takes place.

Due to magnitude of applied stress fatigue can be examined under two types

a) High cycle fatigue: This type of fatigue is observed when the applied stress is under the yield stress of the material. Number of cycles is greater than 10^4
b) Low cycle fatigue: This type of fatigue is observed when the applied stress results in plastic deformation; in other words is greater than yield stress. Number of cycles is less than 10^4

2.6.2 Basic Mechanisms of Metal Fatigue

The fatigue process can be divided into three phases:
a) Phase 1: crack initiation;
b) Phase 2: crack growth;
c) Phase 3: final fracture.

The crack initiation usually takes place on the surface. In the microscopic scale this mechanism is explained by a slip band mechanism caused by the maximum shear stress. When the stress given to the material causes plastic deformation at some grains, some of the crystallographic planes slide. This situation is limited to a few grains and stops when the sliding crystallographic planes reach an unfavorable geometry with the direction of the maximum shear stress. When the stress is released the planes will not go back to their original positions and this will end with the distorted neighboring

planes. The final result of this mechanism is microscopic extrusions and intrusions on the metal surface. The schematic illustration is given in Figure 15.

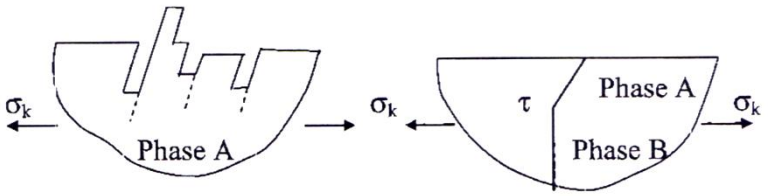

Figure 15 Sketch of various phases of fatigue process. Left: Phase A with shear stress driven intrusion/extrusions. Right: Phase a with transition to Phase B driven by normal stresses [22]

Once the crack is initiated it will extend to pass several grain boundaries. When the crack front passes over several grains, the crack will continue to grow in a direction perpendicular to the largest tensile principal stress. Figure 15 illustrates also the transition from microscopic scale to macroscopic scale of the crack growth. So it can be claimed that crack initiation is related with surface quality and shear stresses whereas crack growth is related with material bulk properties and affected by tensile stresses.

When the crack becomes too large that the remaining part of the material which is without crack can no longer carry the load, final fracture at phase 3 happens. So the local strains and stresses at the crack front cause a fast fracture. The fracture surface consists of two regions. First one is smooth in which the fatigue crack propagates. The second surface is rough because of the final brittle fracture. [22]

2.6.3 Factors Affecting Fatigue Life

2.6.3.1 External Loadings and Stresses in an Item

The external forces create normal, bending, torsion effects on a structural item and they cause stress situations close to potential cracks. The normal and bending loading mode will result in normal stresses that will be the main reasons for crack initiation and growth. These stresses are denoted as stress Mode I. If there are more than one stress axes, it is assumed that one of them will dominate. Shear stresses due to torsion may cause a different fatigue mechanism than Mode I, however this is a very rare mode.

Force or stress variation is considered to be factor that matters when compared to stress magnitude or time. Number of cycles is the other important factor. However the frequency of the cycling loading usually does not affect the fatigue life. [22]

2.6.3.2 Geometry, Stress and Strain Concentrations

Stresses and strains are created in structural items as responses to forces and loads. The localized stress response is important because due to geometrical discontinuities it can be quite high. Geometric factors change fatigue life a lot and it is an issue that can be corrected at design stage. The stress intensity factor K_t which is defined as local rise in the stress value due to geometrical discontinuities must be aimed to be reduced in areas that are susceptible to fatigue. Typical examples are threads, cope holes and welds. The value of the stress intensity factor of a notch can vary from 3 to 8. The stresses can be reduced by increasing the general dimensions of the item or improving the local

geometry of the notch. However increasing the size of the item would have a negative effect on the fatigue life as the surface area will increase and it will also increase the weight. The best way is to have a design that the notch geometry is optimized for fatigue durability.

Figure 16 shows two typical situations of localized stress is raised due to stress concentrations. On the left there is a plate having 2 notches symmetrically up and down. It can be seen that the stresses is high at the notched section due to reduced cross-section. Nevertheless the stress raise caused by the notch is far more important as it will result in fatigue damage. At the right side of the Figure 16 there is a butt weld. This time there is no reduction in the cross section but overfill of the weld will act as a notch. This area is called the weld toe. it can be characterized by its flank angle θ and radius ρ.

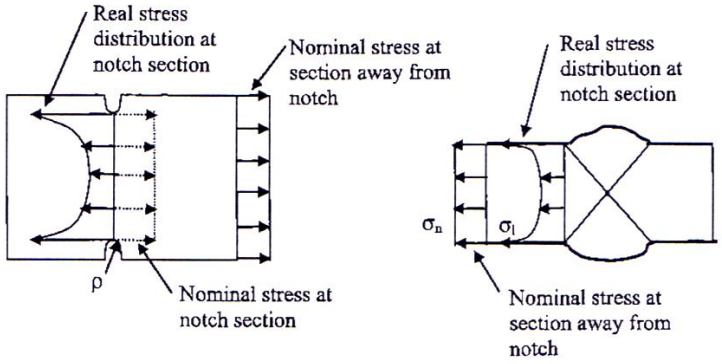

Figure 16 Stress concentrations at notches. Left: plate with edge notches. Right: butt joint [22]

Stress concentration factor is defined by the following formula

$$K_t = \frac{\sigma_l}{\sigma_n}$$

Where;
K_t is stress concentration factor,
σ_l is local stress and
σ_n is normal stress.

2.6.3.3 Material Parameters

Fatigue strength of the metal is influenced by other properties such as yield strength, tensile strength and elastic modulus. However further tests are done to characterize the metals' durability. These tests are usually done under an applied stress range. Most common method is to determine number of cycles before fracture under constant amplitude stress range. The key parameter here is the stress range but mean stress is also important (Figure 17).

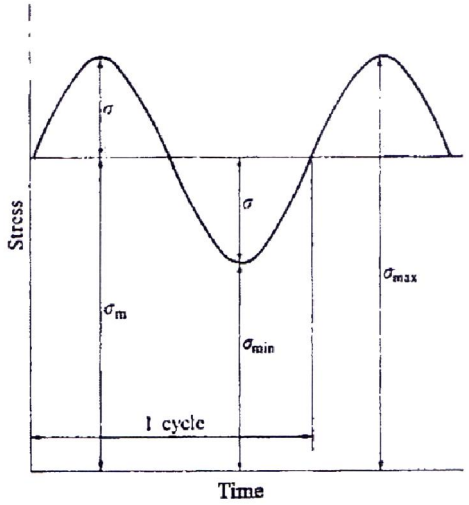

Figure 17 Notation for constant amplitude fatigue loading [19]

Following equation is the linear approximation of the upper part of the curve for a log-log scale.

$\log N = \log A - m log \Delta\sigma$

Where log A is the intercept of the curve with the vertical axis and -1/m is the slope of the curve.

Figure 18 and Figure 19 gives examples of S/N curves (Wöhler curves). As can be seen vertical axis is the applied stress and the horizontal line is the corresponding number of cycles before fracture.

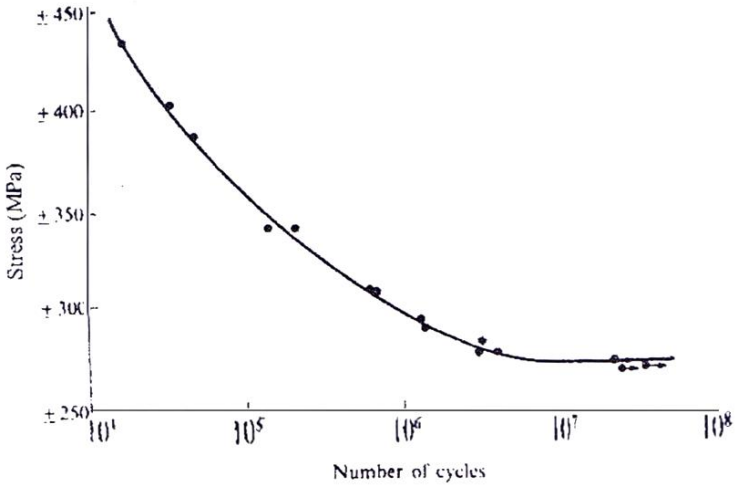

Figure 18 S/N curve for carbon steel specimens tested in rotating bending [25]

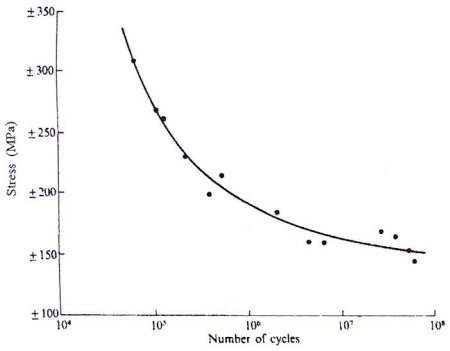

Figure 19 S/N curve for high strength aluminium alloy specimens tested in rotating bending [25]

Usually steels that have tensile strengths up to 700 MPa are not tested after $2x10^7$ cycles. If a specimen is not broken at 10^7 cycles this means that the stress level applied in the test is below the fatigue strength. Tests on other non-ferrous materials are continued up to 10^8 cycles. So fatigue strength can be defined as the maximum stress on the S/N diagram that the material is durable for infinite number of cycles.

Not all the materials' S/N curves become horizontal even the tests are continued to very long endurances. Failures can still occur at 10^9 cycles. This is called gigacycle fatigue and is first experienced by Shabalin in 1958 [23] A high strength 4.5% Cu aluminium alloy's S/N curve is shown in Figure 19. Fracture still occurs approaching to 10^8 cycles. In such cases fatigue strength of the materials is specified at a given endurance. The fatigue strength at this stipulated value is called endurance limit.

The fatigue strength mentioned above can be regarded as material property nevertheless it is best to keep in mind that the fatigue resistance of the material depends also on the size and geometry of the specimens and surface conditions.

2.6.3.4 Residual Stresses

Residual stresses are present whenever a welding is done. They can be defined asstatic inherent stresses present in the item before the external forces are applied. They are self equilibrated such as tensile stress zones are balanced by compressive stress zones. The tensile stress zones are vulnerable to fatigue. The affect of the residual stresses with a partly compressive external stress cycle is shown in Figure 20.

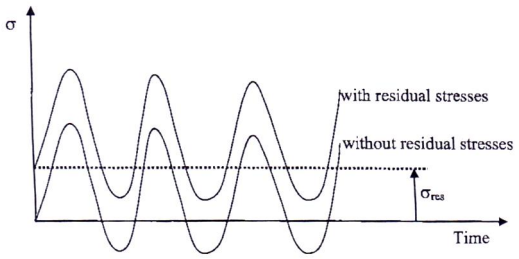

Figure 20 The effect of residual stresses in the stress cycles [22]

2.6.3.4 Fabrication Quality and Surface Finish

Surface roughness is another important factor that influences the fatigue life. Roughness on the surface is generally caused by the fabrication processes such as rolling, extrusion, forging etc. Welding is another process affecting surface quality.

It is also known that surface hardening processes have a positive effect on fatigue durability.

2.6.3.5 Influence of the Environment

Above discussions are all made thinking the normal air environment but things can be different other types of environments. Steel in seawater can be a good example. In this case corrosion and fatigue will enhance each other synergistically and fatigue life will be reduced by a factor of 3 to 5.

Load frequency becomes important as corrosion is a time dependent process. This creates a problem as the fatigue tests in the laboratory can't be accelerated in the same way for air environment.

2.6.3.6 Grain Size Effect

Decreasing the grain size increases the fatigue life. The reason for this can be explained by grain boundaries slowing the crack propagation. Alloying is also important for fatigue durability as grain size is reduced and dispersed particles are introduced, both of them slowing crack propagation rate.

2.6.4 Fatigue Durability of Welded Joints

The topics discussed above are of course also important for welded joints. However there are a few more things to say about fatigue durability of welded joints as they have some peculiar features.

Starting with Figure 21 which is comparing the S/N curve of a fillet weld to one smooth plate and one plate with a hole, it can easily be seen that the welded joint has a lower fatigue life.

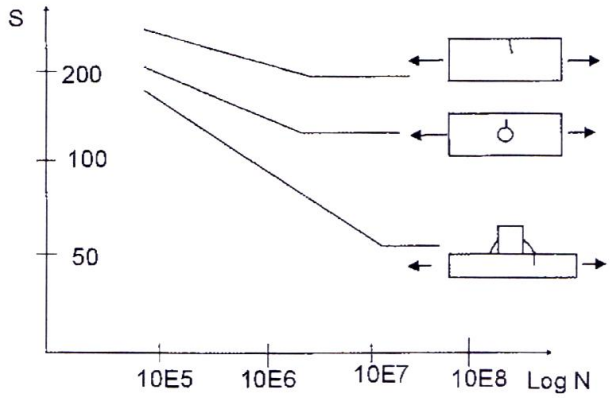

Figure 21 Fatigue life of curves for various details [26]

Looking at the crack positions in the Figure 21 plate's crack would be anywhere but it has to be in the longitudinal sides. The situation with the hole is different as the hole acts as stress raiser. Nevertheless the crack has to be again transverse to the applied load meaning that inner edges of the hole. In the case of the fillet joint weld toe acts as stress concentrators and the crack initiates at that point growing perpendicularly to the direction of the applied principal stress. These cracks are shown in Figure 21. Stages for crack development in the fillet welds are shown in Figure 22.

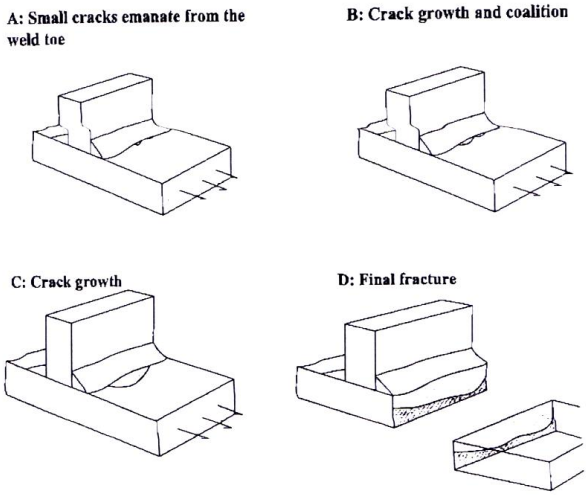

Figure 22 Various stages of crack growth in the fillet welded joint [22]

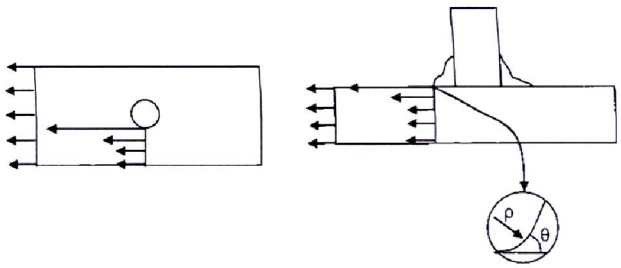

Figure 23 Notch effect at the edge of a bore hole and at the weld toe [22]

Cracks may initiate among several points along the weld seam. They grow and coalesce creating larger cracks. Finally when the uncracked part of the item becomes so small that it can't carry the load, fracture occurs.

The fatigue life of the welded specimen being shorter than the smooth plate is reasonable but it is interesting that the plate with a hole has a longer fatigue life than the welded specimen as the hole creates a stress concentration factor of 3. There are 3 main factors explaining this situation.

- Notch effect due to attachment and the filler material

- Non-metallic precipitates are created during welding
- Large tensile residual stresses are created during welding

The notch effect created by the fillet weld can be more severe if the weld has a steeper toe flank angle. Geometric effects on fatigue life of this fillet weld can be reduced by lowering the flank angle θ and increasing toe radius ρ. But it is better to keep in mind that these angles can change along the weld.

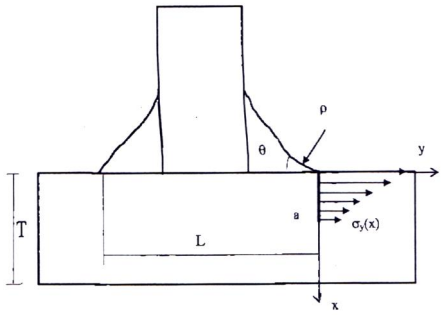

Figure 24 Definition of geometrical parameters of a fillet welded joint [22]

Weld toe is not only subjected to highest stress concentration, it has also the presence of the imperfections like intrusions. There is also the effect of the residual stresses. Consequently it becomes inevitable that the fatigue life is reduced.

The residual stresses are introduced into the material during cooling after the welding and they show up both as compression and tension zones along the weld. Figure 25 give a typical example of the residual stress distribution along a butt weld both transverse and parallel to the welding direction. The effective mean stress increases in the tensile stress zones. The welded joints are less sensitive to applied mean stress because the effective mean stress is not only the applied stress but the sum of it with the residual stress tensile stresses (Figure 20). But if post-weld heat treatment is applied this statement is not valid.

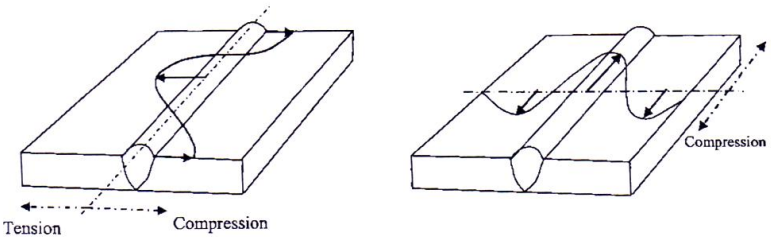

Figure 25 Left: Welding residual stresses transverse to the welding direction Right: welding residual stresses parallel to the welding direction [22]

Two different welds are shown in Figure 26. On the left side there is full penetration butt joint with axial loading perpendicular to the welding direction. This joint type is known for its high strength. On the right side there is again a fillet weld but this time it is subjected to bending type of loading. The main difference between these two welded joints is that the butt joint has to transfer the loading through the weld but in the fillet joint the main plate is regarded as non-load carrying. Besides the butt joint undergoes less geometrical changes whereas the fillet weld will have large geometrical disturbances. Hence, the stress concentration factor will be greater for the fillet joint. This is the main reason that the butt joint has higher fatigue life. Nevertheless both joints will have cracks initiated at the intersection of weld and the plate.

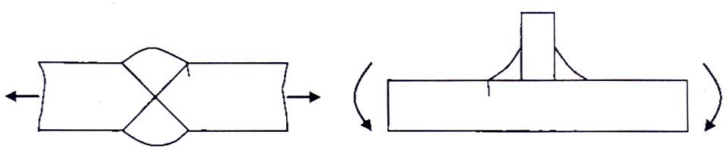

Figure 26 Comparison of two different types of welded joints [22]

CHAPTER 3

EXPERIMENTAL PROCEDURE

3.1 Materials Used

In the experiments 6xxx and 5xxx types of rolled aluminium alloys were joined together in fillet form by using gas metal arc welding process. 5xxx series of plate was type 5754 with 15 mm thickness. The 6xxx series of plate was 6063 in T6 state with 3 mm thickness.

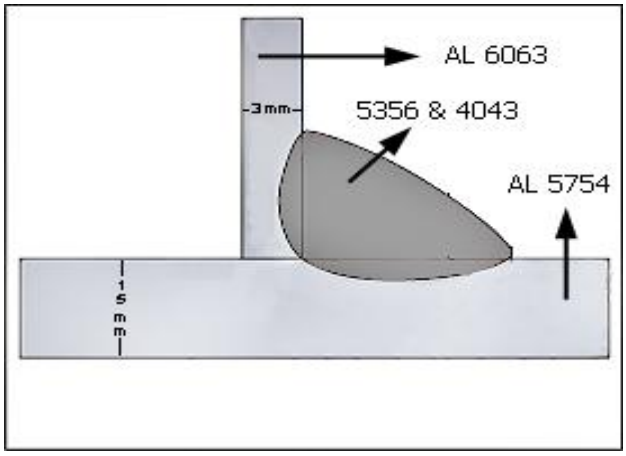

Figure 27 Schematic drawing of a typical fillet joint of this study

In Figure 27 used base materials and filler wire combinations are given. The chemical compositions of the alloys used in this study are given in Table 2.
The 5754 plates were previously hot rolled for strengthening. Magnesium is largely present in solid solution in wrought alloys. Mg_2Al_3 may precipitate in grain boundaries and in grains [28].
On the other hand 6063 plates are first solution treated and then aged artificially in T6 condition. Actually these alloys are designed to make use of solubility of Mg_2Si [28].
In the joining experiments of these two base metal alloys two different filler wires were used and the properties of the weld joints were compared. Used filler wires were Al 5356 and Al 4043. Their chemical compositions are given in Table 2.

Table 2 Chemical compositions of the used base and filler metals

		Chemical composition of the alloying elements (wt %)								Tensile Strength
Material Type	**Trade Name**	Cu	Fe	Si	Mg	Mn	Zn	Ti	Cr	
Base	6063	<0.1	0.35	0.2/0.6	0.4/0.9	<0.1	<0.1	<0.1	<0.1	214 MPa
	5754	<0.1	<0.4	<0.4	2.6/3.6	<0.5	<0.2	<0.1	<0.3	215 MPa
Filler	5356	0.1	0.4	0.25	4.5/5.5	0.1/2	0.1	0.2	.1/.2	
	4043	0.3	0.8	4.5/6.0	0.05	0.05	0.1	0.2	--	

3.2 Joining Experiments

Plates that were to be joined by Gas-Metal arc welding were prepared in size 100±1 mm x 50±1 mm. 15 mm thick AL 5754 plates were located in horizontal position and 3 mm or 5 mm thick 6063 plates were in vertical position. Plates were selected with different thicknesses in order to see the effect on welding.

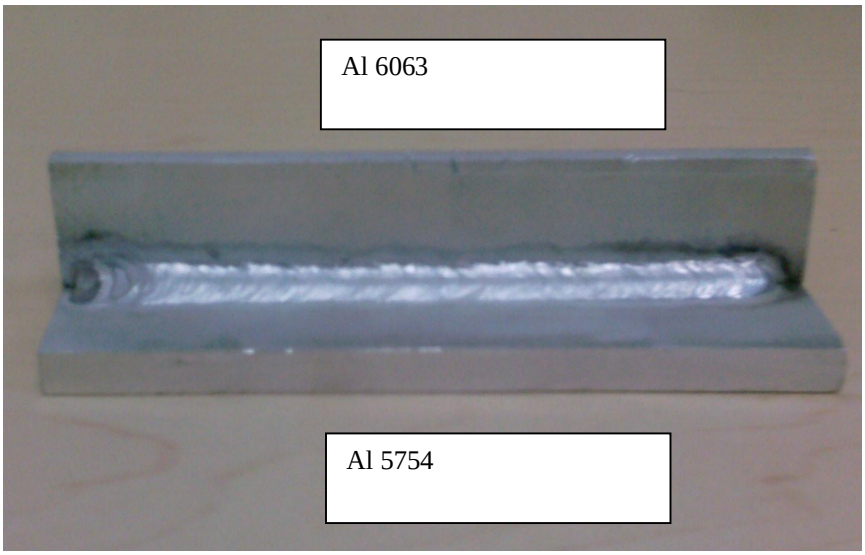

Figure 28 A welded sample

Before welding surface of the plates were ground to eliminate any oxide layer. Afterwards they were also cleaned chemically using acetone to eliminate any oil present on the surface. After this preparation, plates were welded with gas metal arc welding process in which the welding speed kept constant. Energy input given during welding of the specimens was calculated by using the formula given in equation 1. According to equation 1 heat input depends on voltage , current and welding speed. In this study welding speed was held constant and line energy was adjusted by changing the voltage and current values. Welding speed was selected according to the weldability limit through the flow behavior of the molten bath. The machine was adjusted for metal inert gas welding which uses

argon as the shielding gas. Experiments were initially performed with the Al 5754 filler wire; afterwards repeated with using Al 4043 filler.
In the initial experiments welding operation was performed manually. However, in order to achieve automation and consistent repetition of the results, main experiments were conducted by using the semi-automatic setup which contains an automated torch carrier (Figure 29). The whole welding equipment consists of welding power source and wire feeder (Figure 30), a welding torch and a torch carrier.

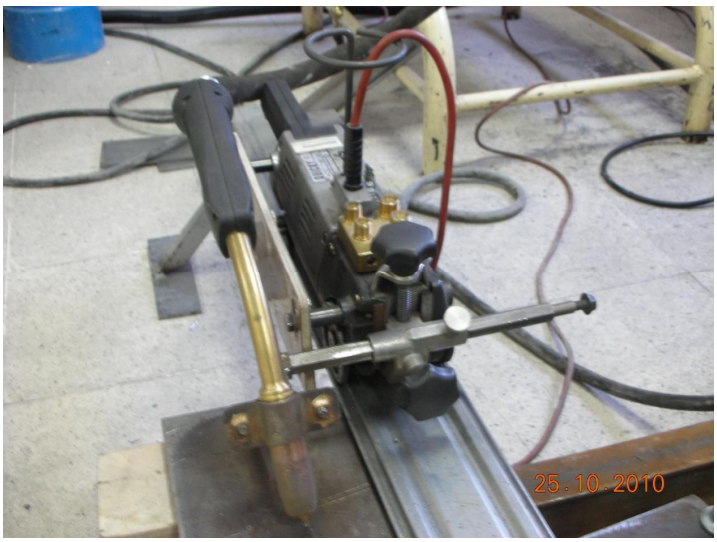

Figure 29 Torch carrier

Figure 30 Lincoln power wave 405m MIG welding machine

Lincoln power wave 405m MIG welding machine was used for welding the plates. Voltage value given by the machine can be trimmed to higher and lower values if needed. Welding current and voltage values can be read on the screen of the welding machine during the welding and average values are displayed when the welding period was finished.
Firstly Al 5356 filler wire was used to join the aluminium plates. Welding current and voltage values were changed between 150 A-18 V and 260A-26V.
Eight different line energies were chosen and applied to the welding experiments using both of the filler wires Al 5356 and Al 4043. These parameters cover a range which is wide enough to observe the whole weldability range. Line energy (Heat input) is calculated from equation 1 with 90% efficiency. Line energies and used parameters are given in Table 3.

$$Line\ Energy\ (kj/mm) = 0{,}9 \times \frac{\text{Volt(V)} \times \text{Current (amp)}}{Welding\ Speed\ \left(\frac{mm}{sec}\right)}$$

Equation 1

As can be seen from Table 3 heat input values were increased continuously. Then it was decided to change the filler wire to 4043 after specimen 8. The same parameters starting from highest to lowest values were applied with filler wire 4043. Experiments 16-17-18 were performed using a torch carrier whereas the experiments 1 to 15 were carried out manually.

Table 3 Used weld parameters and calculated heat inputs

Specimen Group#	WFS (m/min)	trim	GFR (lt/min)	WLS (mm/s)	I (A)	V (V)	E (kJ/cm)
1	9	0,95	16	9,5	152	18	26
2	9,52	1	16	9,5	165	20	31
3	9,65	1,04	16	9,5	183	21	36
4	10,31	1,1	16	9,5	191	23,2	42
5	10,51	1,17	16	9,5	200	24,5	46
6	11,05	1,16	16	9,5	210	24	48
7	11,2	1,11	16	9,5	225	24,5	52
8	12,01	1,15	16	9,5	260	26	64
9	12,01	1,15	16	9,5	260	26	64
10	11,2	1,11	16	9,5	223	24,5	52
11	11,05	1,16	16	9,5	215	25	51
12	10,51	1,17	16	9,5	201	24,5	47
13	10,31	1,1	16	9,5	192	24,2	44
14	9,65	1,04	16	9,5	183	21	36
15	9,52	1	16	9,5	175	20	33
16	10	1,09	16	8,55	215	21	48
17	9,49	1,05	16	8,55	185	20	39
18	9,49	1,05	16	8,55	185	20	39

Torch angles were chosen as shown in Figure 31 in all welding experiments. It can be seen that the torch was mainly inclined towards the thick plate in order to not melt the thin plate completely. It can also be seen that the welding experiments were performed in the "pushing torch" position.

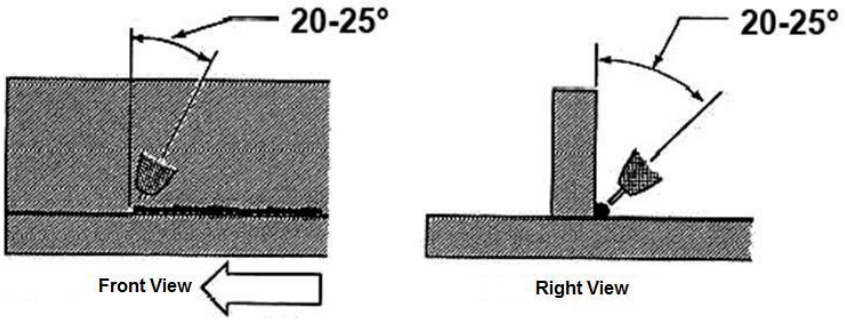

Figure 31 Used welding angles

In all of the welding experiments of this study argon was used to create protective atmosphere and gas flow rate was held constant at 16 lt/min. Also the welding speed was held constant at two levels.
Welding speed was held constant both in the welds performed by manually and by the torch carrier automatically.
After the welds were finished completely they were all cut at the third centimeter from the starting point of the weld seam. All the welds were cut at the same position because characteristics of a weld changes through the starting and the end points. The cutting process was performed vertical to the welding direction and a 2 cm wide cross sections were cut which was considered to be enough for metallographic preparation.
For macro and micro-examinations the sections obtained from welded specimens were ground with emery papers from numbers 120 to 320, 500, 800 and 1000.
At this stage, before micro-examination macro-examination was conducted. Cross sections of welds were etched with Flick's solution. Prepared specimens were examined by naked eye and stereo-microscope in order to observe the weld penetration and quality. The macro sections of the specimens were photographed for the further dimensional measurements.
Afterwards, the specimens were subjected to polishing initially with 6 micron and then 1 micron sized diamond paste containing polishing disc. Finally the specimens were etched with Keller's etching solution. Weld zones were examined under light-microscope to investigate the microstructure and presence of any cracks.
Keller's etchant includes:

- 2 ml of HF
- 3 ml HCl
- 5 ml HNO_3
- 190 ml water

Flick's etchant includes:

- 10 ml of HF
- 15 ml of HCl
- 90 ml of water

3.3 SEM Examinations

SEM examinations were carried out at SEM Laboratory of Department of Metallurgical and Materials Engineering at METU and Anadolu University.
Both the welded samples and welded-fatigue fractured samples were prepared and examined. Welded samples were 4043 filler wire used specimens. Welded and dynamically tested specimens were welded using 4043 filler wire. Fracture surface, heat affected zones, grain boundaries, crack propagation paths and crack initiation locations of these specimens were examined. EDX analyses were also performed on these locations to see if there were any segregated precipitates favoring crack initiation and propagation.

3.4 Hardness Tests

Hardness tests were performed on the cross-section of the specimens by Vickers Hardness Test under 5 kg of load (HV5).

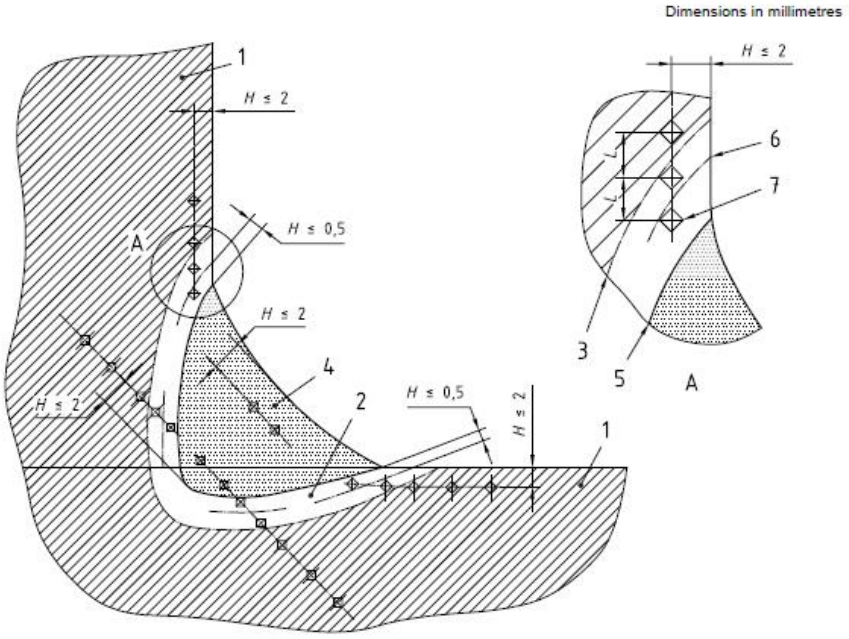

Key

1 Parent metal
2 Heat affected zone
3 Limit of HAZ
4 Weld metal
5 Fusion line
6 Limit for indentations parallel to fusion line
7 First indentation

Figure 32 Locations of indentations in fillet welds [27]

Figure 32 shows the points at which hardness tests were made. Measurements were taken from the 2 mm below the outer surface and at the root of the section as shown in Figure 32. Two specimens were tested. The aim was to make a comparison between joining experiments that were conducted using the different filler wires. Specimen #7 for filler wire 5356 and specimen #18 for filler wire 4043 were selected for the hardness tests.

3.5 Tensile Tests

The aim of tensile tests was to compare the strength of the joints welded by two different filler wires. Specimens were prepared in butt weld form using the parameters considered as an optimum that is shown in Table 4 and tested according to the European Standard EN 895.

Table 4 Weld parameters used for tensile test specimen preparation

WFS (m/min)	Trim	GFR (lt/min)	WLS (mm/s)	I (A)	V (V)	E (kJ/mm)
9,60	1,05	16	10,75	185	21	0,33

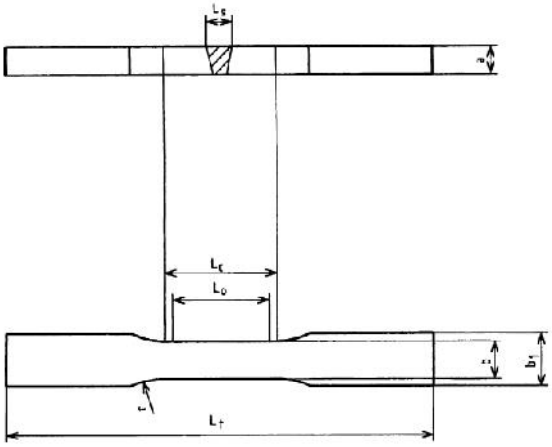

Figure 33 Tensile test specimen [31]

Table 5 Tensile test specimen dimensions [31]

Denomination	Symbols	Dimensions (mm)
Total Length	L_t	To suit test machine
Width of Shoulder	b_1	b + 12
Width of Calibrated Parallel Length	b	25 for a>2
Parallel Length	L_c	$>L_s + 60$
Radius at Shoulder	r	>25

3.6 Specimen Preparation for the Dynamic Loading Test

The aluminium fillet weld that is to be tested must be in certain sizes to fit in the machine. The sizes were given as millimeters as shown in Figure 34.

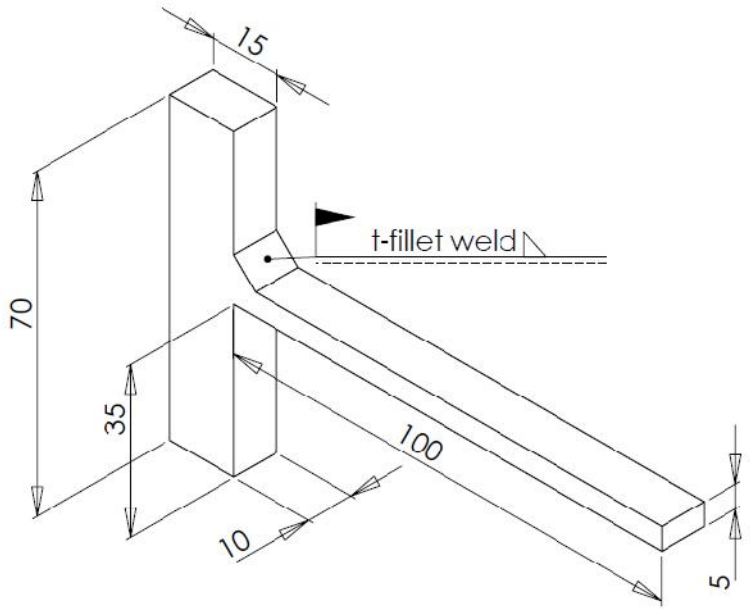

Figure 34 Isometric drawing of a dynamic loading specimen (All dimensions are in millimeters)

For dynamic loading tests another group of welded joints were used. The aluminium plates which were cut in selected sizes were joined by using again the gas-metal arc welding method. The used weld parameters are given in Table 6.

Table 6 Weld parameters used for dynamic loading test specimen preparation

Specimen Group#	WFS (m/min)	Trim	GFR (lt/min)	WLS (mm/s)	I (A)	V (V)	E (kJ/cm)
1	10,00	1,05	16	8,55	210	21	46
2	9,60	1,05	16	10,75	185	21	33

After the welds were completed they were cut into pieces such as that one specimen has 1±0.1 cm width. The starting and finishing points of the welds were removed. From one weld joint three such specimens were obtained. (Figure 35)

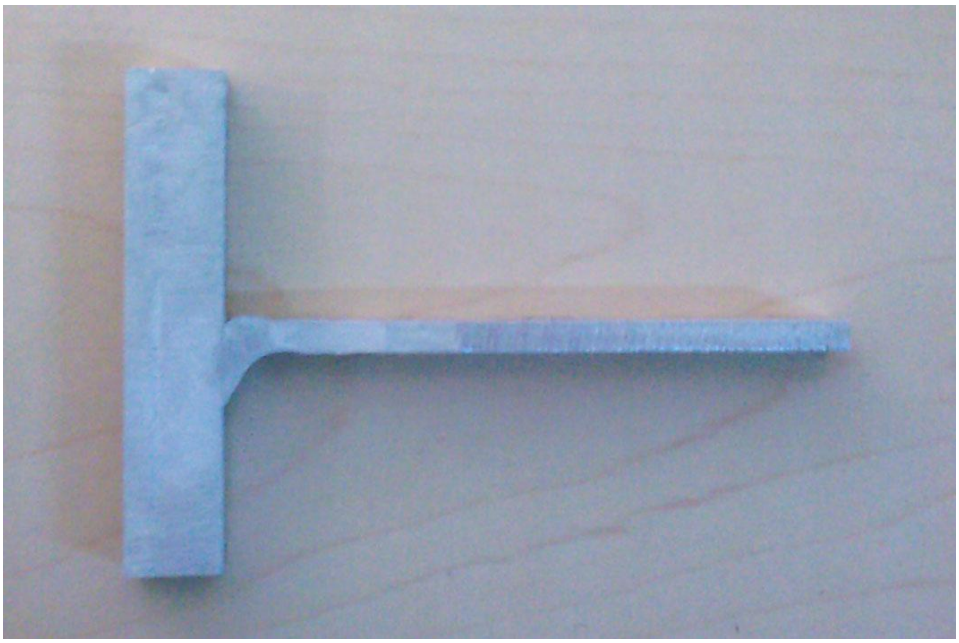

Figure 35 Example specimen for dynamic loading tests

Before starting the test, all of the specimens were subjected into macro examination to control if there is any weld defect. Great care was taken for specimens that were welded with the same specimen group to be identical with each other. Cross sections of welds were ground and etched with Flick's solution. Prepared specimens were examined by naked eye in order to see the weld quality.

3.7 Design and Manufacturing of the Dynamic Loading Machine

To estimate the service life of the fillet weld under real life conditions it was thought essential to design and build a machine which can make a successful simulation. A CAD program (Solidworks) was used for the technical drawings of the machine (Figure 37). Detailed drawings of the machine and its parts are given in appendix.

Figure 36 Dynamic Loading Machine

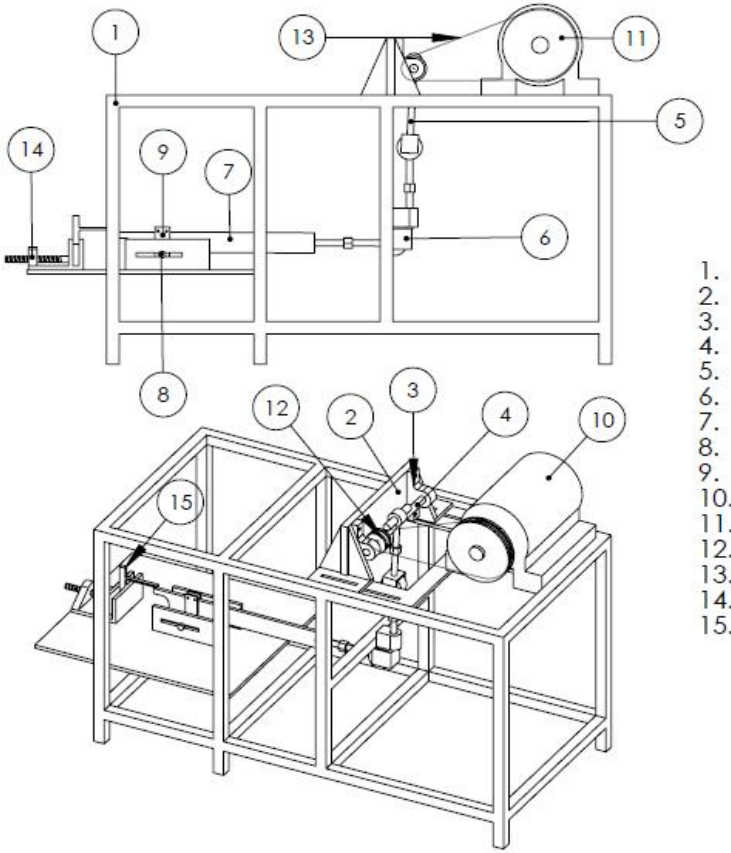

1. Main Frame
2. Supporting Wall
3. Bearing
4. Shaft
5. First Transmission Rod
6. Second Transmission Rod
7. Lever Arm
8. Stroke Control & Support of Lever Arm
9. Lever Arm Holder
10. Engine
11. Engine Pulley
12. Shaft Pulley
13. Belt
14. Bench Clamp
15. Specimen

Figure 37 Drawing of the Dynamic Loading Machine

The main frame of the machine was built from steel profiles which would have enough strength for carrying the engine and other parts. An electrical engine was used which has a control unit that can adjust the number of rotations per minute. The engine was capable of rotating 120 times in a minute which was thought not enough for the planned test. So it was tried to increase the number of rotations per minute by using two pulleys and a belt. The ratio of the diameters of the wheels was 3 so the machine can hit the specimen 360 times in a minute. The smaller wheel was attached to a shaft which was aimed to be working like the crank shafts of the internal combustion engines. Cranks convert rotary motion into a piston-like linear motion. Two bearings which carry the shaft are fixed through a supporting wall of steel which can move in the direction of the belt. The aim here was to stretch the belt for efficient transmission of the work between wheels. (Figure 38)

The universal joints (Figure 39) under the shaft and the shaft itself together convert rotary motion created by the electrical engine to linear motion which was wanted.

Figure 38 Engine, Pulleys and Shaft

Figure 39 Second transmission rod and universal joints

A pipe attached to a steel profile of the main frame is guiding the rod between two universal joints to obtain a motion perfectly in one direction. To avoid friction, grease oil was used inside this pipe. Usually welding was selected as the joining method in the construction of the machine. Examples are guide pipe and main frame, main frame parts etc…

It was decided to use a sheet bar (Figure 40) for the unit that is supposed to be the lever arm and hit the specimen. The reason for that is moment of inertia of the sheet bar in the direction that it hits the specimen was very high.

It can be seen that this sheet bar was used as a lever. The force coming from the engine was transmitted through this lever to the specimen. Here the place of the support point was adjustable. The aim of this design was very important. Amount of the strain which is created on the specimen during the test couldn't be changed if support point was fixed. Two metal plates were used to manufacture this structure (Figure 40). Milling grooves opened and a rod was placed between these plates which were welded parallel to each other. If this rod was moved through the specimen, the amount of the strain created in the specimen would decrease. If it was moved in opposite direction, the amount of the strain would increase.

In the middle of the rod again two small parallel plates were used to hold the lever arm. Lever arm passes between them. These two plates were connected by two screws at the top and at the bottom the lever arm supporting rod passes into them (Figure 40).

Figure 40 Lever arm, Stroke control and support of lever arm, Bench clamp

The lever was designed in such a purpose to increase the force created by the engine. That's why the distance between the end of the sheet bar which takes the force from the engine and the support point is much higher than the distance between the end of the vertical plate that hits the specimen and support point.

The aim of this design is to eliminate the problems that could occur because of force coming from the engine could be insufficient to deform the fillet weld. The specimen was hold by a bench clamp which was fixed very strongly to the main frame. (Figure 41)

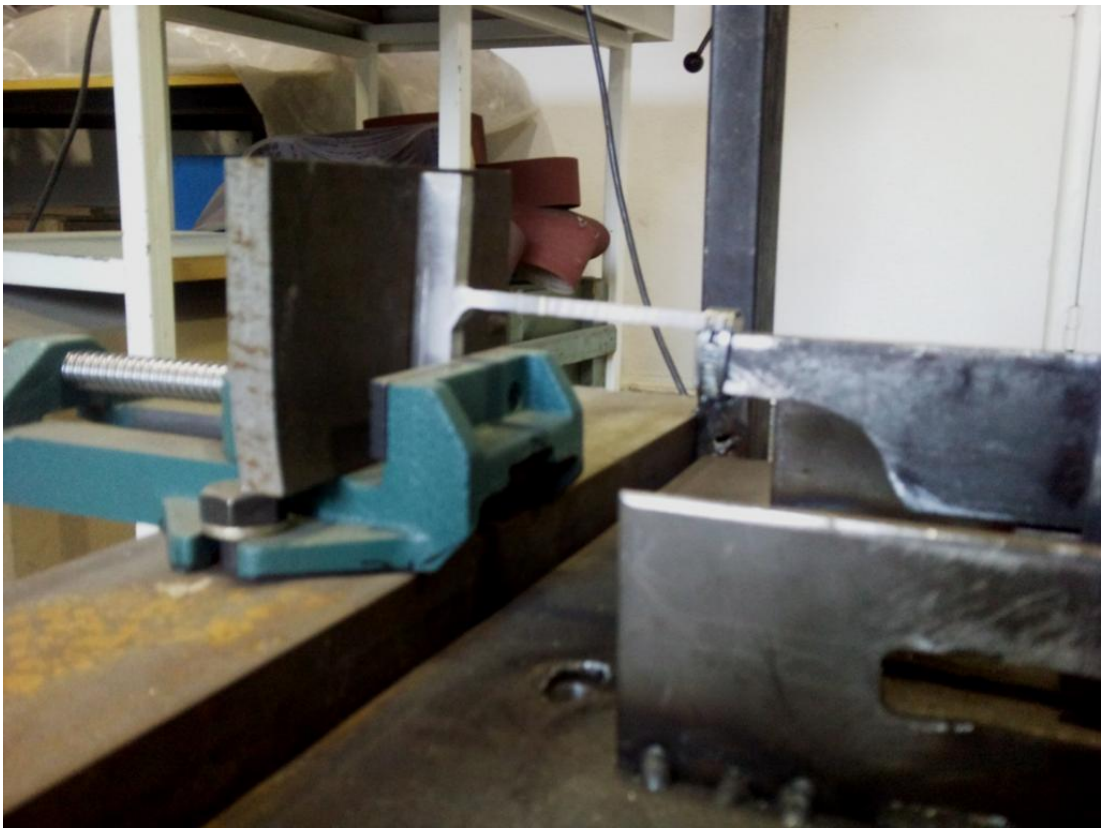

Figure 41 Bench clamp, Specimen

In Figure 41 it is seen that a thick plate was placed behind the aluminium fillet joint. The reason for this was to eliminate the bending of the vertical aluminium plate which was not hit by the lever arm.

3.8 Dynamic Loading Tests

The aim of the test series was to be able to make a comparison between weld parameters. The amount of the load or the amount of the elongation was not measured. Specimens that were prepared with different weld parameters were compared by their number of cycles before fracture.

Great care was taken to prepare the specimens uniformly. The only thing that differs from specimen to specimen was weld parameters and after all, these tests were done to compare weld parameters.

Figure 42 illustrates the load direction given to the specimen by the dynamic loading machine.

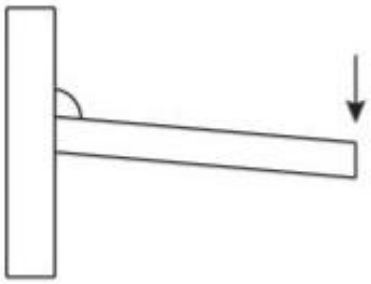

Figure 42 Loading direction on the specimen

The aim was to see the effect of stress concentration at the toe. It was expected that the resulted number of cycles would give ideas about the crack propagation rates at the partially melted zone between weld metal and Al 6063 base metal side heat affected zone. Cycle number before fracture was calculated according to the elapsed time and the rotational speed of the electrical motor.

CHAPTER 4

RESULTS AND DISCUSSIONS

In this study firstly weldability of two types of aluminium alloys with different thicknesses using MIG welding and properties of the weld joint were examined. In the second part a dynamic loading machine was designed and constructed. Tests were performed by using this developed machine. Using this machine fracture surfaces were obtained and examined under SEM microscope.

4.1 Weld Penetration Results and Discussions

Experiments were designed to examine the weldability of 6063 and 5754 alloys. Different parameters were tried to achive a successful weld which means;

- Suitable penetration especially on the corner and on both base metals
- No discontinuities such as crack on weld metal or on the HAZ
- Smooth hardness distribution

Initial experiments were performed using the filler wire type 5356. In these experiments welding speed was held constant at 9,5 mm/sec.

Table 7 Weld parameters of specimens 1-8

Specimen	WFS	TRIM	GFR (lt/min)	WLS (mm/s)	I (A)	V (V)	E
1	9	0,95	16	9,5	152	18	0,26
2	9,52	1,00	16	9,5	165	20	0,31
3	9,65	1,04	16	9,5	183	21	0,36
4	10,31	1,10	16	9,5	191	23,2	0,42
5	10,51	1,17	16	9,5	200	24,5	0,46
6	11,05	1,16	16	9,5	210	24	0,48
7	11,2	1,11	16	9,5	225	24,5	0,52
8	12,01	1,15	16	9,5	260	26	0,64

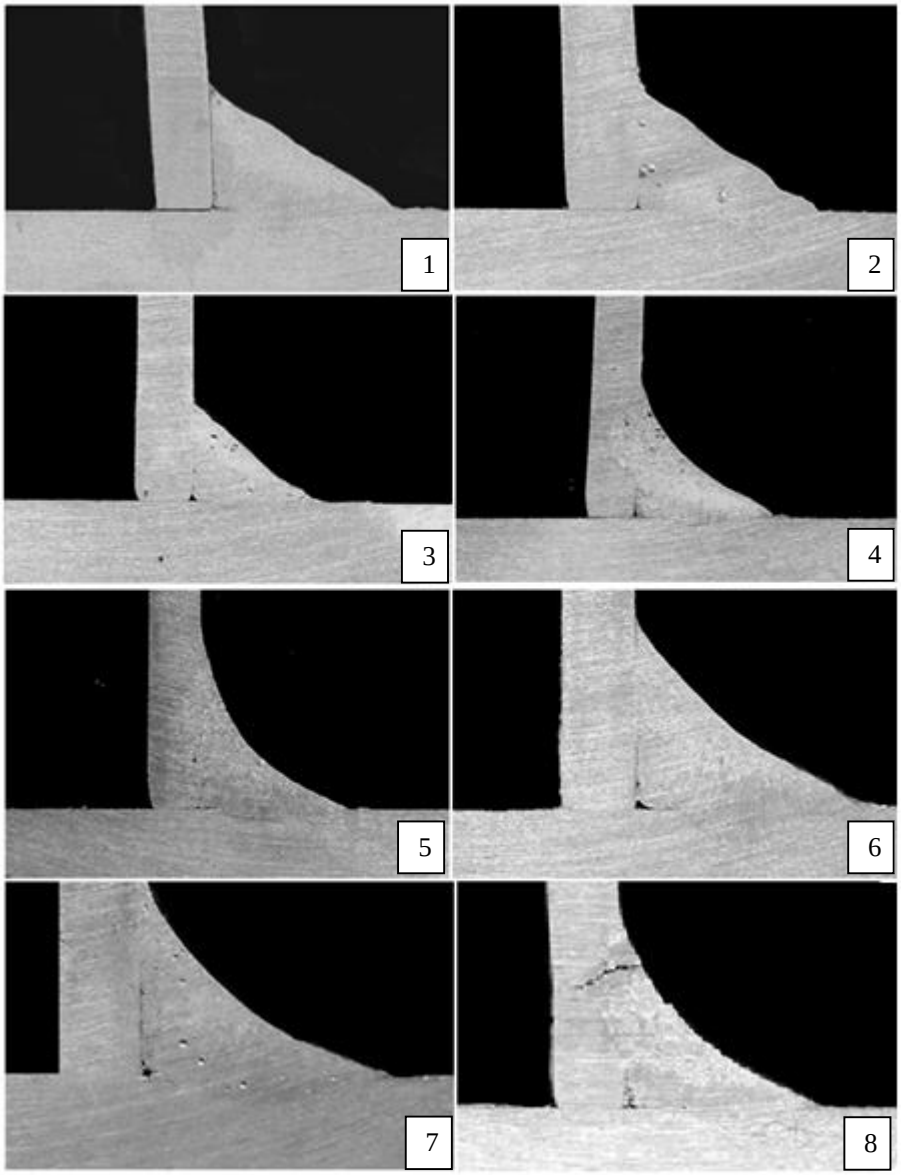

Figure 43 Macro-graph of the specimen #1-8, Etchant: Flick's Solution, Magnification: 2X-3X

Figure 43 shows the macro-graphs of welded fillet joints. The specimens were all etched with Flick's solution and the images were magnified by three times. In the macro-graphs of the weld cross-sections that were welded with higher heat inputs, hydrogen porosity was observed. The main reason of this porosity was thought to be due to the larger weld pools and as a result higher amount of gases dissolved in the pool. Due to the relatively higher solidification rate dissolved gases which contain mainly hydrogen could not have enough time to dissolve out; leading to the entrapped gas holes in the weld metal. Celina Leal Mendes da Silva et. Al. in their study [24] explains the effect of pulse welding on reducing hydrogen porosity on welding of Aluminium alloys. They also indicate that double pulse welding gives better results on reducing porosity. In this study only the pulsed gas metal

arc welding was applied. Since the trials with the double pulsed gas-metal arc welding did not show enough weld penetration, it was not possible to use this variation of the method. Indeed single pulsed GMAW was thought to be sufficient to reduce porosity up to some level. Devletian and Wood [4] in their review clearly states that porosity problem in aluminium welding is very much related in bead chemical composition. Considering all these literature remarks about hydrogen porosity in aluminium, using pulsed gas-metal arc welding and careful cleaning of the plates and filler wires before welding was thought to be sufficient for the reduction in the entrapped gases in the weld pool.

Since this study aims to have successful joints without pre-heating, Figure 43 which show the macro-graphs of welded specimens having 5356 filler wire, indicate "incomplete penetration" defect in common at the corner. Starting from specimen 1; lack of fusion was observed at the vertical wall along with incomplete penetration. The applied energy parameters were thought to be low. Torch angle was also thought to be high and needed an adjustment. The joint in specimen 2 was welded with higher energy parameters but still incomplete penetration was observed. Lack of fusion problem on the vertical wall was solved. In order to overcome the incomplete penetration problem at the corner, heat input was increased step by step by giving higher current and higher voltage holding the weld speed constant. Incomplete penetration at the corner was thought to be a major problem in this study. The corner of the fillet weld would effect as notches and this would result in tremendous decrease in fatigue life. The effect of stress concentrators were widely discussed in Chapter 2 "Theory".

Specimens 3-8 show that although the current and voltage were increased to ultimate values for the given thickness range sufficient penetration could not be obtained. In specimen 8 hot cracking was observed. The reason for the hot cracking was thought to be excessive heat input and therefore lower solidification rate against the thermal stresses. The heat input could not be increased anymore to solve insufficient penetration problem because it was already too high that hot cracking occurred due to excessive heat input. In this situation changing the filler wire could be a solution because some filler wires especially the ones with high Si content are known to be more penetrative. The reason could be understood by examining the phase diagrams of the filler wires. Liquidus and solidus temperatures for Al 5356 alloy are 638^{o}C and 574^{o}C respectively. For 4043 alloy liquidus and solidus temperatures are 630^{o}C and 575^{o}C [28]. There is only a slight difference between these temperature intervals. At this point, it would be interesting to examine the Al-Si phase diagram. Al-Si alloy goes into eutectic reaction at 575^{o}C whereas Al-Mg does not. This means that 4043 filler wire has most probably very high amount of liquid phase at 1^{o}C above eutectic temperature although 5356 has 99% solid. Between solidus and liquidus temperatures 4043 has always far more liquid phase than 5356 and that's why it wets and flows better resulting in more penetration.

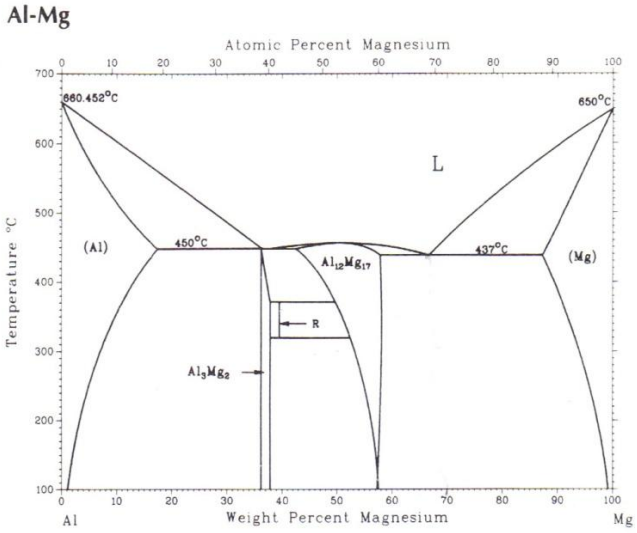

Figure 44 Al-Mg Phase Diagram [28]

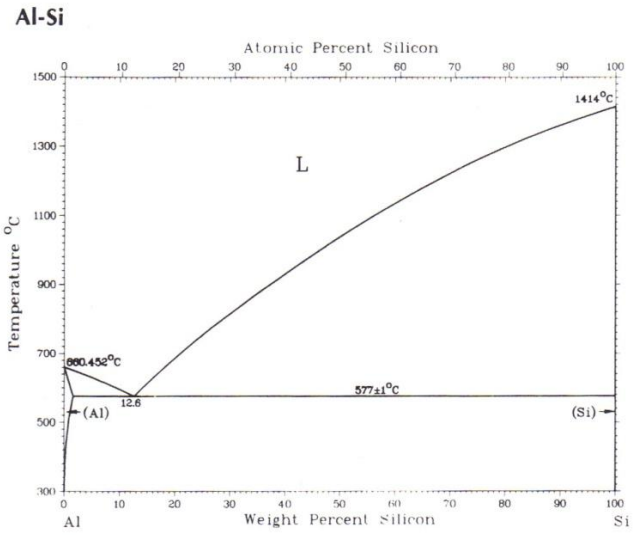

Figure 45 Al-Si Phase Diagram [28]

One of the reasons for the hot cracking is filler composition and dilution [1]. Kerr at al. [33] and Miyazaki et al. [34] in their study with a similar composition aluminium alloy (Al 6061) hot cracking was found to depend on weld-metal compositon. Al 4043 filler wire resulted with no hot cracking wheras with Al 5356 filler wire longitudinal hot cracks occurred in a study by Rao et al [2]. Tirkes S. [35] also stated in his study that hot cracking susceptibility is dependent on the Mg amount in Al- Mg alloys.

Considering all of these reasons it was decided to change the filler wire to 4043. The chemical composition of this filler wire is given in Table 2. New welding experiments were performed starting from the last and the highest parameters. Figure 46 show the macro-graphs of the weld joints which were produced using the filler wire Al 4043.

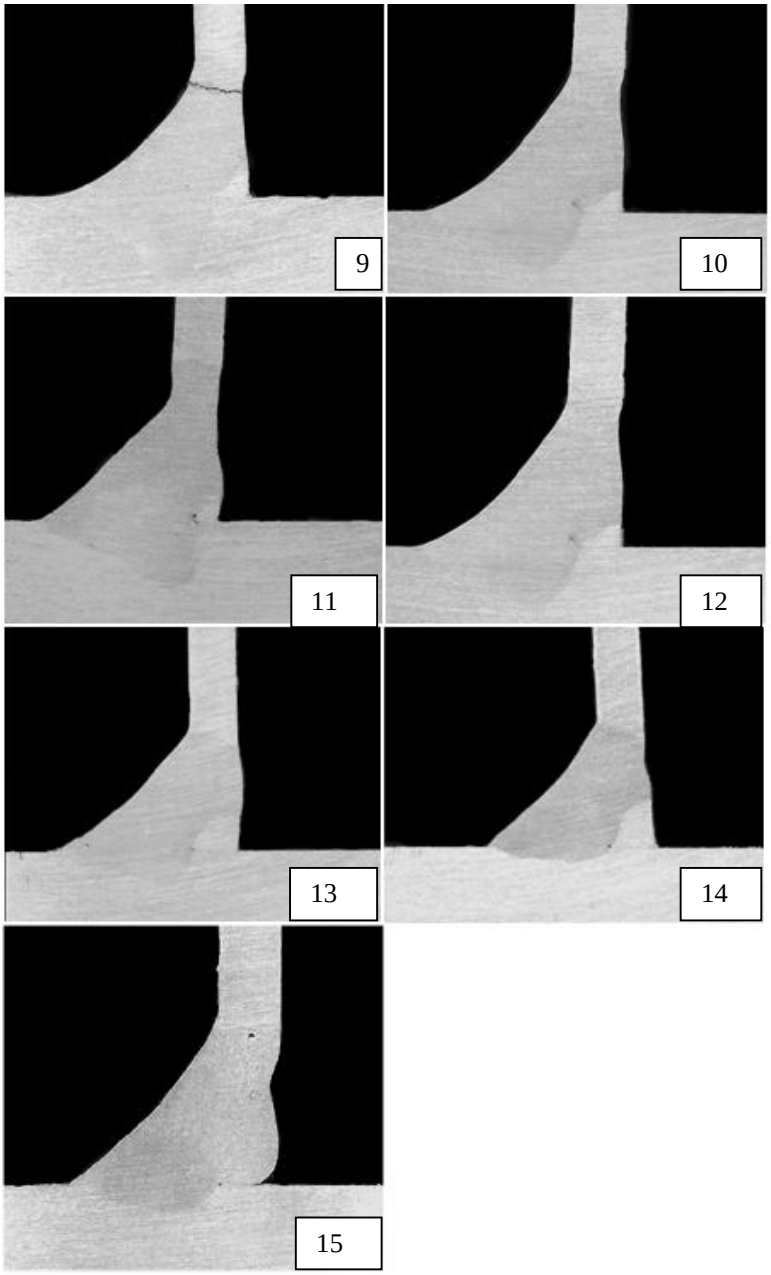

Figure 46 Macro-graph of the specimen #9-15, Etchant: Flick's Solution, Magnification: 2X-3X

Table 8 Weld parameters of specimens 9-15

Specimen	WFS	TRIM	GFR (lt/min)	WLS (mm/s)	I (A)	V (V)	H
9	12,01	1,15	16	9,5	260	26	0,64
10	11,2	1,11	16	9,5	223	24,5	0,52
11	11,05	1,16	16	9,5	215	25	0,51
12	10,51	1,17	16	9,5	201	24,5	0,47
13	10,31	1,1	16	9,5	192	24,2	0,44
14	9,65	1,04	16	9,5	183	21	0,36
15	9,52	1	16	9,5	175	20	0,33

Figure 46 shows the macro-graphs of welded fillet joints. Specimen 9 shows the cross-section taken perpendicular to direction of the welding which was done under 260 Amperes of current and 26 Volts. This parameter caused hot cracking with filler wire 5356 and it caused hot cracking with filler wire 4043 too. There is of course one major difference. With filler wire 5356 along with having hot crack, incomplete penetration was observed. However in the welding experiment in which the filler wire 4043 was used resulted in quite enough penetration. Further experiments were performed for reducing the hot cracking tendency by decreasing the heat input and keeping the sufficient penetration result.

From specimen 10 to 15, heat input was decreased step by step. Hot crack formation was avoided due to the decreased heat input. However, further experiments were performed to find out optimum parameters. Provided that, besides having sufficient penetration, the penetration depth in the thin section should not exceed the thickness of the thin material.

To obtain reproducibility in the seam character and fix the welding angle, further experiments were performed semi-automatically using a torch carrier. The aim of using the torch carrier and paying more attention to the torch angle was to prevent the weld region to cover the entire thin wall (vertical plate).

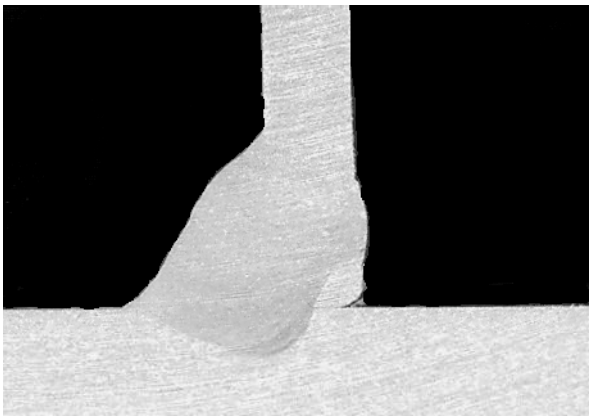

Figure 47 Macro-graph of the specimen #16, Etchant: Flick's Solution, Magnification: 4X

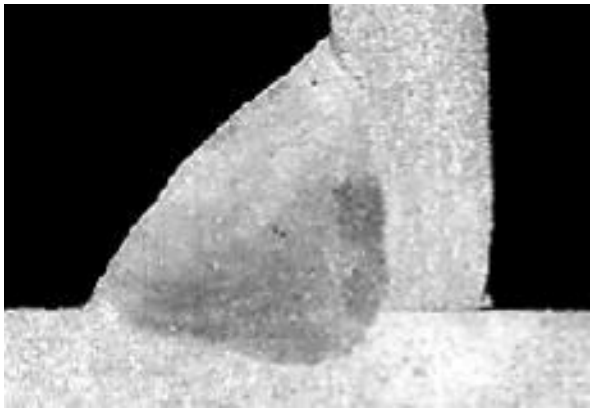

WFS: 9,49 m/min
Trim: 1,05
Current: 180 Amps
Voltage: 20Volts

Figure 48 Macro-graph of the specimen #17, Etchant: Flick's Solution, Magnification: 8X

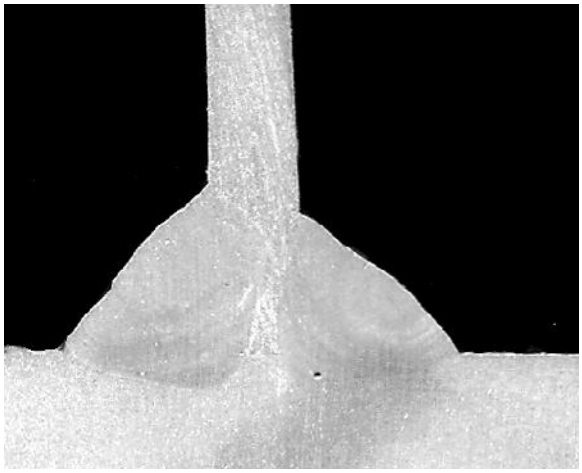

WFS: 9,49 m/min
Trim: 1,05
Current: 182 Amps
Voltage: 21 Volts

Figure 49 Macro-graph of the specimen #18, Etchant: Flick's Solution, Magnification: 4X

Specimen 16 in Figure 47 was considered to be in the range of a successful joint. Decreasing the parameters resulted in finding the optimum parameters precisely at specimen 17 (Figure 48). In order to achieve equivalent penetration on both of the legs welding angle was increased to have a more vertical torch angle (Figure 31). Result was successful and acceptable as there was no incomplete penetration, no lack of fusion and no excessive porosity.

The specimen at Figure 49 was double side welded semi automatically in other words with the help of the torch carrier and with optimum parameters. The result was again successful having very good penetration with no weld defects were observed on macro examination.

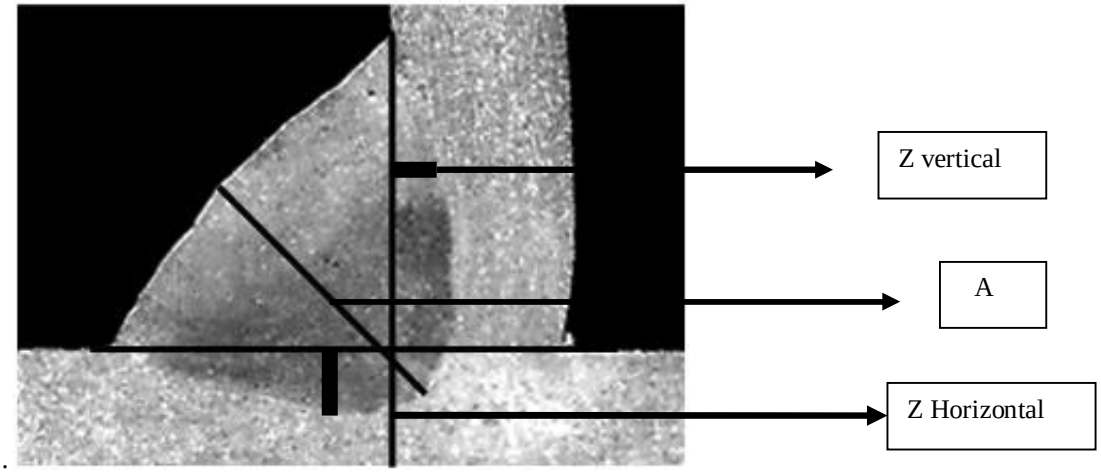

Figure 50 Illustration of A, Z Vertical and Z Horizontal values

Above figure explains the three important lengths that were measured to compare the penetration of joints. A value is the penetration from the corner of the joint. Z vertical is the penetration to the vertical wall and finally Z horizontal is the penetration to the horizontal aluminium plate. All these lengths are measured from specimen #1 to specimen #18. Results above make possible to examine vertical and horizontal penetrations separately.

Table 9 A, Z horizontal, Z vertical Values

Specimen #	A (mm)	Z Horizontal(mm)	Z Vertical(mm)
1	4,1	0	0,5
2	4,0	0,8	1,0
3	4,0	0,7	1,1
4	4,9	0,5	1,5
5	4,5	1,0	1,5
6	5,1	0,5	0,5
7	4,0	0,6	0
8	4,7	0,5	1,3
9	4,4	5,1	3,0
10	4,9	3,9	3,0
11	5,2	3,1	3,0
12	4,8	3,0	3,0
13	5,0	1,9	3,0
14	5,3	1,0	3,0
15	4,6	1,5	3,0
16	3,9	1,5	3,0
17	4,3	1,1	0,8
18	4,1(left) 4,1(right)	1,2(left) 1,3(right)	2,1(left) 0,8(right)

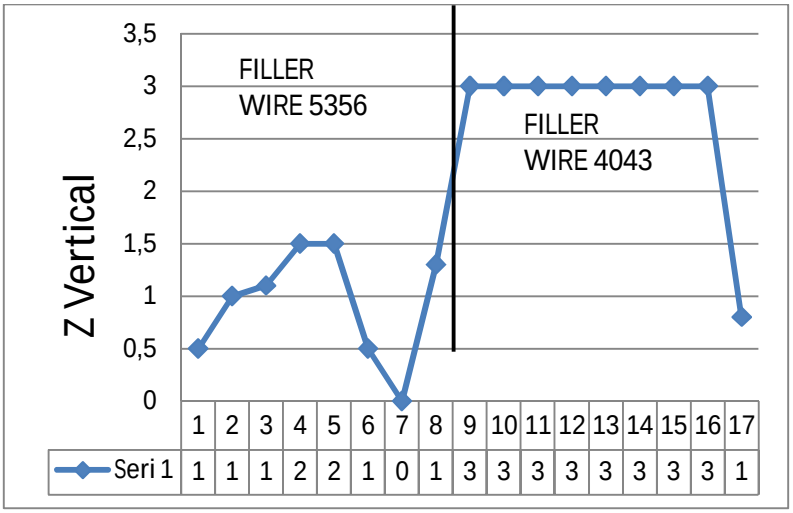

Figure 51 Z vertical values vs specimen plot

Penetrations values in the joining experiments in which the filler wire 5356 used were found to be inadequate. However the problem with the filler wire 4043 was the too deep penetration which caused to melt the vertical wall thickness completely. Optimum parameters were obtained in specimen #17.

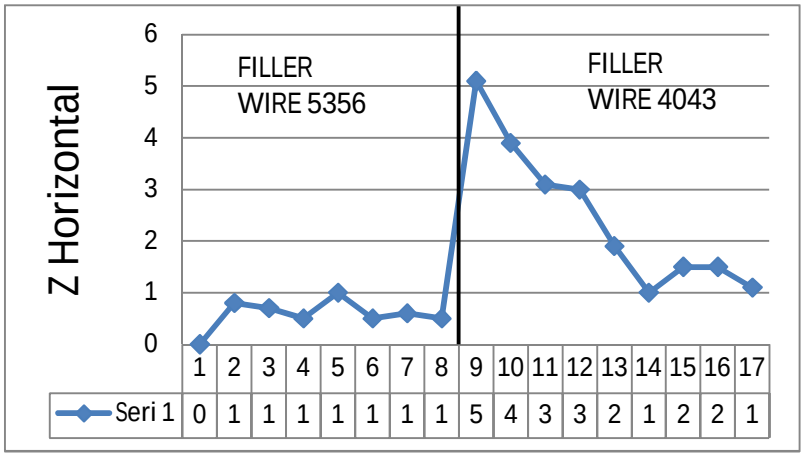

Figure 52 Z Horizontal values vs specimen plot

Considering the horizontal wall penetration, results were again too low for the 5356 filler wire. 4043 filler wire resulted in higher penetration and weld parameters were decreased to optimize it.

The cooling rate increases with the thickness of the workpiece because the thicker workpiece finds larger area to conduct heat to surroundings.

The penetration values at the vertical thin wall to be higher than the penetration results at the horizontal thick wall especially in 4043 used experiments can be explained with this phenomenon. Kihara et al. [29] also mentioned this effect in their studies. Inagaki and Sekiguchi [30] showed that, under the same parameters cooling time is shorter for the fillet welds than other types of welds because of greater heat sink effect.

These literature reviews explain the situation in this study that although the vertical wall thickness is melted completely there can still be insufficient penetration in the horizontal thick plate.

4.2 Tensile Tests

The aim of the tensile tests was to compare the strength and ductility for joints welded by two different filler wires and also compare the base metals' strength before and after the welding. 5356 filler wire used specimens suffered from incomplete penetration and 4043 filler wire used specimens had good penetration results as it can be remembered, 8 specimens for each filler wire were tested with tensile test machine. Results are given in Table 10 and Table 11:

Table 10 Tensile test results for specimens welded with filler wire Al 4043

Specimen #	Tensile Strength (Mpa)	% Elongation
1	119,34	% 2,73
2	105,79	% 3,21
3	110,65	% 2,66
4	108.58	% 2,36
5	109,36	% 2,45
6	130,25	% 3,21
7	122,21	% 2,89
8	118,36	% 2,14

Table 11 Tensile test results for specimens welded with filler wire Al 5356

Specimen #	Tensile Strength(MPa)	% Elongation
1	191,36	% 4,33
2	185,34	% 3,92
3	188,69	% 4,12
4	174,36	% 3,21
5	189,66	% 2,36
6	198,33	% 2,65
7	197,23	% 3,47
8	182,32	% 3,12

Results have showed that the joints that were welded with filler wire 5356 had higher tensile strength and higher percent elongation than the joints welded with 4043 filler wire. Fracture occurred in weld metal zone on all of the specimens. It should be taken into account that although the specimens

welded with Al 5356 filler wire resulted in higher tensile strength, weld penetration in the corner of the fillet could not be achieved with that filler wire so service life will be much shorter. On the other hand Al 4043 filler wire used specimens resulted in lower tensile strength but complete penetration was observed on the corner of the fillet. So it is up to the design intent to decide which filler wire shall be used.

4.3 Hardness Tests

Hardness tests were performed mainly to see any extreme increment in HAZ and weld metals as it can be a sign of brittle phase formation. Following graphs were obtained by Vickers Hardness tests under 5 kgf load. The hardness plots of two different used filler wires showed no significant difference. Both of them had increased hardness values in weld metal regions and in heat affected zones. The reason for the hardness increment in HAZ may be the increased amount of intermetallics and both Al 4043 and Al 5356 filler wires showed higher hardness values in weld metal zones. Al 6063 base metal had lower hardness than 5754 base metal. Correspondingly heat affected zone at Al 6063 side had lower hardness than heat affected zone in 5754 side.

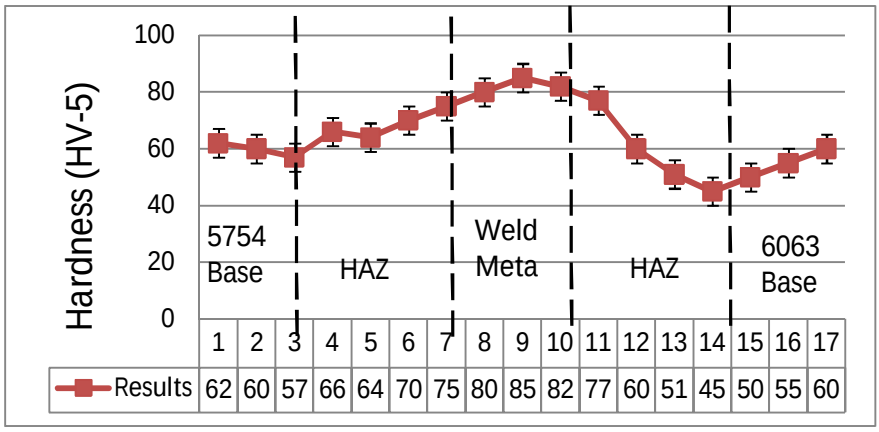

Figure 53 Hardness Profile along the fillet weld with 4043 filler wire

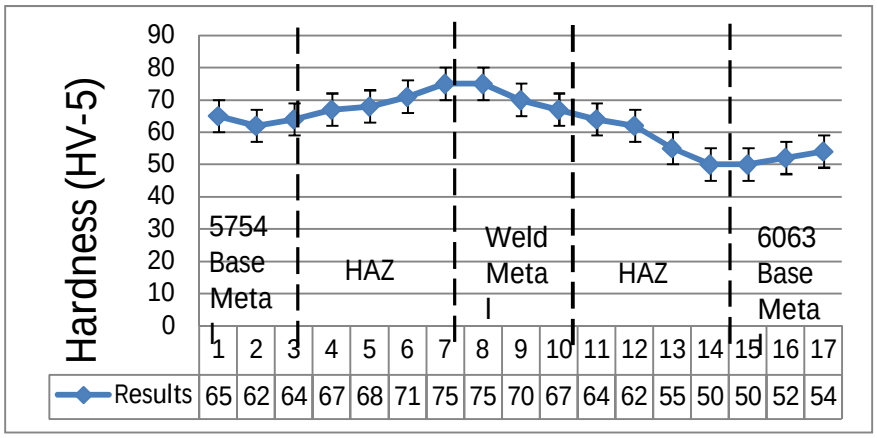

Figure 54 Hardness Profile along the fillet weld with 5356 filler wire

4.4 Dynamic Loading Tests

As soon as the manufacturing of the dynamic loading machine was finished, new specimens were prepared and example tests were started. Figure 55 shows an example specimen which has failed after being subjected to fatigue.

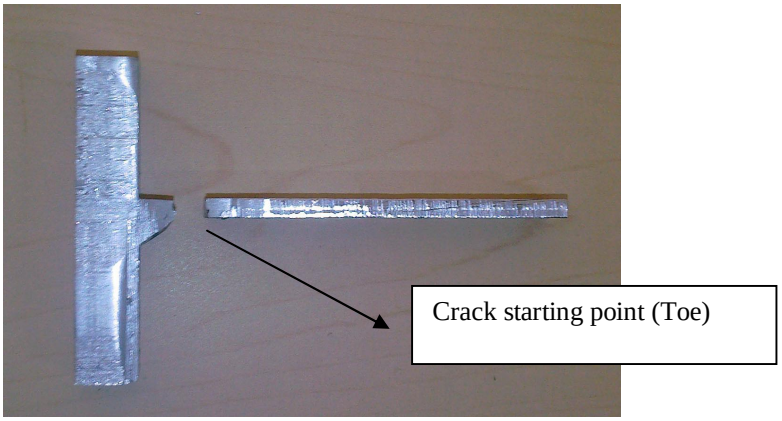

Figure 55 Specimen having fracture under dynamic loading

Dynamic loading strength of the welded specimens is greatly affected by the notch effect on the toe. In order to have an idea about the effect of weld parameters on service life of the welded joint, the notches had to be eliminated by grinding. Nevertheless cracks started from the toe but this time crack initiation time and propagation rate were not affected from the depth of the notch since they were already grinded.

Two groups of specimens were prepared using two different groups of weld parameters. Line energies were calculated according to equation 1. Used weld parameters and corresponding Line energies are given in Table 12.

Table 12 Weld parameters used for dynamic loading test specimen preparation

Specimen Group#	WFS (m/min)	Trim	GFR (lt/min)	WLS (mm/s)	I (A)	V (V)	E (kJ/cm)
1	10,00	1,05	16	8,55	210	21	46
2	9,60	1,05	16	10,75	185	21	33

In the above table “WLS” refers to welding speed, “GFR” refers to gas feeding rate. “H” which refers to line energy calculated for two parameter groups. Each parameter was applied to 6 specimens and they were tested by the manufactured dynamic loading machine. Results are shown in

Table 13.

Table 13 Results of the dynamic loading tests by dynamic loading machine

Parameter Group	Specimen #	Cycles Before Fracture
1	1	19800
1	2	30600
1	3	22320
1	4	32400
1	5	21600
1	6	21240
2	7	38520
2	8	34200
2	9	27000
2	10	31680
2	11	29160
2	12	36000

Cracks initiated at the toe and propagated. It can be realized that a difference appears between the parameter groups. The parameter with the lower line energy resulted in having larger number of cycles in average. Parameter 1 with high line energy had average 24660 cycles before fracture. On the other hand parameter 2 with lower line energy had 32760 cycles average.

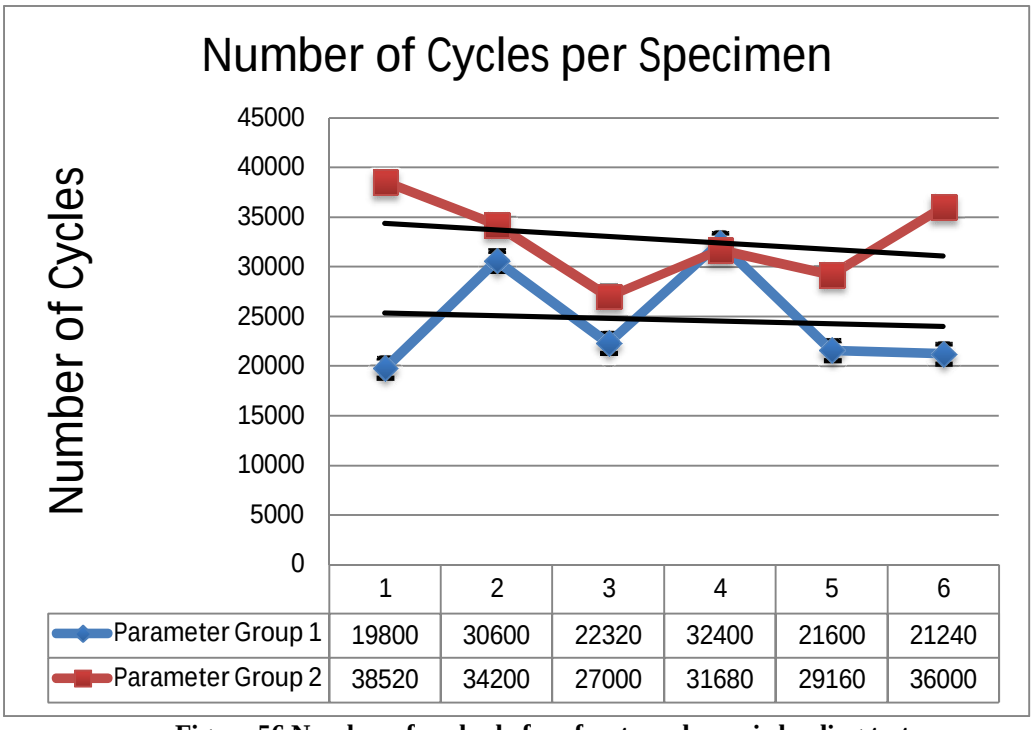

Figure 56 Number of cycles before fracture dynamic loading tests

In the graph error bars are corresponding to ±1000 cycles which is representing approximately 3 minutes of machine working. The error may arise from the operator while noting the starting and finishing time of the test.

It is already discussed that fatigue life of welded joints greatly depends on stress concentrators. Welding is a very random process geometrically so there is big scattering even between the specimens of the same parameter group.

The big variations on the results might be coming from the specimen set-up on the dynamic loading machine. The specimens should be placed on the machine identically using proper gages which was not possible for the used machine. There should be a system measuring the initial and final displacement of the end of the specimen which was connected to the machine. In other words initial stress and strain introduced on the specimen should be identical.

The geometric dimensional tolerances of the specimens must be narrowed down and inspected after the production, again to produce more identical specimens to make the initial stress and strain on the specimen more identical.

As explained in chapter 4 “Experimental Procedures” three specimens were taken from one welded joint by cutting in equal lengths. But welding is a very random process and parameters like flank angle or the phases formed on the weld metal or heat affected zone could change between the start and end of a weld line.

At this stage it would be wrong the make a characterization about the results although in average, the higher input specimens resulted in lower number of cycles, because there is quite a big scattering between the results and there is no major difference between parameter group 1 and parameter group 2. Large amount of identical specimens must be tested in order to make a judgement about the service lifes between parameter groups. However the tests took attraction to the failure locations and opened a way for the analysis of fracture surfaces.

4.5 Microstructural Examinations of Specimens

During microstructural examinations, a special attention is given to specimens welded with Al 4043 wire. Specimens that are identical to the specimens welded for dynamic loading tests were examined under light microscope.

The purpose of the examination was to observe and characterize any distortions and discontinuities such as grain alignment, grain size, precipitates, cracks especially around the fusion lines at Al 6063 base metal side.

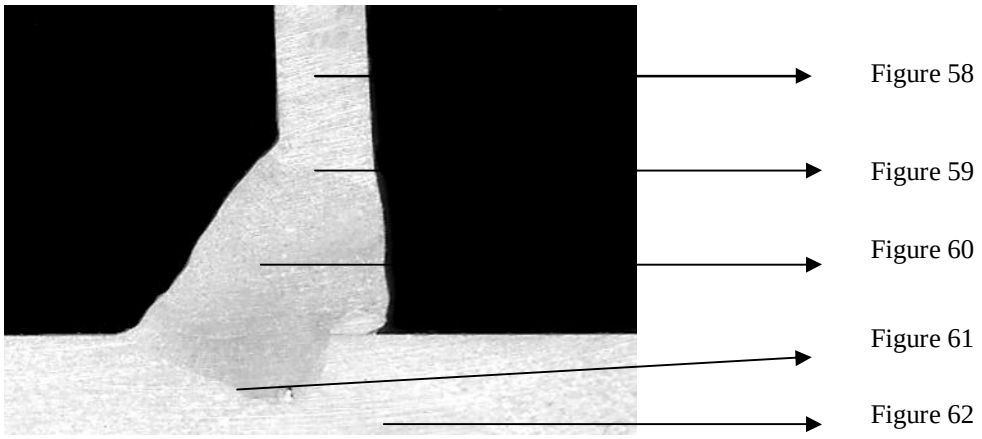

Figure 57 Locations of taken microstructure photos of specimen #1

Figure 57 illustrates the micrograph taken from specimen 1 that is welded with parameter 1 (the parameter with higher heat input). Figure 58 shows the microstructure of 6063 base metal. Figure 59 contains the micrograph of the heat affected zone and partially melted zone at 6063 base metal side. Figure 60 shows weld metal microstructure.Figure 61 belongs to heat affected zone but this time at Al 5754 base metal side. Finally Figure 62 shows the base metal microstructure of Al 5754.

Studies in the literature showed that the precipitates in Figure 58 (dark areas) are Mg_2Si particles [37]. They have a homogeneous distribution in the matrix.

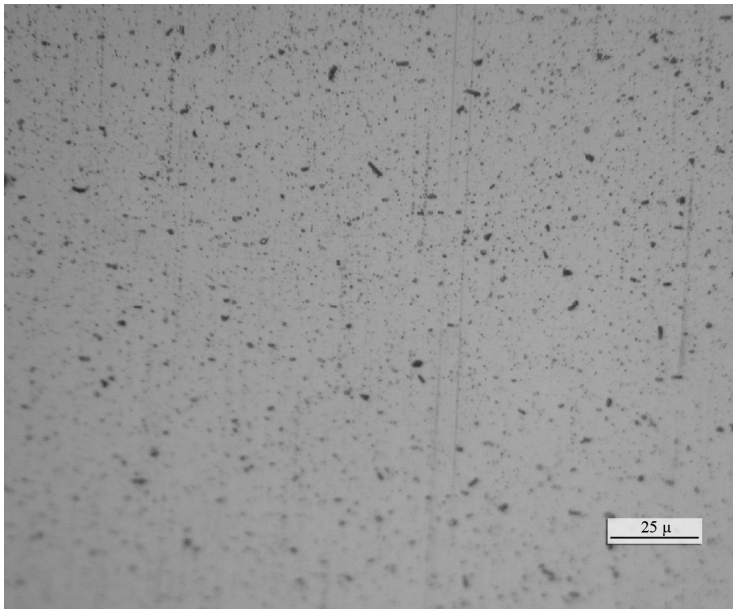

Figure 58 Base metal microstructure of 6063 Aluminium alloy, Etchant: Keller

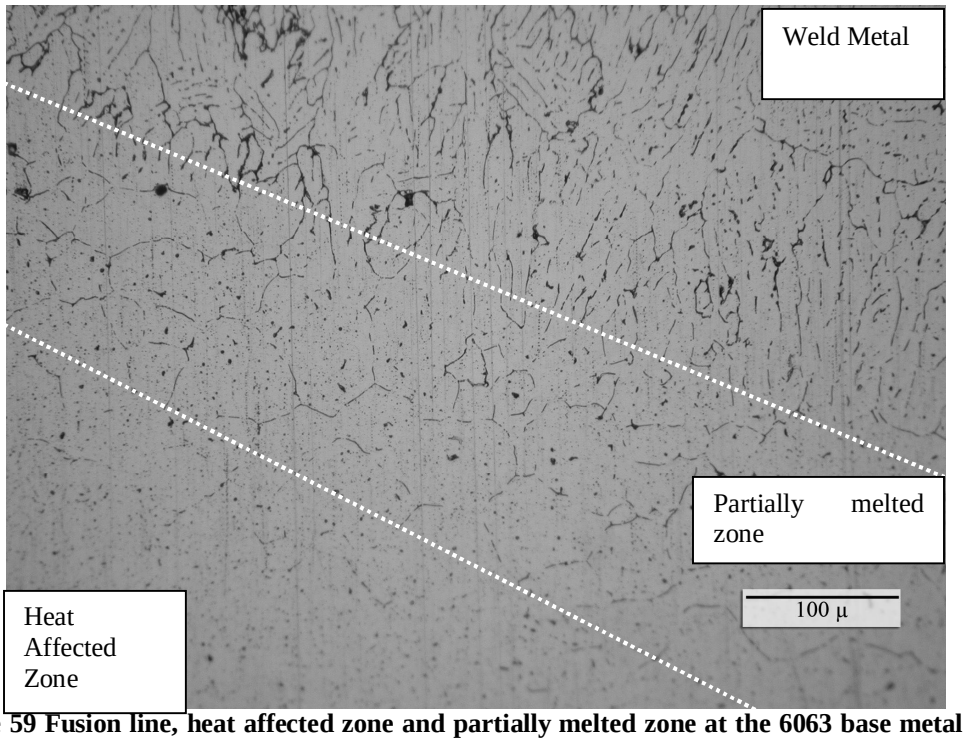

Figure 59 Fusion line, heat affected zone and partially melted zone at the 6063 base metal side, Welded with parameter group 1, Etchant: Keller

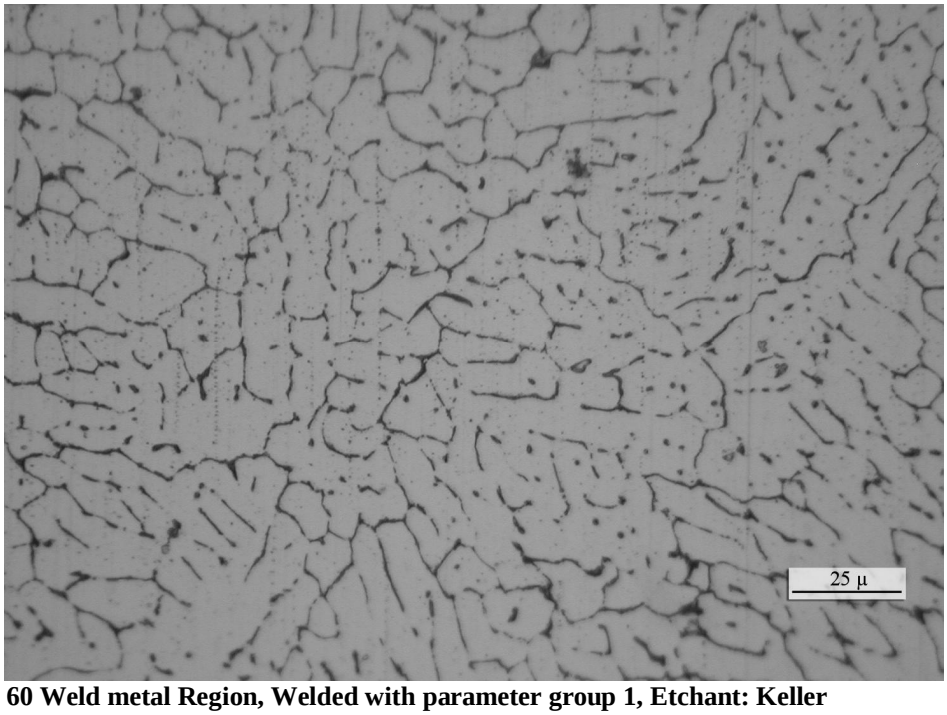

Figure 60 Weld metal Region, Welded with parameter group 1, Etchant: Keller

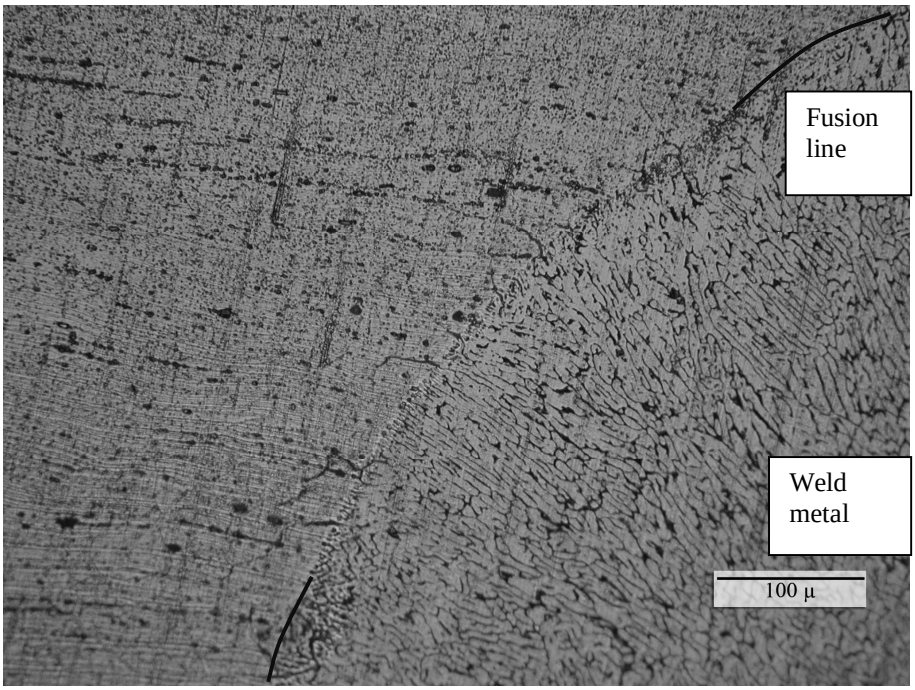

Figure 61 Fusion line, heat affected zone and partially melted zone at the 5754 base metal side, Welded with parameter group 1, Etchant: Keller

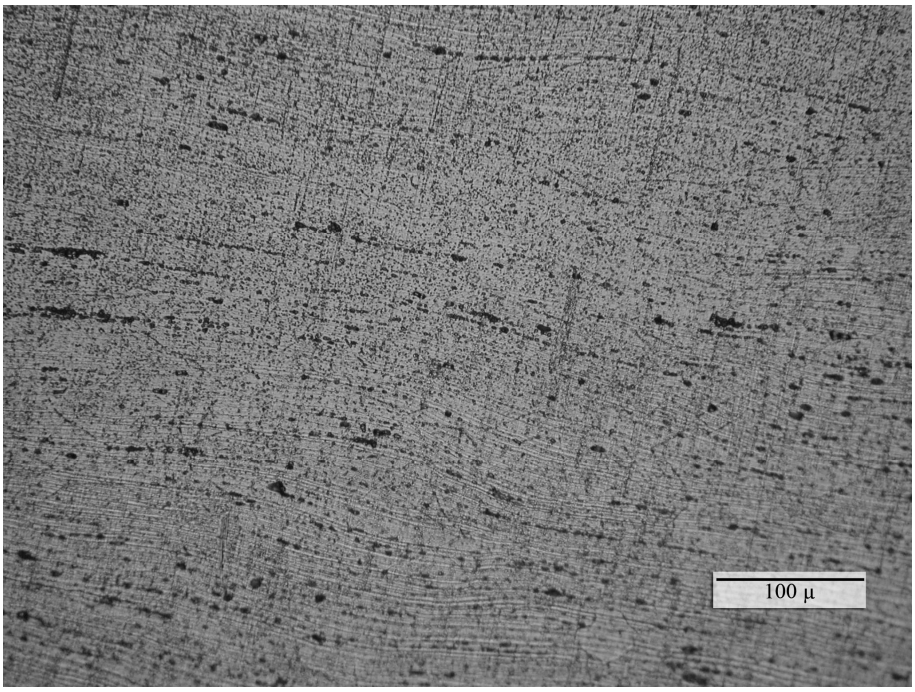

Figure 62 Base metal microstructure of 5754 Aluminium alloy, Parallel to the rolling direction, Etchant: Keller

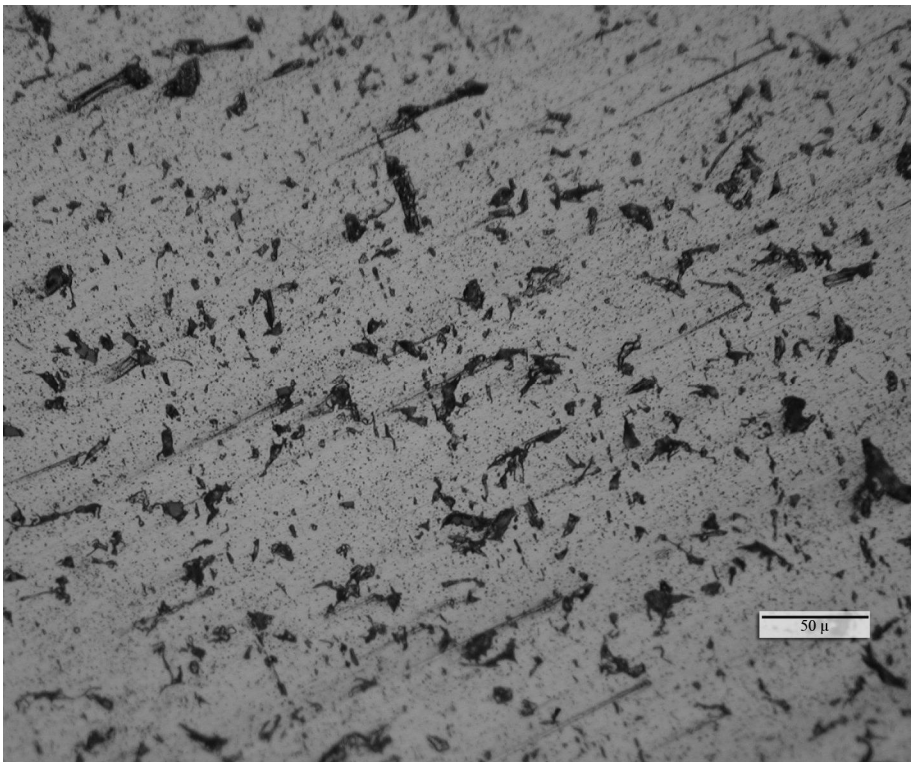

Figure 63 Initial microstructure of 5754 plate, Perpendicular to the rolling direction, Etchant: Keller

In Figure 59 which is taken from the fusion line at Al 6063 base metal side, a different microstructure is observed with respect to the base metal. From fusion line to the base metal temperature profile decreases. At the other side of the the fusion line the maximum temperature during weld process is lower than the liqiudus however it is still above the solidus. So the partially melted zone occurred. Between the HAZ and fusion zone, there is partially melted zone (Figure 59). On the partially melted zone grain boundary enrichment with Mg and Si was observed on SEM examinations together with the grain boundary coarsening. In their study with the same filler wires and base metals K. Prasad Rao et al [2] made EDX analysis at the grain boundaries of PMZ and they also observed Mg and Si enrichment on grain boundaries. There was also grain boundary coarsening. In our study from fusion line towards the weld metal dendritic grain growth is observed due to rapid cooling.

Grain boundaries have the lowest melting point constituents of an alloy system. Considering the ternary Al-Mg-Si system lowest melting point is the 559^{o} C where ternary eutectic reaction occurs as liquid transforms into α-Al + Mg_2Si + Si. It can be stated in the partially melted zone, that the precipitated phases at the grain boundaries may consist of mainly α-Al, Mg_2Si and Si.

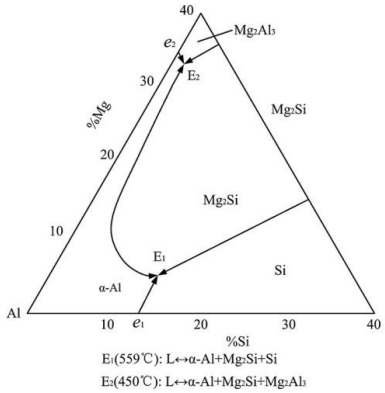

Figure 64 Ternary phase diagram of Al–Mg–Si system [38]

In Figure 60 weld metal microstructure is seen. Again Si and/or Mg enrichments were observed at grain boundaries.Figure 61 is an image taken from the fusion line at Al 5754 side. Dendritic grains were observed starting from the fusion line to the weld metal due to rapid solidification.

The main metal of Al 5754 alloy (Figure 62) indicated a high degree of orientation that precipitates are oriented in the direction of rolling. Besides these, both of the base metals Al 5754 and Al 6063 (Figure 58 and Figure 62) are not altered by the welding process.

Figure 65 Locations of microstructural investigation in specimen #13

Microstructural examination of specimen #1 has revealed neither cracks nor intolerable grain size increment. Figure 65 illustrates the locations of the photos of dynamic loading test specimen #13 taken by light microscope. This specimen was prepared with parameter group 2 which had lower heat input. Figure 66 shows the heat affected zone and especially the partially melted zone at 6063 side. Figure 67 shows weld metal microstructure, Figure 68 belongs to heat affected zone at Al 5754 base metal side.

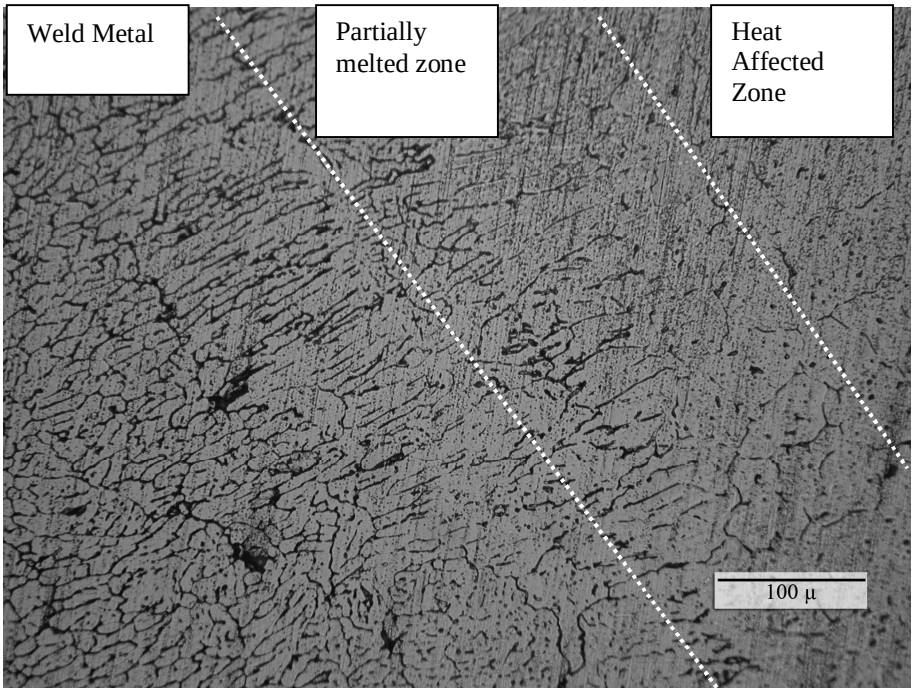

Figure 66 Fusion line, heat affected zone and partially melted zone at the 6063 base metal side, Welded with parameter group 2, Etchant: Keller

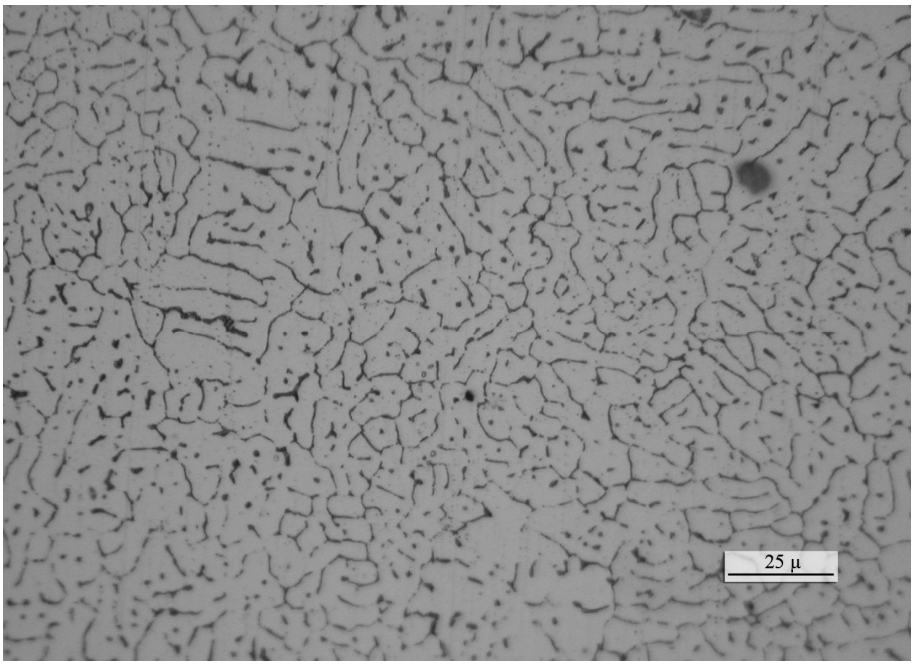

Figure 67 Weld metal Region, Welded with parameter group 2, Etchant: Keller

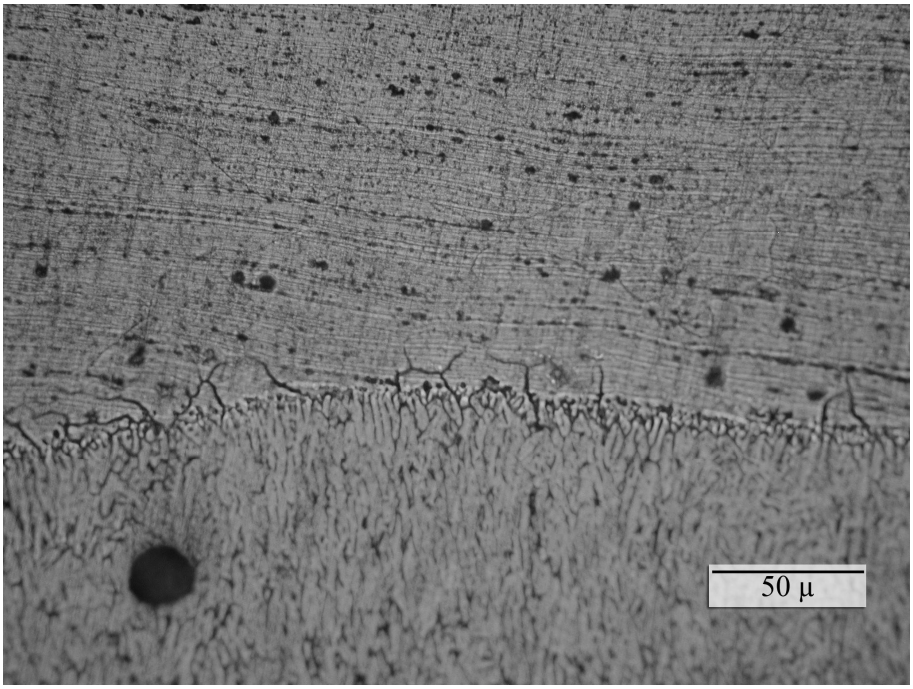

Figure 68 Fusion line, heat affected zone and partially melted zone at the 5754 base metal side, Welded with parameter group 2, Etchant: Keller

Microstructure examination of specimen #13 has indicated that there were no cracks and no grain coarsenings. In Figure 68 grain boundary enrichment by Mg and Si is more clearly observed near fusion line on partially melted zone. Dendritic grain growth is again observed starting from fusion line towards weld metal.

Comparing the microstructures of high heat input specimen to the low heat input specimen, no significant difference was observed. It can be stated that the heat input difference between parameters was not enough to create a significant difference on the microstructures.

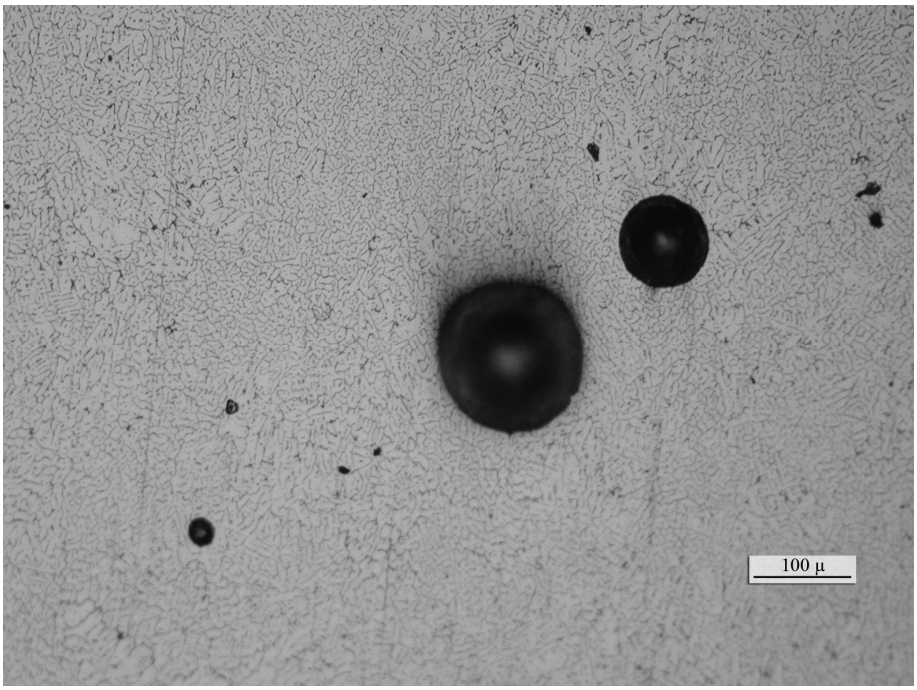

Figure 69 Porosities around the weld metal, Welded with parameter group 1, Etchant: Keller

As mentioned previously, porosity is a general problem in aluminium welding. Although the precautions were taken as using pulsed arc welding [24]; and paying attention to the cleanliness of the plates to be welded (since it is a very important parameter as dirt and moisture can release hydrogen during welding), porosity formation was still observed in weld metal (Figure 69). To obtain the desired weld properties, heat input should be as low as possible because higher heat input increases the cooling rate and so the amount of hydrogen trapped inside weld metal.

4.5 SEM Examinations

4.5.1 Fatigue Fracture Surfaces

Figure 70 shows the initiation point of the crack and the direction of the force. It is explained briefly in Chapter 2 (Theory) (Figure 22 and Figure 23) that the highest stress is created at the toe due to geometric stress intensity factors and this is the dominant parameter that determines start point of the cracks.

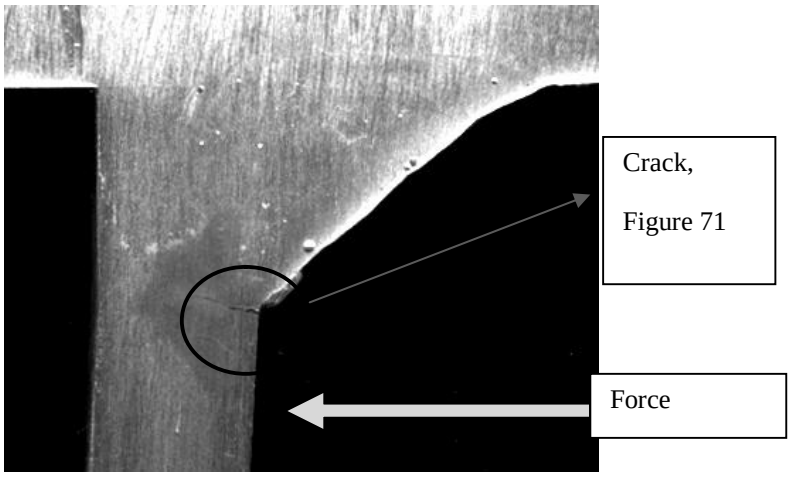

Figure 70 Crack initiation at the heat affected zone, Magnification: 6X

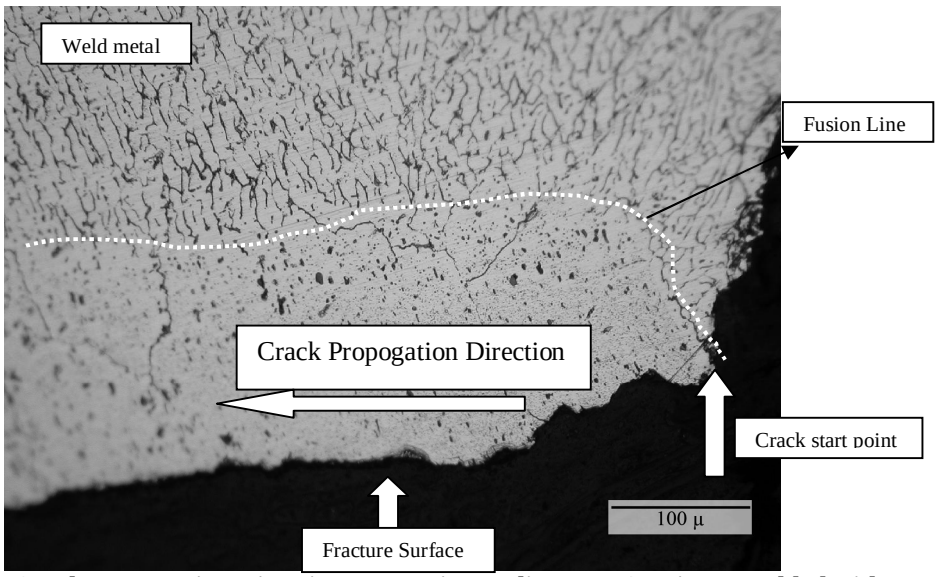

Figure 71 Crack propagation Direction, Dynamic Loading Test Specimen Welded with parameter group 1, Etchant: Keller

Figure 71 shows the section of the broken specimen which is taken perpendicular to the fracture surface. It is seen that the crack initiated at the toe as shown in Figure 70 and propagated through heat affected zone.

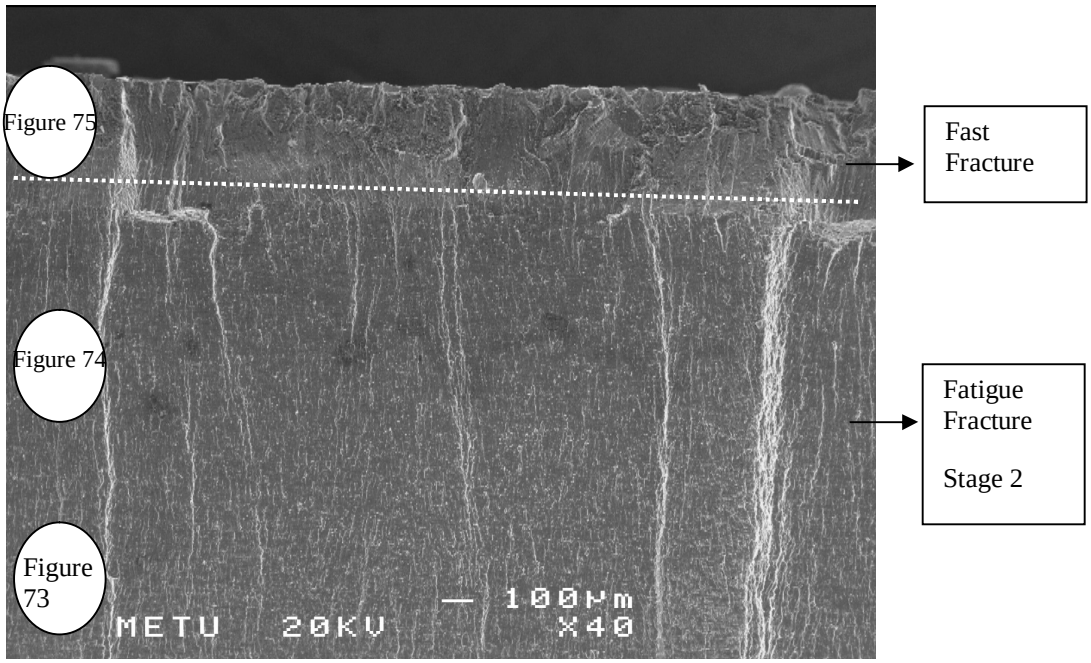

Figure 72 Dynamic Loading Specimen Fracture Surface (Location of the images)

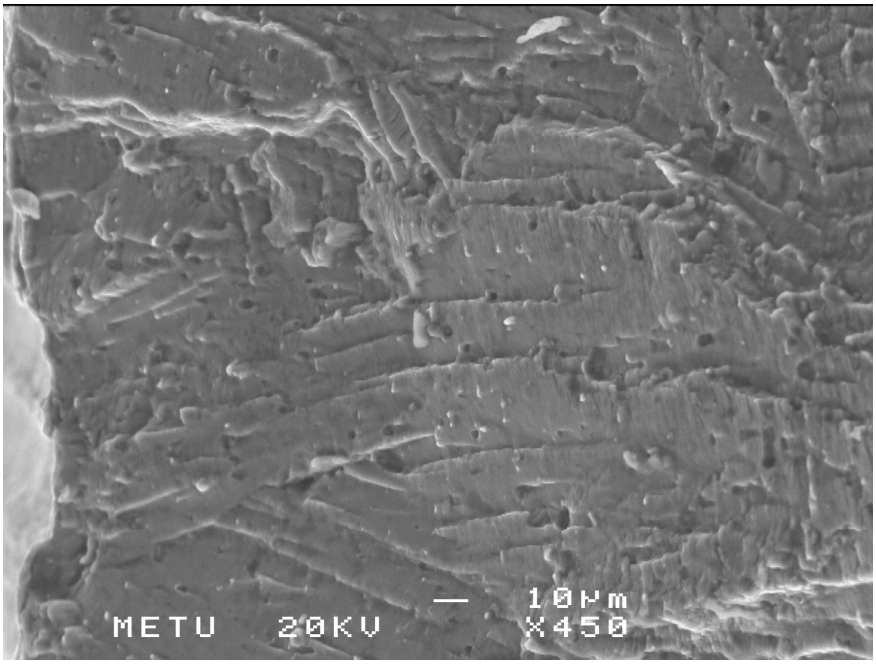

Figure 73 Dynamic Loading Specimen, Stage 1 fatigue fracture surface SEM image

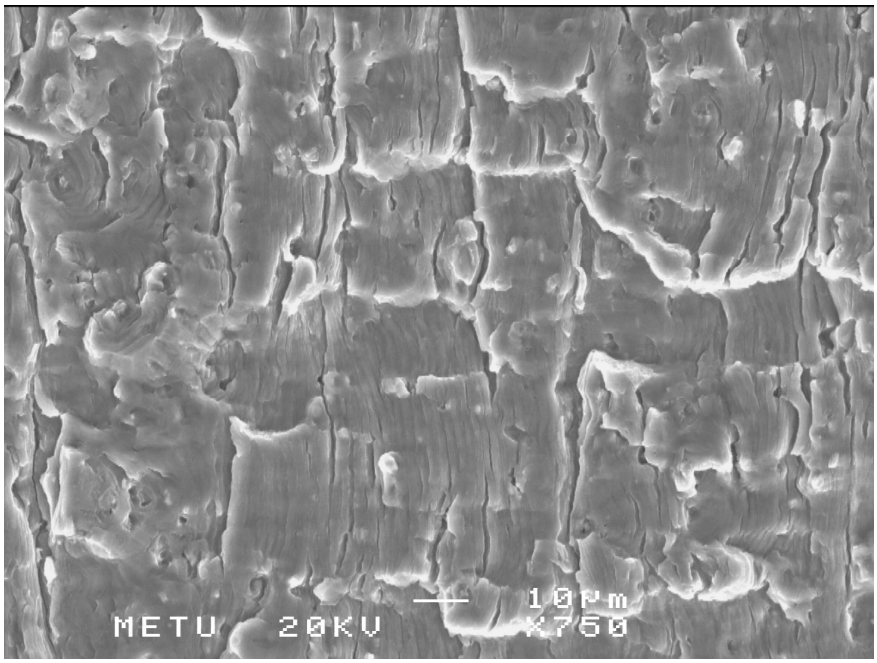

Figure 74 Dynamic Loading Specimen, Stage 2 fatigue fracture surface SEM image

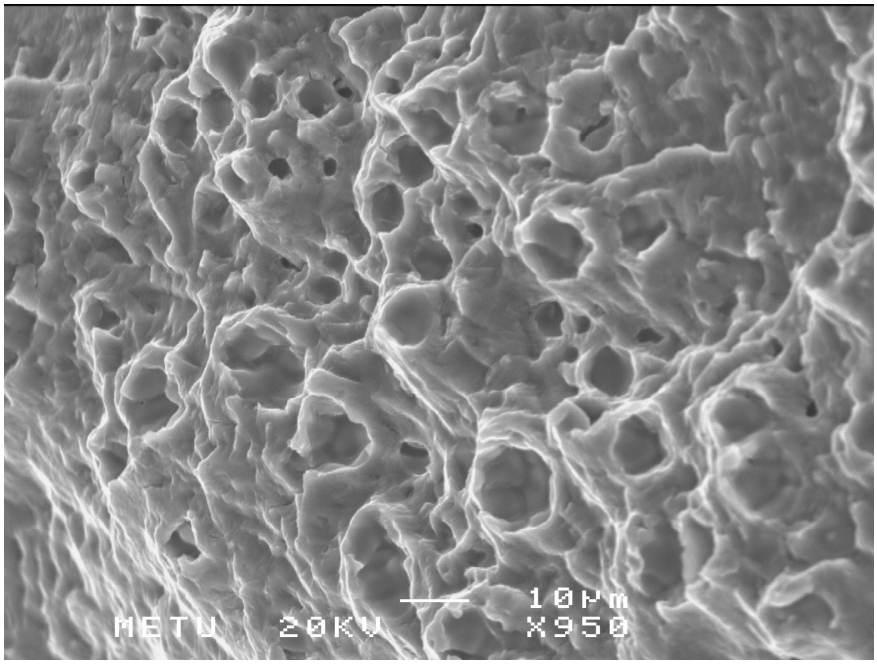

Figure 75 Dynamic Loading Specimen, Stage 3 fatigue fracture surface SEM image

Figure 73 shows the SEM image taken from the crack initiation (Stage 1) location of the fracture surface which appears faceted, cleavage like, crystallographically oriented as a result of the maximum shear stress created. This location on the fracture surface did not exhibit fatigue striations. It is known that Stage 1 fatigue surfaces occur on high cycle low stress fractures and fatigue striations are not seen.

Figure 74 is the SEM image showing the stage 2 fatigue facture surface of the specimens. Fatigue striations were observed. After the crack became too large and the remaining part of the material could not carry the load, the local strains and stresses at the crack front caused a ductile fracture with dimples (Figure 75).

4.5.2 Tensile Test Fracture Surfaces

As mentioned previously, the crack propagated through weld metals during tensile tests. Ductile fracture was observed.

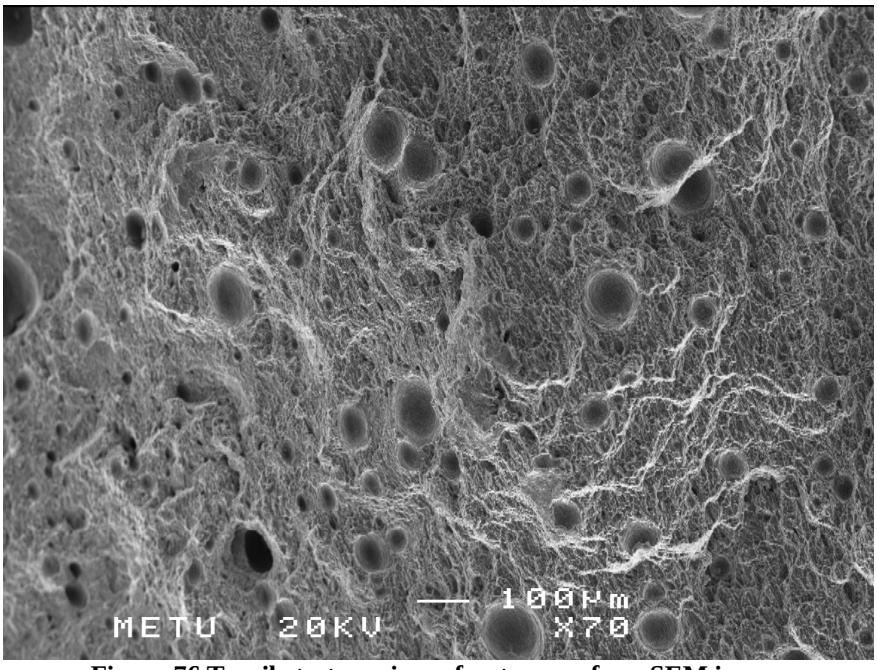

Figure 76 Tensile test specimen fracture surface, SEM image

Hydrogen porosity was widely discussed in the previous chapters. Figure 76 again shows the porosity caused by hydrogen on the fracture surface of tensile test specimen fracture surface . When inside the pores are examined in detail, dendrite arms can be seen inside them Figure 77.

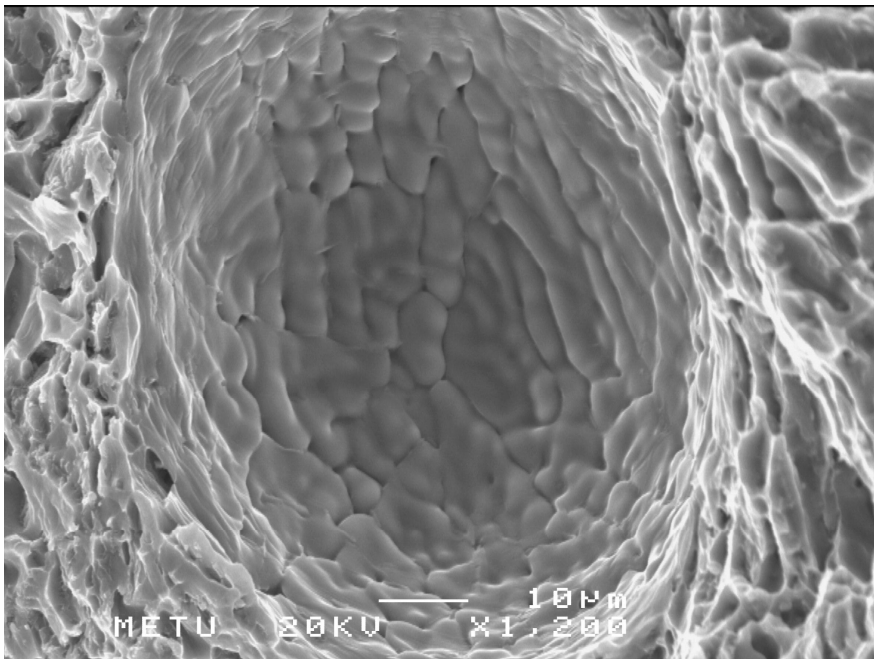

Figure 77 The detail inside the porosity which was revealed after tensile testing, (SEM)

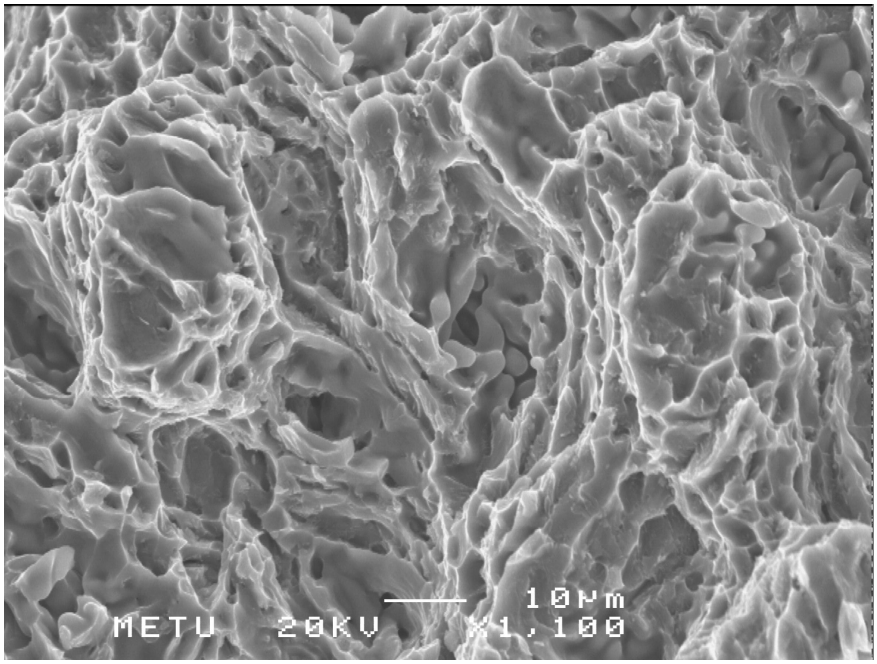

Figure 78 Fracture surface of tensile test specimens, SEM image

On the fracture surface there were dimples which are the sign of plastic deformation (Figure 78).

4.5.3 Partially Melted Zone and Heat Affected Zone

It is important to remember that during the dynamic loading tests crack started from the toe at Al 6063 side and propagated through the PMZ and HAZ. So these areas were taken into SEM for further examinations.

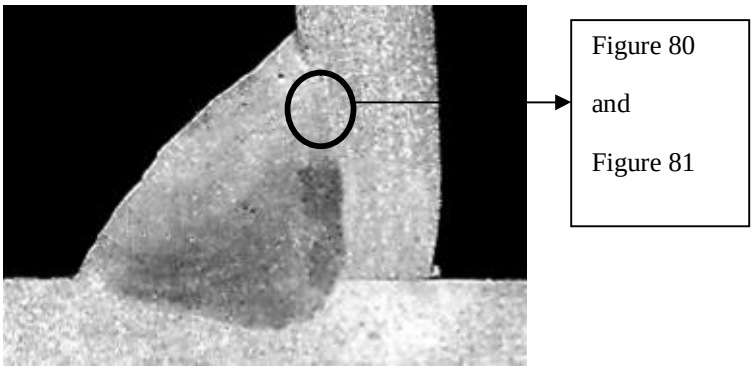

Figure 79 Locations of the taken images of SEM examinations

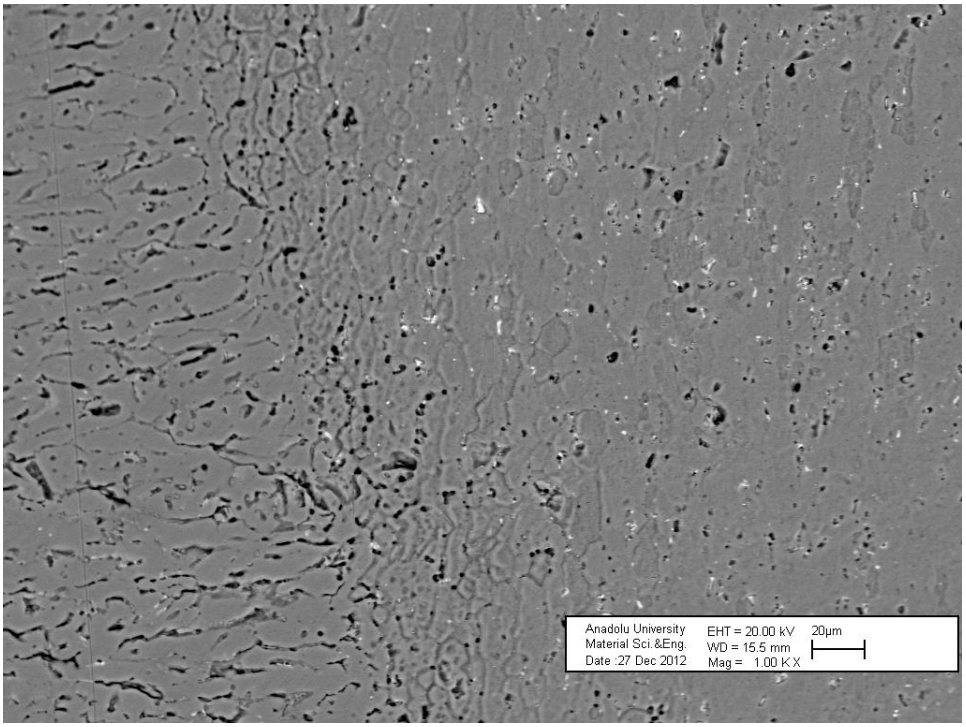

Figure 80 Weld metal, Fusion Line, PMZ and HAZ, Al 6063 side, BSE SEM image, 1000X magnification

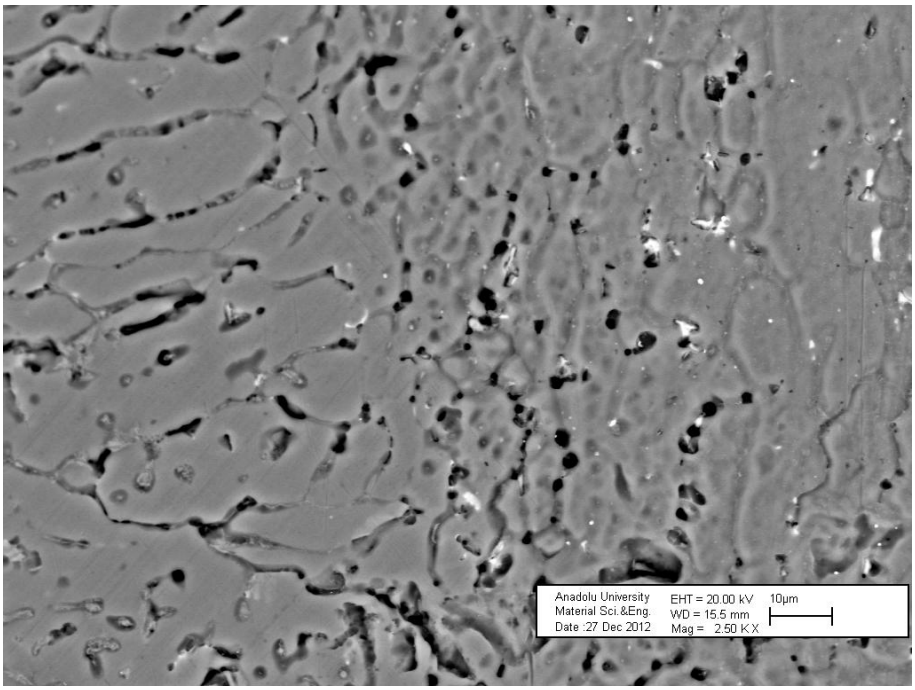

Figure 81 Weld metal, Fusion Line, PMZ and HAZ, Al 6063 side, BSE SEM image 2500X magnification

Again dendritic grain growth was observed on the weld metal from fusion line. EDX analysis taken from the grain boundaries on PMZ gives peaks of silicon, magnesium and copper at the grain boundaries. It is known in the literature that the aluminium liquid which have high silicon are more fluid. Therefore the lower solidus temperature of the Al 4043 filler may enhance liquid penetration through the Al 6063 base metal

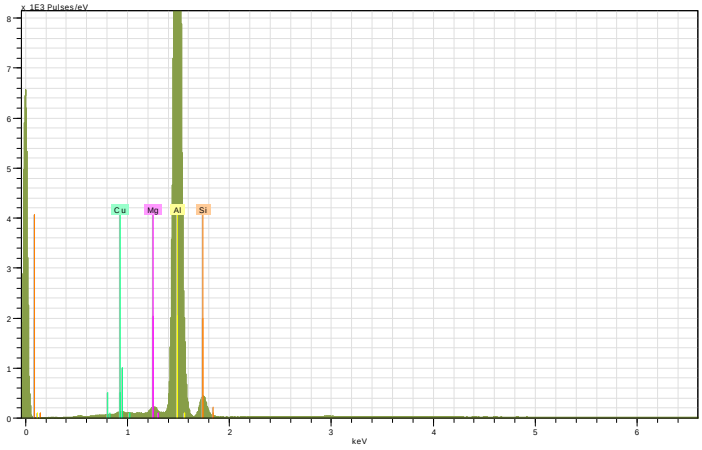

Figure 82 EDX analysis taken from the grain boundaries on PMZ

Table 14 EDX analysis taken from the grain boundaries on PMZ

Element	***Weight Conc %***	***Atom Conc %***
Al	86.03	87.17
Si	11.56	11.26
Mg	1.42	0.75
Cu	1.63	0.70

EDX analysis of the white precipitates observed in Figure 80 was also done, which yielded high Fe peak. Considering the study of Y Osada [36] α-AlFeSi and β-AlFeSi may be present at these locations. Together with the distortion of heat effect, the particle sizes may have increased considering the larger white regions in PMZ in Figure 80. It was also observed in Figure 81 that these particles are both present in grains and at the grain boundaries.

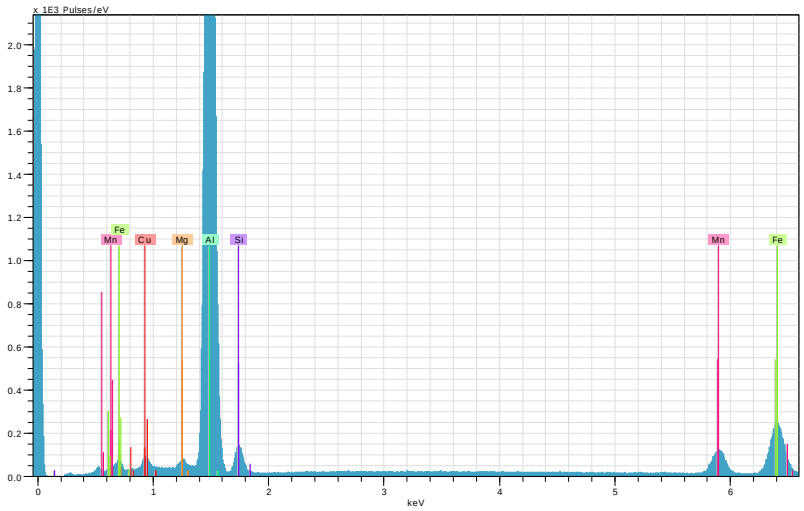

Figure 83 EDX analysis of the white precipitates on Figure 80

Table 15 EDX analysis of the white precipitates on Figure 80

Element	***Weight Conc %***	***Atom Conc %***
Al	76.88	86.64
Si	4.70	4.97
Mg	1.01	1.23
Cu	2.16	1.01
Fe	11.02	5.86
Mn	4.24	2.29

4.5.4 Fatigue Crack Path of Dynamic Loading Tests

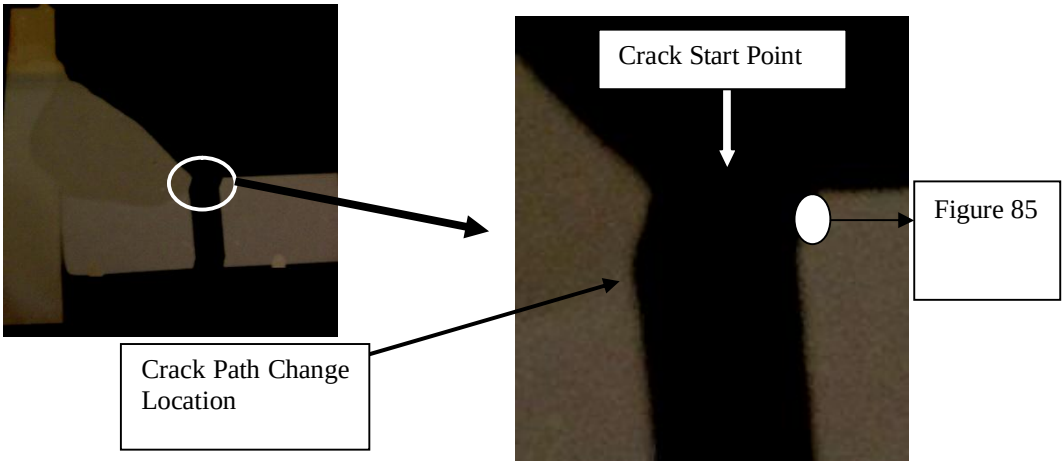

Figure 84 Fracture exhibited dynamic loading test specimen, Etchant: Keller's

On Figure 84 it was aimed to see the favored path for crack propagation. It was observed that geometry, stress and strain concentrations at the toe was the dominant factor over material properties and cracks started at this location. Besides after the cracks were initiated, the path followed was the heat affected zone up to some point which means material properties are dominant over geometry, stress and strain concentrations. At that point, shown as crack path change location on

Figure 84, geometric factors again became dominant over material properties and crack path is directed into Al 6063 base metal.

It is a known fact that Al 6063 material has fine Mg_2Si particles inside grains which are obtained by age hardening. On the other hand during SEM and light microscope examinations over PMZ and HAZ regions it was observed that Mg and Si enrichment occurred on grain boundaries together with grain boundary coarsening. Grain size increment was seen. Large particles containing Fe, Mg, Si, Cu formed inside grains and grain boundaries. Because of these distortions on the original microstructure of Al 6063, crack path may have favored PMZ and HAZ over original Al 6063 base metal microstructures.

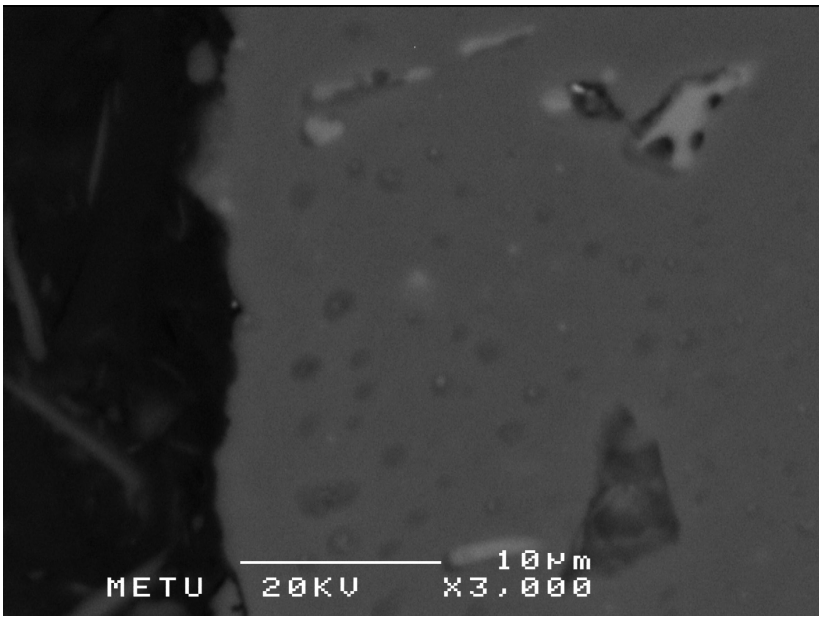

Figure 85 PMZ and HAZ, Fracture exhibited Specimen, BSE SEM image

Figure 85 is an SEM image to observe crack path location. EDX analysis was taken from the dark and white precipitates.

Table 16 EDX results for the dark regions of Figure 85

Element	***Weight Conc %***	***Atom Conc %***
Al	86.13	92.60
Si	1.28	1.33
Mn	1.42	0.75
Fe	3.56	1.85
Cu	7.60	3.47

Table 17 EDX results for the white regions of Figure 85

Element	***Weight Conc %***	***Atom Conc %***
Al	62.87	75.01
Si	6.73	7.71
Mn	6.78	3.97
Fe	19.30	11.13
Cu	4.32	2.19

Again it is understood that the heat input during welding process resulted in particle size increment. Observing Figure 85 from left to right white and dark precipitates are getting smaller.

On their study CHEN Jun-Zhou et al. [38] have arrived a result that grain boundary precipitates don't have a significant effect on crack growth as compared with that of the precipitates inside grains. Likewise in this study fatigue crack tended to pass over the PMZ and HAZ because they contain coarser particles. Also it can be concluded that the distortion on the fine particled microstructure of Al 6063 base metal may have decreased the fatigue life.

CHAPTER 5

CONCLUSION

In this study weldability of aluminium 6063 plate to aluminium 5754 plate with different thicknesses and with no preheating was examined. Mechanical, macrostructural and microstructural properties were compared. A dynamic loading machine was designed and manufactured in order to simulate real life service conditions of the fillet joint. From the analysis and discussion of the results obtained in the study following conclusions can be drawn:

1. 15 mm plate of Aluminium 5754 is successfully welded to 3 mm plate of Aluminium 6063 by using filler wire Al 4043. Plates having different thicknesses are successfully joined without using preheating.
2. A dynamic loading machine that can cause fatigue fracture on the produced fillet welds is manufactured. Manufactured machine is able to make a simulation of the real life loading conditions on the aluminium joints.
3. Gas-metal arc welding (MIG) is a convenient welding method for the fillet joint of this study.
4. Using Al 4043 filler wire in welding gives more fluid and penetrative weld pool compared to Al 5356 filler wire due to its high silicon content.
5. Tensile strength and ductility of the joints welded by Al 5356 filler wire was measured to be higher than the joints welded by Al 4043 filler wire.
6. No significant change on cycle numbers of two parameter groups was observed on the tests for their durability under dynamic loading tests using dynamic loading machine
7. Microstructure of the Al 6063 base metal near weld was distorted as the coarse particles was formed so that crack propagation was favoured on these locations compared to fine particled original Al 6063 base metal.

REFERENCES

1. Katoh M, Kerr HW. Investigation of heat-affected zone cracking of GTA welds of Al–Mg–Si alloys using the Varestraint test. Weld J 1987;66:360-s–8-s.
2. K. Prasad Rao, N. Ramanaiah , N. Viswanathan, "Partially melted zone cracking in AA6061 welds", Materials and Design 29 (2008) 179–186
3. R.J. Shore, R.B. McCauley, "Effects of porosity on high strength aluminium 7039", Welding J. 49 (July (10)) (1970) 311s–321s.
4. J.H. Devletian, W.E. Wood, "Factors affecting porosity in aluminium welds- a review", Welding Research Council Bulletin 290, USA, December 1983, p. 20.
5. ASM Metals Handbook. Welding, Brazing and Soldering. Vol. 6. 1993: ASM International.
6. AWS Welding Handbook, Volume 1 "Welding Technology", 8th edition, American Welding Society
7. Fact Sheet—Choosing Shielding for GMA Welding, Weld. J., 79: 18, 2000.
8. Gibbs, F. E., Weld. J., 59: 23, 1980.
9. Jones, L. A., Eagar, T.W., and Lang, J. H., Weld. J., 77: 135s, 1998.
10. S. Kou "Welding Metallurgy" 2nd edition (2002) pp19-22 pp170-199 John Wiley & Sons
11. Weman, Klas (2003). Welding processes handbook. New York: CRC Press LLC. ISBN 0-8493-1773-8.
12. Kelkar G.P., *Weld Cracks – An Engineer's Worst Nightmare*, WJM Technologies.
13. D.G. Eskin, Suyitno, L. Katgerman "Mechanical properties in the semi-solid state and hot tearing of aluminium alloys" Progress in Materials Science 49 (2004) pp629–711
14. Novikov II, Novik FS. Doklady Akad Nauk SSSR, Ser Fiz 1963 vol.7 pp1153.
15. Prokhorov NN. Russian Castings Production 1962 vol.2 pp172
16. W.S Pellini,. "Strain theory of hot tearing". The Foundry vol. 80(11) (1952) pp. 125-199.
17. W.I. Pumphrey and P.H. Jennings "A consideration of the nature of brittleness and temperature above the solidus in castings and welds in aluminium alloys" J. Inst. Metals 75 (1948) 235-256.
18. J.C Borland "Generalized theory of super-solidus cracking in welds (and castings)" Br. Weld. J. Vol.7 (1960) pp508–512.
19. Les Pook "Metal Fatigue" p15-136, Springer
20. Miller KJ, McDowell Overview In: Miller KJ, McDowell DL(Eds) Mixed-Mode Crack Behavior. ASTM STP 1359. American Society for Testing Materials, West Conshohocken, PA, pp. vii-ix.
21. Miller KJ, McDowell DL(Eds) Mixed-Mode Crack Behavior. ASTM STP 1359. American Society for Testing Materials, West Conshohocken, PA
22. Tom Lassen, Naman Recho "Fatigue Life Analyses Of Welded Structures" ISTE
23. Romanovskaya AV, Botvina LR (2003) Effect of crack path on statistical distribution of the fatigue lifetime. In: Carpinteri A, Pook LP (Eds) Proceedings of the International Conference on Fatigue Crack Paths (FCP 2003), Parma (Italy), 18-20 September 2003. University of Parma. Parma on CD (6 pp.).
24. Celina Leal Mendes da Silva , Am´erico Scotti, "The influence of double pulse on porosity formation in aluminium GMAW", Journal of Materials Processing Technology 171 (2006) 366–372
25. Frost NE, Marsch KJ, LP (1974) "Metal Fatigue". Clarendon Press, Oxford. Reprinted with minor corrections (1999), Dover Publications, Mineola, NY.
26. S.Maddox, "Fatigue Strength of Welded Structure", Abington Publishing, 1991
27. ISO 9015-1 - EN 1043-1 - Destructive Tests on Welds in Metallic Materials - Hardness Testing - Part 1 Hardness Test on Arc Welded Joints - First Edition
28. ASM Specialty Handbook, Aluminium and Aluminium alloys, ASM International-The materials Information Society, p380-680

29. Kihara, H., Suzuki, H., and Tamura, H., Researches on Weldable High-Strength Steels, 60th Anniversary Series,Vol. 1, Society of Naval Architects of Japan,Tokyo, 1957.
30. Inagaki, M., and Sekiguchi, H., Trans. Nat. Res. Inst. Metals, Tokyo, Japan, 2(2): 102 (1960).
31. British Standard: EN 895, Destructive tests on welds in metallic materials – Transverse Tensile Test
32. ASTM E 112-88, Standard Test Methods for Determinin Average Grain Size, 1996, ASTM International
33. Kerr HW, Katoh M. Investigation of heat-affected zone cracking of GMA welds of Al–Mg–Si alloys using the Varestraint test. Weld J 1987;66:251-s–9-s.
34. Miyazaki M, Nishio K, Katoh M, Mukae S, Kerr HW. Quantitative investigation of heat-affected zone cracking in aluminium Alloy 6061. Weld J 1990;69:362-s–71-s.
35. Tirkeş S., Hot Cracking Susceptibility of Twin Roll Cast Al - Mg Alloys, PhD Thesis in Metallurgical and Materials Engineering. 2009, Middle East Technical University: Ankara. p. 108.
36. Y Osada , EPMA mapping of small particles of a-AlFeSi and β-AlFeSi in AA6063 alloy billets, Journal of Materials Science;Apr2003, Vol. 38 Issue 7, p1457
37. ASM Metals Handbook. Properties and Selection - Nonferrous Alloys and Special-purpose Materials. Vol. 2 1993: ASM International
38. Shuhai Chen, Liqun Li, Yanbin Chen , Jihua Huang, Joining mechanism of Ti/Al dissimilar alloys during laser welding-brazing process, Journal of Alloys and Compounds 509 (2011) 891–898

APPENDIX A

TECHNICAL DRAWINGS

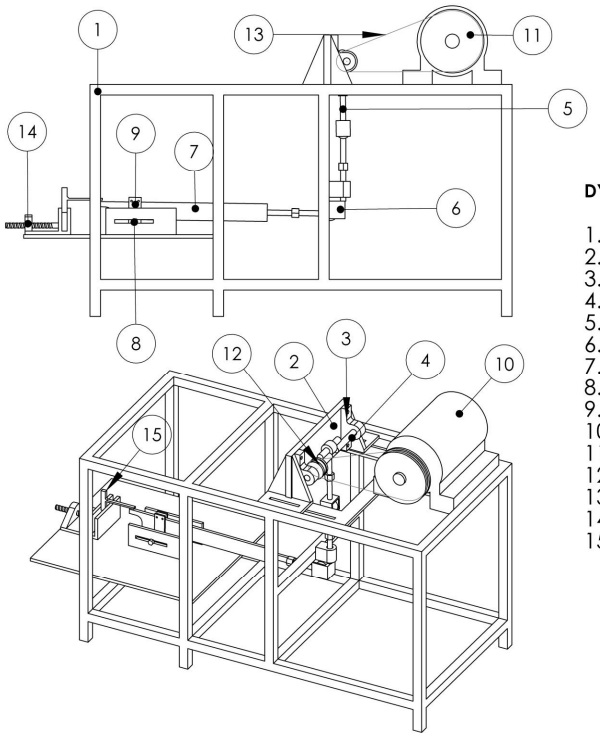

DYNAMIC LOADING MACHINE

1. Main Frame
2. Supporting Wall
3. Bearing
4. Shaft
5. First Transmission Rod
6. Second Transmission Rod
7. Lever Arm
8. Stroke Control & Support of Lever Arm
9. Lever Arm Holder
10. Engine
11. Engine Pulley
12. Shaft Pulley
13. Belt
14. Bench Clamp
15. Specimen

Figure 86 Dynamic Loading Machine

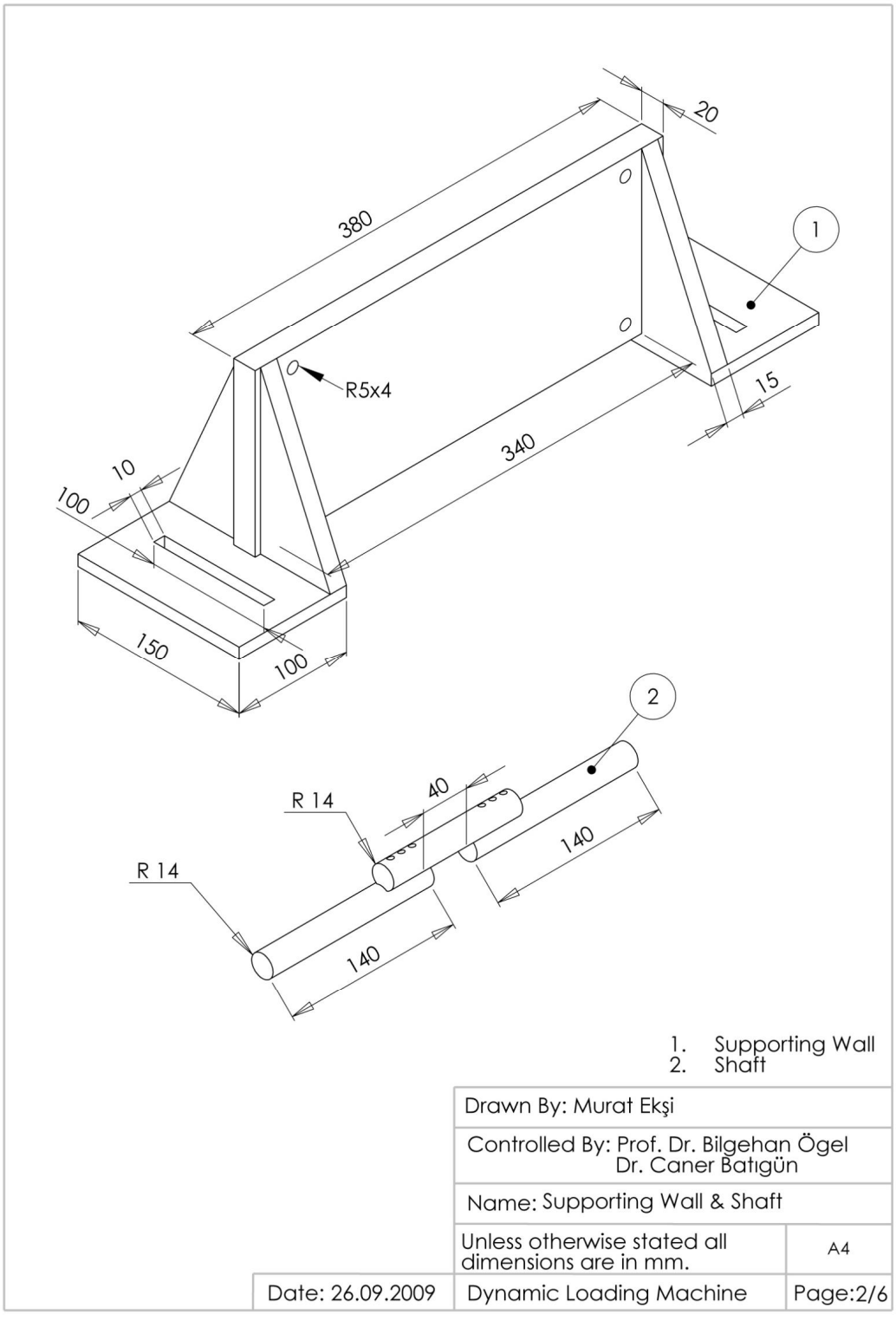

Figure 87 Supporting wall and shaft

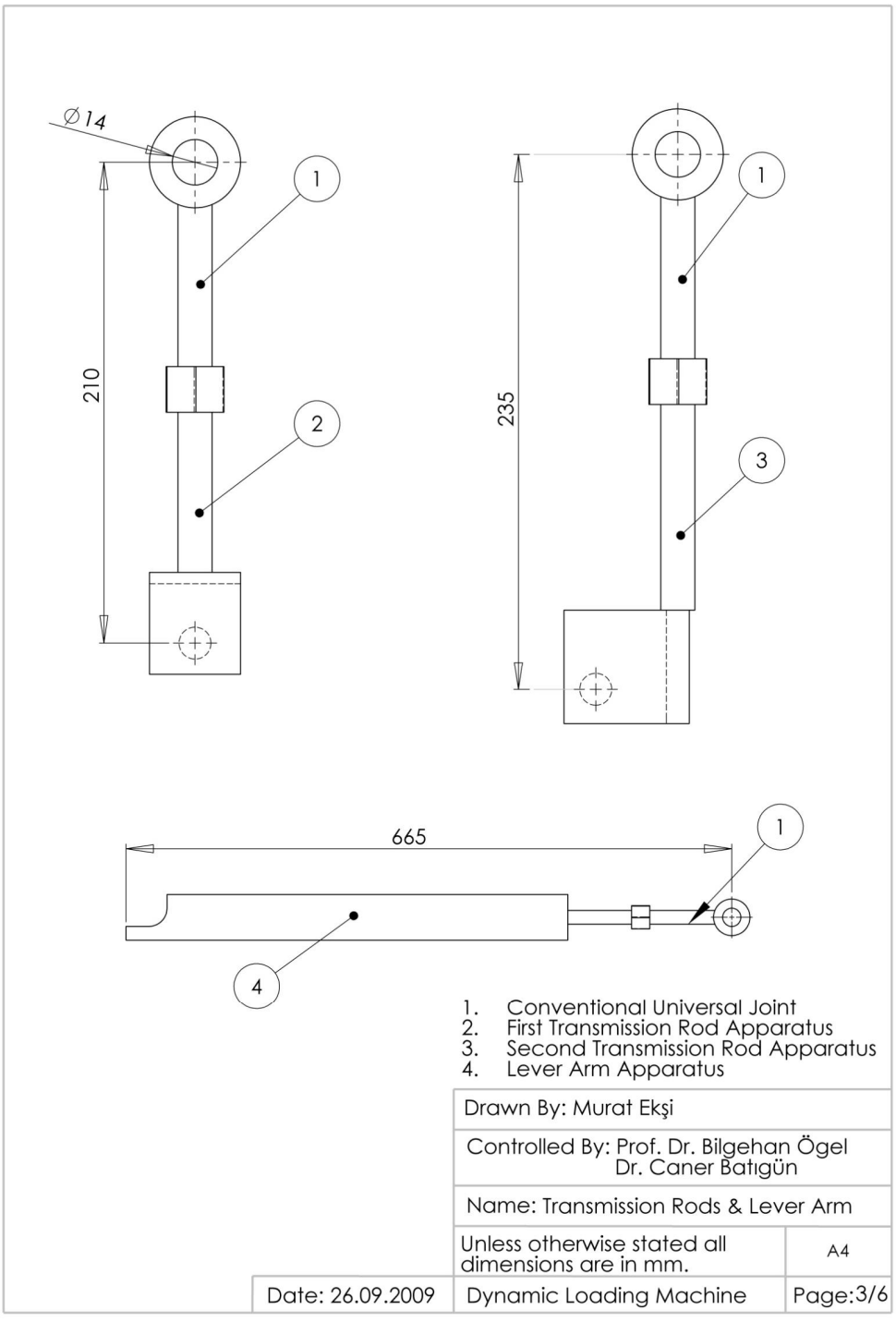

Figure 88 Transmission rods and Lever arm

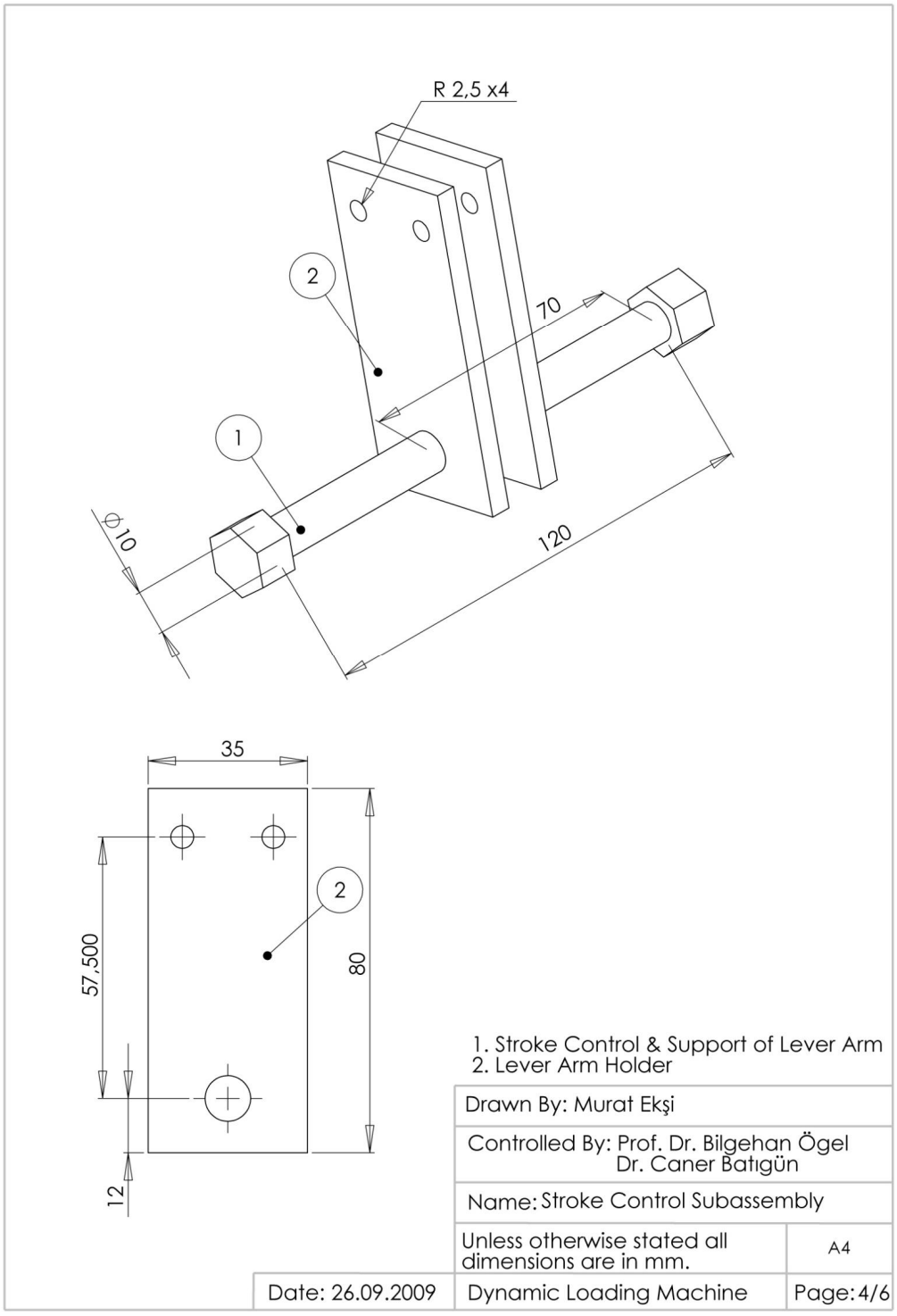

Figure 89 Support of lever arm and Lever arm holder

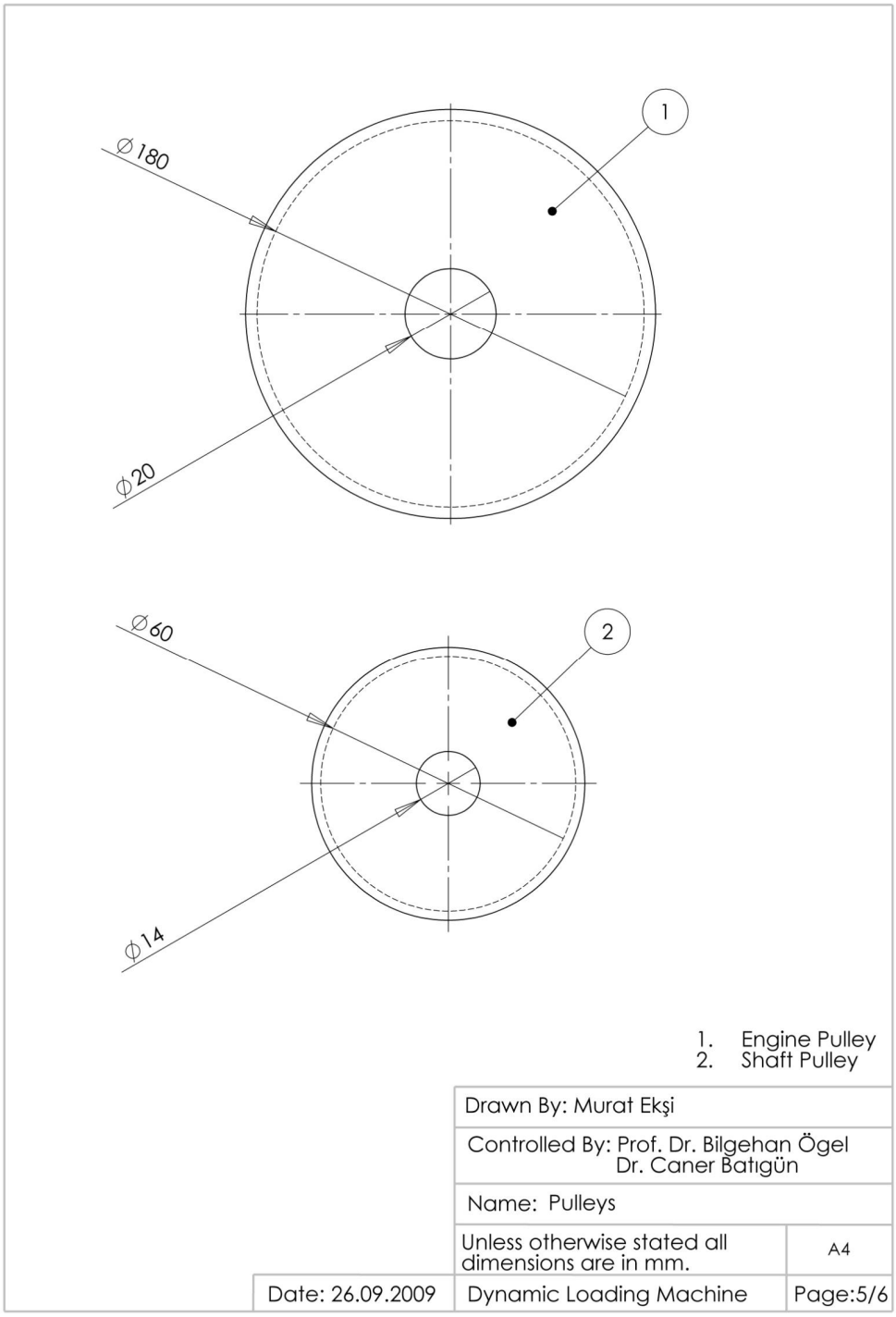

Figure 90 Engine pulley and shaft pulley

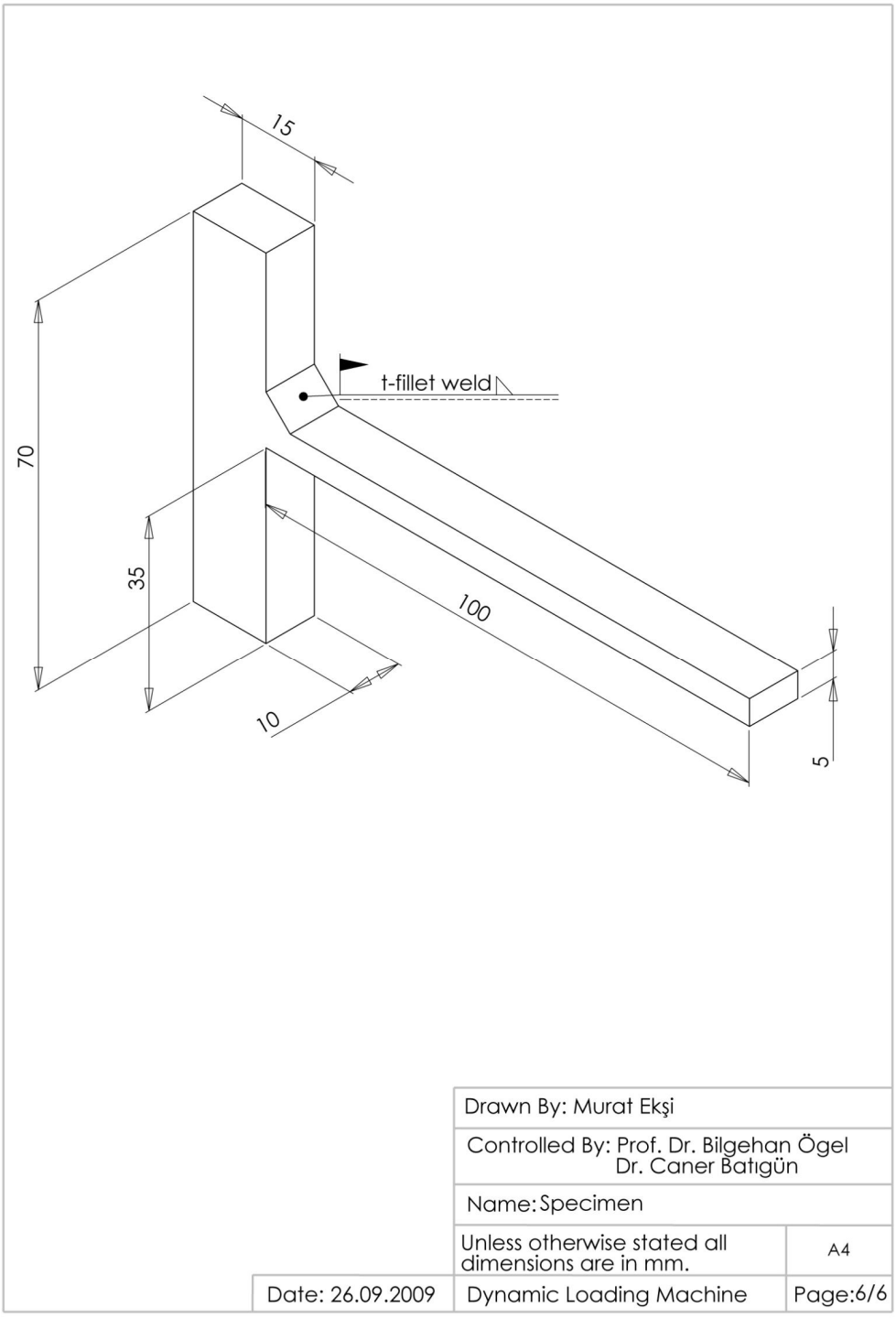

Figure 91 Dynamic Loading Specimen